NTNU – Trondheim
Norwegian University of
Science and Technology

Evaluation of Split Ratio for Plug Flow at a Meso-Scale T-Junction

Andre Wolden

Master of Science in Mechanical Engineering
Submission date: August 2012
Supervisor: Maria Fernandino, EPT
Co-supervisor: Young Lee Sang, KAIST

Norwegian University of Science and Technology
Department of Energy and Process Engineering

NTNU
Norwegian University
of Science and Technology

Department of Energy
and Process Engineering

EPT-M-2012-95

MASTER THESIS

for

Andre Wolden

Spring 2012

Evaluation of split ratio of plug flow at a meso-scale T-junction

Background and objective

Plug flow in meso-scale channels connected by a T-junction is frequently encountered in industrial applications, e.g. in heat exchangers for thermal management of electronic devices. A T-junction consists of an inlet referred to as "main", an outlet referred to as "run" which are connected straightly with regards to the main, and a perpendicularly connected channel referred to as "branch". Information regarding the flow behavior and flow-split ratio to the run and the branch are crucial in designing T-junctions.

It is of interest to review existing models or, if proven necessary, construct a reliable way of modeling two-phase flow through a T-junction system. Frequently used models include the superficial velocities for the two phases, but regard the impact of variations in bubble length (or bubble frequency) as unimportant or negligible. Previous work performed in the Multiphase Flow Laboratory of KAIST suggests otherwise, but is yet not conclusive. Hence a continuation of the investigation regarding the importance of bubble length for sufficiently accurate modeling is of interest to investigate further.

The goal of this project is to experimentally evaluate the importance of introducing the bubble length as an additional parameter in modelling the system at hand. It is of interest to evaluate and to improve existing models counting this quantity, and thereafter evaluate the performance of the model.

The following tasks are to be considered:

1. An extensive literature review will be necessary to compare the results of the researches conducted respectively on macro-scale channels and micro-scale channels with regards to the plug flow at a T-junction. Both researches focus on the similar topic, but do not share a similar objective because of the difference in applications. Therefore, a thorough literature survey should be performed if the work conducted by the micro-scale groups can be somehow helpful for the topic at hand, especially on the basic phenomena, primary parameters and the method of modelling.
2. Assembly of experimental loop in the lab.
3. Measurement of the transient pressure at the reference point of the T-junction as well as the pressure distribution along the main, run and the branch for various flow rates for the two phases and various bubble lengths.

Within 14 days of receiving the written text on the master thesis, the candidate shall submit a research plan for his project to the department.

When the thesis is evaluated, emphasis is put on processing of the results, and that they are presented in tabular and/or graphic form in a clear manner, and that they are analyzed carefully.

The thesis should be formulated as a research report with summary both in English and Norwegian, conclusion, literature references, table of contents etc. During the preparation of the text, the candidate should make an effort to produce a well-structured and easily readable report. In order to ease the evaluation of the thesis, it is important that the cross-references are correct. In the making of the report, strong emphasis should be placed on both a thorough discussion of the results and an orderly presentation.

The candidate is requested to initiate and keep close contact with his/her academic supervisor(s) throughout the working period. The candidate must follow the rules and regulations of NTNU as well as passive directions given by the Department of Energy and Process Engineering.

Risk assessment of the candidate's work shall be carried out according to the department's procedures. The risk assessment must be documented and included as part of the final report. Events related to the candidate's work adversely affecting the health, safety or security, must be documented and included as part of the final report.

Pursuant to "Regulations concerning the supplementary provisions to the technology study program/Master of Science" at NTNU §20, the Department reserves the permission to utilize all the results and data for teaching and research purposes as well as in future publications.

The final report is to be submitted digitally in DAIM. An executive summary of the thesis including title, student's name, supervisor's name, year, department name, and NTNU's logo and name, shall be submitted to the department as a separate pdf file. Based on an agreement with the supervisor, the final report and other material and documents may be given to the supervisor in digital format.

Department of Energy and Process Engineering, 6. February 2012

Olav Bolland
Department Head

Maria Fernandino
Academic Supervisor NTNU

Academic supervisor at KAIST, Korea: Prof. Sang Yong Lee (sangyonglee@kaist.ac.kr)

Preface

This thesis has been written while working for the Multiphase Flow Lab in Korea Advanced Institute of Science and Technology (KAIST) in South Korea under the supervision of Professor Sang Yong Lee. The author of this thesis was admitted to KAIST as an exchange student.

The topic of this thesis was chosen so as to partly be able to contribute to the Multiphase Flow Lab's interest, even though it is to be graded as a MSc Thesis at NTNU. The topic at hand were investigated by previous master student Ju Hyuk Hong (홍주혁), and this thesis can be partly regarded as a continuation of his work.

As a side not I would like to mention that through cooperation with PhD student Seok Kim (김석) I was found suited to be a part of a conference paper by the name *Investigation of previous research on two-phase flow distribution at microfluidic junctions* as a co-author. The topic of investigation was closely related to that of this thesis and hence cooperation was found to be a natural and efficient way to proceed with our work together. This paper was presented at the KSME (The Korean Society of Mechanical Engineers) Conference that took place in Yong Pyong Resort from 23rd to 26th of May 2012, and represented by both authors.

Abstract

Numerous applications, such as meso-scale heat exchangers, Lab-on-Chip devices (LOC), different systems within pharmaceutical and food industry, monodispersed emulsion and several other microfluidic systems, include two-phase flow through a meso-scale T-junction. When two-phase gas-liquid flow passes through an asymmetric meso-scale T-junction, a mal-distribution occurs. The phenomenon has proven itself to be unavoidable in most cases. In some applications this phenomenon can put the operational system at risk, while in other applications it is actually preferred. The phenomenon is still far from thoroughly understood. Thus the objective of this thesis is to further investigate this mal-distribution phenomenon. Split ratio for plug flow at a meso-scale T-junction has been investigated. A model for prediction of the split ratio has been proposed. Physical ingredients for determination of the split ratio have been focused upon. Much of the conducted work is based on findings in the MSc thesis by Hong et al. (2011) who proved the importance of the bubble length when predicting the split ratio.

Split ratio, bubble length and pressure has been measured through experimentation. The T-junction used in the conducted experiments has a main channel, referred to simply as the "main". It is connected in a straight line with one outlet referred to as the "run". The second outlet is connected perpendicularly to the main and the run, and is referred to as the "branch". All channels have a square shaped cross section with a hydraulic diameter of $D_H = 0.6\,mm$. Water and air was used as working fluids. For all conducted experiments the flow field took on a plug flow pattern.

The branch channel has been observed to be rich in gas for all cases, except when the flow rate in the run is high. The flux in the main also has to be low to reduce the viscous drag forces between the two phases and the inertial

forces of the plug. For increasingly high total flow rate in the run, a turning point has been located. When the flow rate exceeds this point the run becomes rich in gas. In both extreme cases (high flow rate in the run and in the branch) separation occurs for sufficiently short bubbles. The occurrence of separation is also highly dependent on the total flux in the main. To retain separation the surface tension has to overcome the viscous drag forces acting on the interface between the two phases.

In the centre regime, where bubbles always break up and a plug flow pattern occurs in both outlets, the split ratio shows a strict relation to the bubble length. This strict relation between the split ratio and the bubble length were also concluded upon in the MSc thesis by Hong et al. (2011). In the defined centre regime changes in superficial velocities showed to have a negligible effect on the split ratio in comparison to variation in the bubble length. Long bubbles yields a split ratio located closest to perfect distribution. Decreasing the bubble length yields an increase in the void fraction (gas) in the branch.

A model for prediction of the split ratio has been proposed. It is primarily valid within the centre regime, and is based on the time and area averaged Bernoulli equation. The model takes the bubble length into account, and predicts the split ratio on the main assumption that an increased amount of energy is lost to friction and separation as the fraction of water in the branch is increased. This while keeping the *total* fluxes in each of the outlets constant. An anticipated trend has been located through evaluating the model against experimental data. Therefore the model has been concluded upon to be physically sound.

Sammendrag

En rekke systemer, som for eksempel *meso-scale* varmevekslere, Lab-on-Chip enheter (LOC), ulike systemer innenfor farmasøytisk- og næringsmiddelindustri, *monodispersed* emulsjon og flere andre mikrofluidiske systemer, inkluderer tofasestrøm gjennom et *meso-scale* T-kryss. Når en tofase gass-væske strøm passerer gjennom et asymmetrisk *meso-scale* T-kryss, så oppstår det en mal-distribusjon av fasene. Fenomenet har vist seg å være uunngåelig. I noen tilfeller kan dette fenomenet utsette det operasjonelle systemet for fare, mens i andre systemer er det faktisk foretrukket. Viktigst er det faktum at fenomenet er fortsatt langt fra grundig forstått. Derfor er målet ved denne avhandlingen å ytterligere undersøke dette mal-distribusjons fenomenet. Delingsforhold for *plug*-strømning gjennom et *meso-scale* T-kryss har blitt undersøkt. Det er blitt foreslått en modell for å predikere delingsforholdet av de to fasene. Fysiske ingredienser for å bestemme delingsforholdet har blitt fokusert på. Mye av det utførte arbeidet er basert på funn gjort av Hong et al. (2011), som fokuserte på viktigheten av å ta hensyn til boblelengden for å predikere delingsforholdet.

Gjennom eksperimenter har delingsforholdet, bobblelengden og trykkdistribusjon blitt målt. T-krysset som er blitt brukt i de gjennomførte eksperimentene har en hovedkanal, oppkalt "main". Den er koblet i en rett linje med en utløpskanal som er blitt oppkalt "run". Det andre uttaket er koblet vinkelrett på kanalene main og run, og er blitt oppkalt "branch". Alle kanalene har kvadratisk formet tverrsnitt med en hydraulisk diameter på $D_H = 0.6\,mm$. Vann og luft ble benyttet for væske- og gassfasene. For alle gjennomførte eksperimenter inkluderte strømningsmønsteret et slug-mønster.

Branch-kanalen har blitt observert å være rik på gass for alle tilfeller, foruten for høy total strømningshastighet i run-kanalen, men dette er også en

funksjon av total fluksen i main-kanalen. For høye strømningshastigheter i run-kanalen har et vendepunkt blitt definert hvor run-kanalen istedet for branch-kanalen er rik på gass. For begge ektremtilfellene oppstår separasjon så lenge boblene er tilstrekkelig korte. For strømning med boblestørrelser større enn denne kritiske verdien blir boblene presses inn i begge utløpsrørene, og deling av boblene forekommer. Separasjon er også svært avhengig av den totale fluksen. For å oppnå separasjon så må overflatespenningen overvinne de viskøse kreftene som virker på grensen mellom de to fasene.

I et definert senterregime, hvor bobler alltid deles, og et slug-strømningsmønster forekommer i begge utløpene, viser delingsforholdet en streng relasjon til boblelengdeparameteren. Dette strenge forholdet mellom delingsforhold og boblelengde ble også diskutert av Hong et al. (2011). Innenfor det definerte senterregimet har det blitt vist at variasjon av totalfluksen i main-kanalen har en ubetydelig effekt på delingsforholdet i forhold til variasjon i boblelengde. Lange bobler gir et delingsforhold som ligger nært perfekt fordeling. Reduksjon i boblelengde er vist å føre til en økning av gassinnhold i branch-kanalen.

En modell for å predikere delingsforholdet har blitt foreslått. Den er først og fremst gjeldene innenfor senterregimet, og er basert på Bernoullis ligning, med bruk av gjennomsnittlige verdier for trykk og hastigheter med respekt til tid og areal. Modellen betrakter boblelengde, og predikerer delingsforholdet. Modellen er basert på en antagelse om at en økt mengde energi går tapt i form av friksjon og separasjon nær T-kryssregionen hvis mengden av den tunge fasen som strømmer til branch-kanalen økes. En predikert trend basert på denne fysiske påstanden er lokalisert gjennom evaluering av modellen opp mot eksperimentelle data. Derfor er det blitt konkudert at modelling er i stand til å predikere delingsforholdet. Dette kommer også frem ved evaluering av eksperimentell data.

Table of Contents

Nomenclature

Notation	Unit	Description
Q	[m^3/s]	Total volumetric flow rate
Q_G	[m^3/s]	Volumetric flow rate gas
Q_L	[m^3/s]	Volumetric flow rate liquid
U_G	[m/s]	Volumetric flux gas
U_L	[m/s]	Volumetric flux liquid
U_r	[m/s]	Slip velocity between the two phases
U_B	[m/s]	Bubble velocity
U_{ext}	[m/s]	Mean velocity of the external phase
U	[m/s]	Characteristic velocity scale
W	[kg/s]	Total mass flow rate
W_G	[kg/s]	Mass flow rate gas
W_L	[kg/s]	Mass flow rate liquid
G	[kg/m^2·s]	Total mass flux
G_G	[kg/m^2·s]	Mass flux gas
G_L	[kg/m^2·s]	Mass flux liquid
j	[m/s]	Total volumetric flux / average velocity
j_G	[m/s]	Superficial velocity gas
j_L	[m/s]	Superficial velocity liquid
Re	[1]	Reynolds number (Re_d)
Ca	[1]	Capillary number
We	[1]	Weber number
Bo	[1]	Bond number
σ	[N/m]	Interfacial tension
ρ_G	[kg/m^3]	Density gas phase
ρ_L	[kg/m^3]	Density liquid phase
μ_G	[kg/m·s]	Viscosity gas phase

μ_L	[kg/m·s]	Viscosity liquid phase
g	[m/s^2]	Acceleration of gravity
A	[m^2]	Pipe area
D_H	[m]	Hydraulic Diameter
A_G	[m^2]	Area for gas
A_L	[m^2]	Area for liquid
α	[1]	Void fraction gas phase
α_L	[1]	Void fraction liquid phase
β	[1]	Volumetric quality gas phase
β_L	[1]	Volumetric quality liquid phase
λ	[1]	Viscosity ratio
L_{UC}	[m]	Length unit cell
L_B	[m]	Bubble length
L_{BN}	[m]	Bubble nose length
L_{BT}	[m]	Bubble tail length
L_{plug}	[m]	Liquid plug length
δ	[m]	Film height
Δt_i	[s]	Time of bubble interface in junction region
C_{BT}	[1]	Correction coefficient for time fraction of bubble interface in junction region
Subscripts		
1		Main
2		Run
3		Branch
12		Main to run
13		Main to branch
j		Junction
G		Gas
L		Liquid
$BN\&T$		Bubble nose and tail

1 Introduction

Two-phase plug flow in micro- and meso-scale channels flowing through T-junctions is frequently encountered in numerous applications. These applications might differ from each other drastically in many ways with regards to their functionality, but even so the flow system in each of them resembles each other by having the described fluid flow implemented somewhere in the total system. Some examples of these applications are micro- and meso-scale heat exchangers, many types of process plants, water-cooled nuclear reactors, applications within pharmaceutical and food industry, and so on. Many more applications surely exist, some shall be pointed out in later chapters, and it is assumed that there are still others unknown to the author.

The key point between these all these obviously different applications is that they all somehow include a highly complex two-phase flow stream through channels, and these channels are normally connected through junction points with variations in geometry. The two-phase flow can have different flow patterns, as shall be further explained later on, and several parameters needs to be accounted for to specify which pattern that will occur for a specific system. A frequently encountered two-phase flow pattern in micro- and meso-scale channels is the plug flow pattern. It can be described as consecutive gas bubbles and liquid plugs, sometimes referred to as liquid trains, propagating throughout the system of channels. It is difficult to predict the flow behavior and pressure distribution for this flow pattern, as well as others. Hence it is hard to evaluate important parameters which play a role in the overall performance of the system since they are affected by the flow conditions.

As an example some micro- and meso-scale heat exchangers take use of several tens of T-junctions connected in series to distribute the working fluid

through parallel channels. When the two-phase flow enters the first T-junction a mal-distribution of the two phases occur. Mal-distribution has been verified to occur by numerous researchers. The result is a possibility of dry-out in the channels that has received a higher quality (gas quality), and thereby lowering the cooling ability for these channels. This puts the e.g. electrical device that needs to be cooled at risk.

Therefore, as the objective of this thesis, it is of interest to investigate the split ratio for a two-phase gas and liquid mixture with a plug flow pattern at a meso-scale T-junction. The T-junction used in the conducted experiments has a main channel, referred to simply as the "main". It is connected in a straight line with one outlet referred to as the "run". The second outlet is connected perpendicularly to the main and the run, and is referred to as the "branch". All channels have a square shaped cross section with a hydraulic diameter of $D_H = 0.6\,mm$. The experimental flow conditions was proven to lie within the plug flow regime from comparison with flow pattern maps constructed by Chung and Kawaji (2004) (1) and Owejan et al. (2005) (2).

Physical trend is emphasized upon as being highly important for the understanding of the phenomena since an extensive literature review has revealed that the split ratio is still far from thoroughly understood. The topic has been investigated through experimentation, and a model for the prediction of the split ratio is proposed.

Many researchers have already attacked the same problem with interest in prediction of the split ratio. They usually try to describe the split ratio as a function of superficial velocities, flow pattern, inclination angle and hydraulic diameter. In their experimental data inconsistencies have been located and the reason behind their appearance unknown. Being aware of this fact Ju Hyuk Hong (2011) (3) suggested in his MSc thesis that the bubble length could possibly be one of the main parameters for prediction of the split-ratio. Through their work they managed to prove this assumption to be true. This thesis will mainly focus upon this very interesting conclusion, and

should therefore be seen as an extension and continuation of their work. No evidence of other authors regarding the bubble length as important for evaluation of the split ratio has been located.

As a side note, an interesting coincidence has occurred in the investigation of flow split at a T-junction with meso-scale heat exchangers in mind as the diameter of the channels has continued to decrease for many decades. There are other branches within engineering that are focusing on a similar area, namely split ratio in micro- and meso-scale channels junctions, thought their objective is instead to actually obtain mal-distribution, and even separation in some cases. Due to this coincidence previous work conducted for these other branches will be reviewed and used to enhance the understanding of the split ratio phenomenon.

In chapter 2 and 3 a review of related applications is presented. This is followed by an extensive literature review in chapter 4 5 6 and 7 . Chapter 7 includes experimental data obtained by Hong et al. (2011) (3) and their reasoning behind the conclusion upon the grave importance of regarding bubble length for prediction of the split ratio. Chapter 8 presents the finalized experimental set-up. Chapter 9 presents obtained experimental data and evaluation of pressure data against theory. Finally chapter 10 includes a proposed model for prediction of the split ratio at a meso-scale T-junction and validation of its performance. A conclusion and suggestions for future work is presented in chapter 11 and 12 .

2 Meso-scale Heat Exchangers

The interest of studying the flow field and pressure distribution in capillary tubes, and later on focus on how to be able to predict the split ratio at junctions, has partly arisen due to their existence in small sized heat exchangers (e.g. plate heat exchangers (4)). This particular interest relates far back in time. Suo et al. (1964) (5) investigated this topic for mainly the plug flow regime. The plug flow regime covers a wide range of most flow regime maps, including flows in capillary tubes (i.e. tubes with small hydraulic diameter) and is frequently encountered in many applications such as small sized heat exchangers. Since then several other researchers have conducted work with problem descriptions based on similar specifications for two-phase flow in small-sized channels. Around the same era the interest of predicting the split ratio of the two-phases for when the flow field enters a T-junction became important due to its presence in heat exchangers. Among some of the earlier researchers to attack this topic was Azzopardi et al. (1982) (6) and Bassiouny et al. (1983) (7).

It is important to be able to predict and foresee the qualities of the phases in each channel so as to avoid possible negative effects on entities affected by the heat transfer performance of the flow system. Mal-distribution at the junctions might be in some cases fatal for the overall system due to, for example, the possibility of dry-out in some of the channels, or, if not entirely dried out, lowering of the heat transporting capacity which can result in malfunctioning of the cooled device.

2.1 Cooling of Electrical Components

Cooling of electronic components (microchips etc.) has gained considerable importance, as a result of the high increase in power densities in micro-electronic equipment. By power densities it is meant the increasing amount

of thermal energy that needs to be transported away from the given electrical device so that the temperature of the device stays below its specified maximum working conditions. This is to ensure that the device will work properly and not become overheated followed by malfunctioning. The increase in power densities has been made possible by advances in semiconductor technology (8).

Electrical devices can be cooled by performing heat transfer directly to the surrounding air. This is shown in Figure 2.1 where an air-cooled heat sink is directly mounted on to the heat source. For very high heat fluxes, however, heat transfer by liquids flowing through micro-channels is more effective (9), (10). The working fluid in liquid or vapour form is then carried to a remote heat exchanger were space availability is easier found.

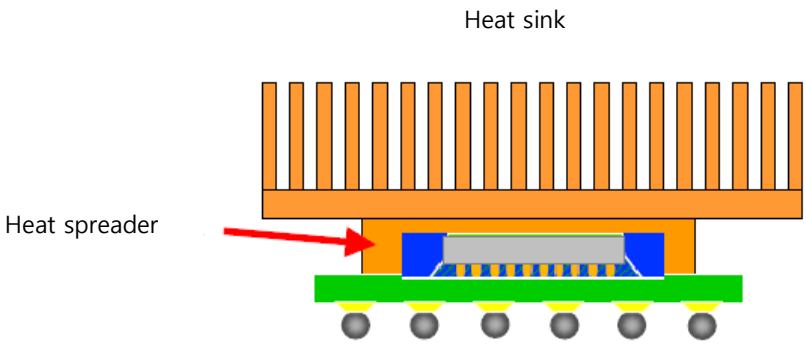

Figure 2.1: Chip with integrated air cooled heat sink (10)

For transportable devices the heat transported eventually has to be transferred to the surrounding air, but by transporting heat away from the device this heat transfer to air can be handled in an easier fashion due the increase in available area. An example of the schematic of this procedure is presented in Figure 2.2.

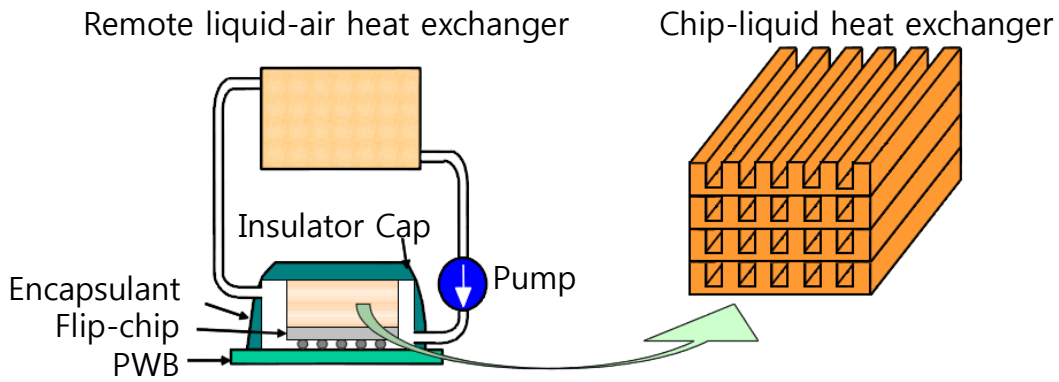

Figure 2.2: Flow loop for thermal management of electrical devices (10)

Heat is rejected to the ambient surrounding in the remote liquid-air exchanger and thereafter the cooled working fluid is transported back to the chip-liquid heat exchanger. This overall cycle is what is referred to as the flow loop.

2.2 Geometry of Heat Exchangers

To elaborate on the relevance of investigating two-phase plug flow in channels with a hydraulic diameter close to $D_H = 600\ \mu m$ this section and the next will focus on ranges for relevant parameters so as to see the connection with the present conducted work. Heat exchangers come with numerous variations in both design and sizes. Heat exchangers that use channel sizes in the range of 0.5-1.0 mm are relatively common in mostly mobile applications due to compactness and performance (11). Also heat exchangers that take use of ever decreasing channel sizes starts to get more and more common for industrial use. Two heat exchangers with internal channel size of 75 x 800 and 150 x 800 μm are presented in Figure 2.3. These types of heat exchangers typically include several hundred parallel meso-scale channels.

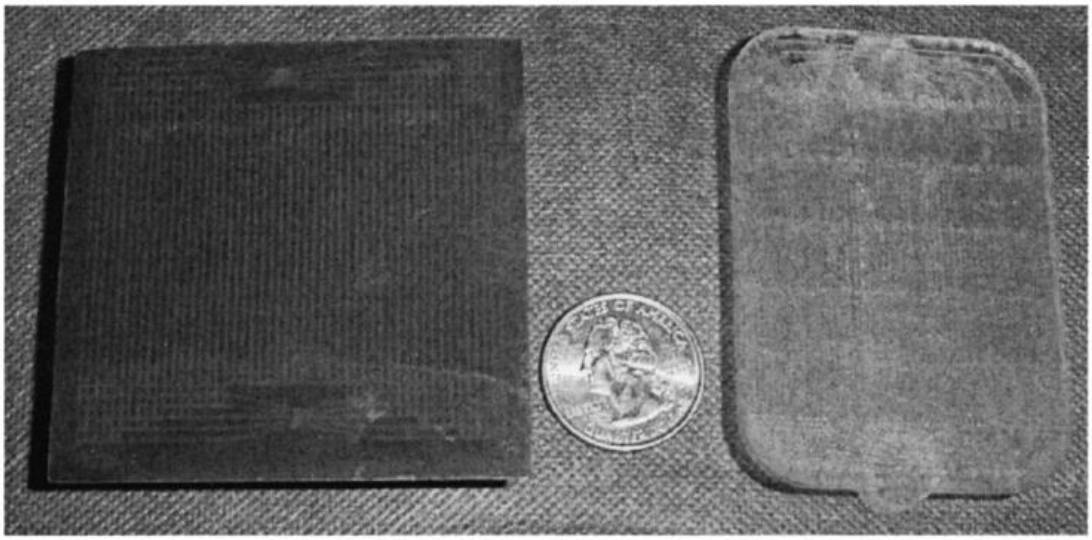

Figure 2.3: Conventional meso-scale heat exchanger (11)

A schematic view of a typical heat exchanger is presented in Figure 2.4. The working fluid enters the header typically as a one component two phase flow, e.g. use of water where some of the water has undergone phase change to gas due to boiling. The quality depends on each specified system.

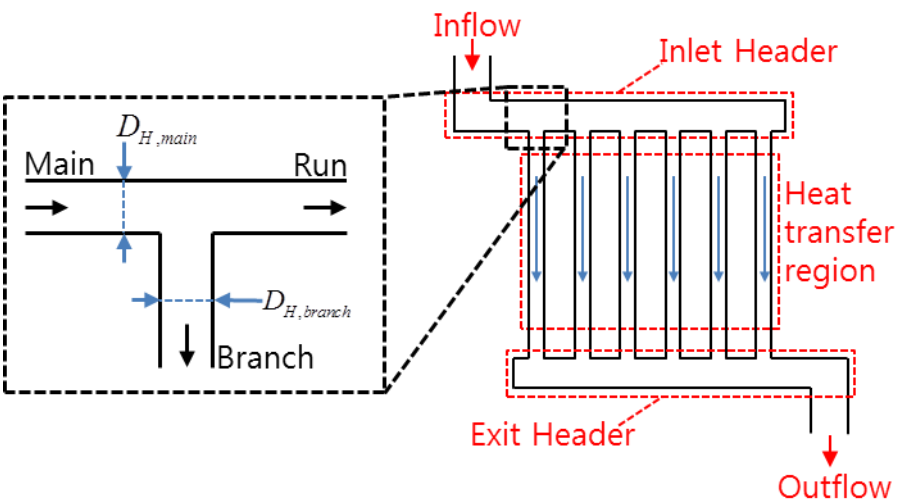

Figure 2.4: Schematic of a Z-type heat exchanger

In the figure the dimensions of the header and each channel appears different in the right hand side of the figure. Even so, as stated earlier, there are numerous different sizes and design of heat exchangers, and so the work conducted for this thesis assumes that the header and each one of the channels have square shaped cross sections of equal size to yield the given

T-junction with the dimensions of the main equal to that of the branch and the run channel. It is of course important to investigate the split ratio at a T-junction for variations in diameters, but in general the physics that governs the split ratio for any given T-junction is far from understood. To rigorously model and predict the split ratio at even the simplest T-junction remains an important challenge in general science. Knowledge about the split ratio for a basic T-junction is utmost important to obtain and will serve as complimentary help with physical understanding for when prediction of split ratio in headers that involve different junction dimensions is designed. The working fluid is distributed in the inlet header, flows through the parallel meso-scale channels where heat transfer from the electrical device to the working fluid occurs, and is then collected in the exit header. In the header, as seen in the figure, the header distributes the working fluid to each channel though several T-junctions connected in series.

2.3 Plug Flow Pattern and Mal-distribution

The plug flow pattern is relatively dominant in flow regime maps for meso-scale hydraulic diameters. It is suspected that for conventional heat exchanger design, the flow pattern consists mainly of plug flow. The plug flow regime can be described by consecutive gas bubbles with bubble length larger that the hydraulic diameter. An example of plug flow through a meso-scale T-junction is presented in Figure 2.5.

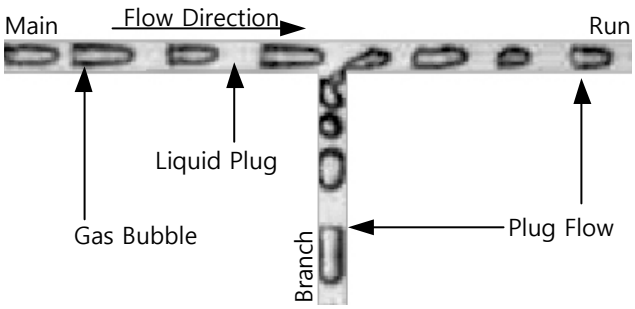

Figure 2.5: Plug Flow at a T-junction (3)

In later chapters flow regime maps for two phase flow in meso-scale channels is presented, and it reviels the domince of the plug flow pattern for such flow conditions

When the multiphase mixture of liquid and gas with a plug pattern enters the header and passes a T-junction, a maldistribution occurs. The occurrence of mal-distribution at an asymmetric T-junction is well known in the literature. The quality in the run and the branch differs from that in the main. For most cases the branch in the system is rich on gas. With different quality in the parallel channels, some channels will be exposed of higher risk of dry-out, and hence a drastic decrease in the heat transporting ability of that channel. This maldistribution will inevitably lead to an undesirable temperature distribution in the electrical entity. In the heat transfer region the working fluid will undergo phase change.

If the electrical device is assumed to have an evenly distributed temperature so that the temperature difference between the working fluid and the electrical device is the same in each channel, then the maldistribution will increase the possibility of dry-out in the channels with the higher quality. On the other hand hot-spots are often encountered in different electrical devices. For cases like this a maldistribution of the working fluid can actually prove itself to be advantageous for cooling purposes, but of course has to be well predicted. In any case the flow split ratio at each T-junction in the header largely determines the overall performance of the cooling unit. This phenomena lead to the objective of interest; prediction of the split ratio for plug flow at a T-junction with meso-scale channels.

3 Other Applications

The hydraulic diameter of the channels located in heat exchangers has decreased to less than a millimetre for the last two or three decades, and it is still decreasing. Because of this drastic decrease in size of a heat exchanger device and thereby the channel size as well this branch within engineering has closed in on other engineering groups with similar topic of interest, namely two-phase flow in micro- or meso-scale channels with possible junctions within the system. These other groups have their roots within several different fields, such as chemical or biomechanical engineering, pharmaceutical or food industries, Lab on Chip (LOC) applications, production of polymer particles etc. Therefore it is obviously of interest to review literature across different engineering fields so as to obtain as good as possible physical understanding of the flow field at hand. It is of interest to try and combine knowledge within all the mentioned engineering fields so as to obtain more information about the physical trend of split-ratio at a T-junction. In this chapter some of the applications that include a similar flow system are presented and described shortly. Later on, in chapter 5 and 6 , findings that can contribute in understanding the physical trend of two-phase plug flow in channels and through junction points will be reviewed.

3.1 Lab on Chip

Research on so-called Lab-on-Chip (LOC) has received a dramatic increase in interest for the last two decades. Entire journals have been dedicated to this field. The interest in analysing complex biological systems such as living cells with the use of microfabricated structures has attracted attention more recently. These microfabricated structures can enable easy integration of all kinds of analytical standard operations with regards to e.g. cell biology, neurobiology and tissue engineering into microfluidic systems (12), (13). It enables methods for manipulating large number of cells simultaneously, and

the size of these cells fits very well with that of commonly used fluidic devices with hydraulic diameters in the range of $10-100\ \mu m$ (12).

3.2 Monodispersed Emulsions

Microfluidic technologies have recently emerged as a new tool for conducting various chemical/biological processes in a miniaturized platform. Monodispersed microdroplets and microparticles can be produced in micro/meso-scale channels which in recent times can be precisely manufactured. Several schemes involving junctions or any type of flow system has been tried out to obtain specific flow fields with different kinds of applications in mind. For instance producing monodispersed emulsions have been used as miniaturized reactors for where the reaction time can be rigorously controlled. Aqueous droplets have also been used to confine small amounts of biological entities such as biomacro-molecules and cells to conduct biochemical screening or selection (14).

4 Multiphase Flow

The most frequently occurring type of flow in both nature and technology consist of two or more phases, i.e. they are multiphase flows. Some applications for where different types of multiphase flow occur has already been introduced in chapters 2 and 3 . Some other specific examples are in steam generators, condensators, cooling towers etc. For the oil and gas industry multiphase flows are present during extraction, transportation and treatment of the products.

Usually multiphase flows have a highly complicated and chaotic velocity distribution. Sometimes the relative velocity between the phases can be almost equal, but this is usually not the case. Multiphase flow systems can have major differences when it comes to possible flow patterns or parameters that describe the transition between these patterns, and has to be dealt with as several subtopics due to their apparent difference in nature. Several parameters, e.g. geometry, velocities, volume flow, and number of different phases affect the final flow. Due to the usually chaotic flow it is sometimes necessary to use statistical methods to evaluate the flows. Parameters like velocity, temperature and pressure distribution needs to be averaged. This is needed to be able to predict a systems behavior so that quantitative statements about the expected phenomena can be made.

The definition of a multiphase flow is a combined mixture of two or more different phases where all phases are in motion. The relative motion between the phases differs. The simplest kind of multi-phase flow is two-phase flow as is encountered in the present work. Even so, almost all two phase flow phenomena are random, due to possible high Reynolds numbers or phase induced instabilities. Therefore statistical mechanics are commonly needed. The difference between the media of the two phases can be its thermodynamic state, called the phase (e.g. solid, liquid or gas) and/or its

multiple chemical components, e.g. a mixture of air and water. The term two-component is used to describe flows in which the phases do not consist of the same chemical substance, but the mathematics which describe both types of mixtures are identical. Therefore it is not needed to emphasize on distinguishing these two types of mixtures.

In many cases it is crucial to be able to physically understand, measure important parameters and predict the flow characteristics for a future system in order to meet environmental and technological demands. Even the simplest kinds of multiphase flows make a consistent mathematical physical description difficult. Rigorous two-phase flow modeling and analysis is one of the great remaining challenges in classical science, and numerous researches have been working within the field for decades. For two-phase flow in pipes and channels small changes to e.g. hydraulic diameter, fluid properties and superficial velocities can give tremendous changes in the observed physical trend, and hence several researchers investigate two-phase flow within specified regimes for the mentioned parameters. At the same time it is of interest to connect the bridge between every specified system while at the same time researchers have to focus on investigating a limited parameter regime close to that of the operating conditions for the specifically related applications.

Two terms that have been traditionally used for two-phase flow classifications are "flow pattern" and "flow regime". A flow pattern indicates the visible distribution or structure of the phases. Some typically occurring patterns consisting of gas and liquid are schematically presented in Figure 4.1.

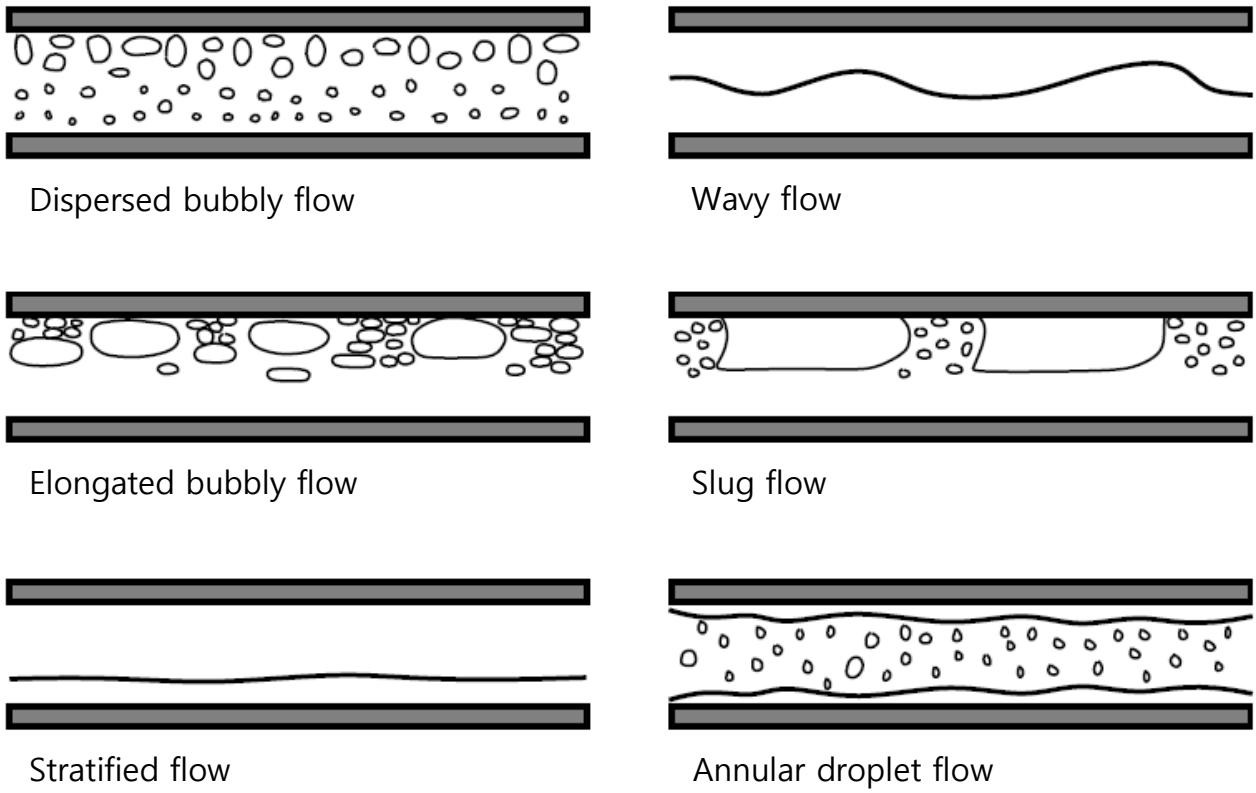

Figure 4.1: Flow patterns for horizontal gas-liquid flow (15)

In contrast to the term flow pattern, a flow regime indicates how the phase distributions affect the physical nature of the system. Hence, different flow regimes indicate the need for different models. Different flow patterns, on the other hand, indicate a visible difference in the phase structure, but not necessarily a need for a new model. Patterns and regimes are terms that are occasionally interchangeable, but they are not synonymous.

The type of flow pattern which occur for a specific setup is highly dependent on the superficial velocities, but at the same it depends on the hydraulic diameter and the properties of each of the two phases. The named flow patterns are illustrated in Figure 4.2 to serve as an example. The location of these borders is highly dependent on hydraulic diameter, viscosity and density for each of the two phases, and the inclination angle of the channel for when gravity effects is important. New maps have to be constructed for changes in the mentioned parameters.

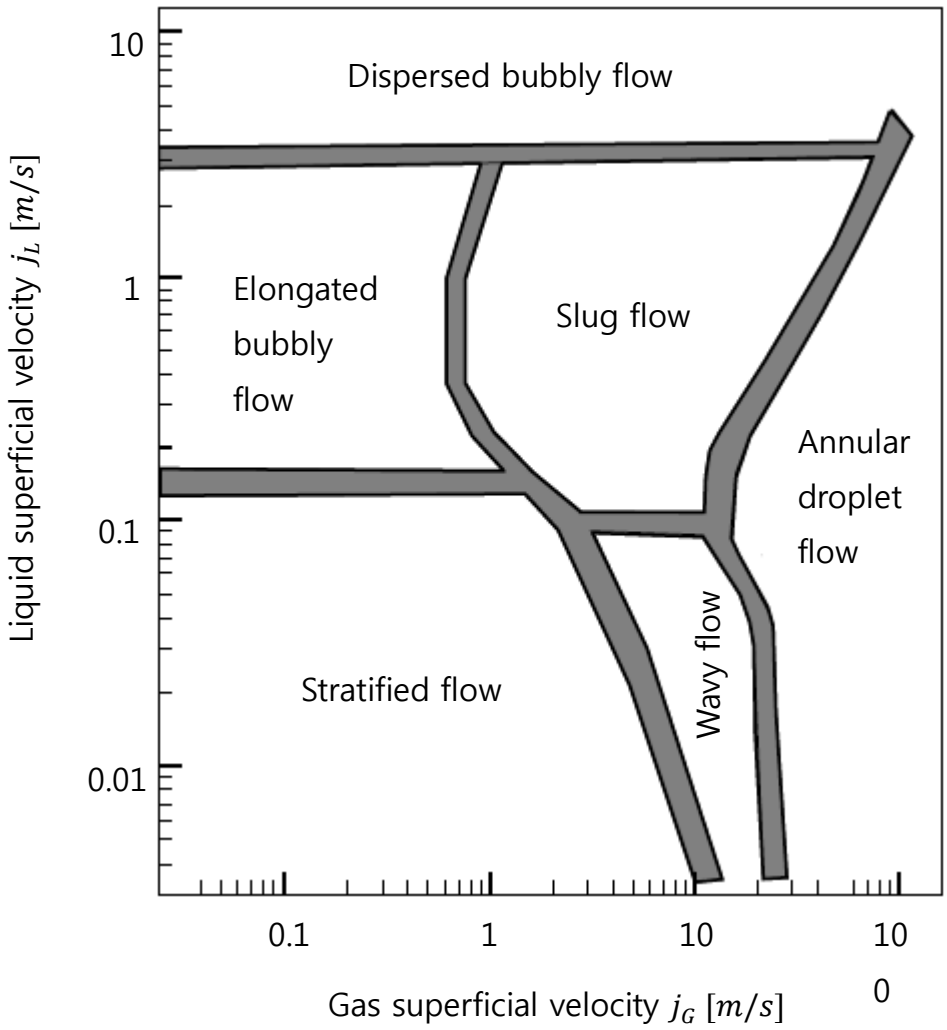

Figure 4.2: Flow regime map (horizontal flow, $0.1\,MPa, D_H = 2.5\,cm$) (15)

For horizontal two phase flow (see Figure 4.2), stratified flow, with increasing interfacial stress, turns into slug flow when the liquid superficial velocity gets large enough, and into annular flow for small liquid volume fractions. Figure 4.2 is an empirical flow regime map for air-water flow in a horizontal pipe with $D_H = 25\,mm$.

4.1 Definitions

Earlier the term meso-scale was used even though its meaning has not been fully revealed, though assumed to be intuitive to some extent. Here a definition is given, though it should be emphasized that different naming of same regions have been discovered in the literature. The micro-scale region is defined to govern

$$1\,\mu m < D_h < 100\,\mu m \qquad 4.1$$

while meso-scale hydraulic diameter refers to the diameter being in the range of

$$100\,\mu m < D_h < 1\,mm \qquad 4.2$$

The hydraulic diameter is defined as

$$D_H = \frac{4A}{wetted\ perimeter} \qquad 4.3$$

and hence for a square shaped cross section (as is used in the experimental set-up) the hydraulic diameter becomes simply

$$D_H = \frac{4A}{wetted\ perimeter} = \frac{4 \cdot L^2}{4 \cdot L} = L \qquad 4.4$$

where L is the length of one of the sides.

For two phase situations the single phase conservation equations cannot be easily applied, primarily because of the discontinuities represented by the gas-liquid interphase and the fact that the interphase is deformable. A wide variety of flow patterns can occur as already introduced. Useful analytical, semi-analytical, and purely empirical methods have been developed for the

analysis of two-phase flows. This is done by adapting one of the following methods:

- Simplifying assumptions, e.g. equal sized gas bubbles uniformly distributed in laminar liquid flow with gas and liquid moving with the same velocity everywhere.
- Averaging parameters and transport equations. Averaging can be performed in time and/or area/volume. Averaging is equal to low pass filtering to eliminate high-frequency fluctuations.

4.2 Averaging

For any property ξ, the local time-averaged value is defined as

$$\overline{\xi}^{t}(t_0,\vec{r_0}) = \frac{1}{\Delta t}\int_{t_0-\frac{\Delta t}{2}}^{t_0+\frac{\Delta t}{2}} \xi(t,\vec{r_0})dt \qquad 4.5$$

Where $\vec{r_0}$ is defined as presented in Figure 4.3 and

- $\Delta t \gg$ characteristic time scale of fluctuations desired to be filtered out.
- $\Delta t \ll$ characteristic time scale of the macroscopic system's transient behaviour.

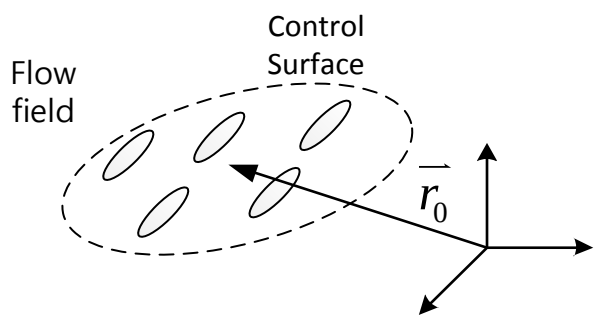

Figure 4.3: Two phase flow

Time averaging is most appropriate for quasi-stationary processes. Also the term *stationary* should be used instead of the term *steady state* for e.g. plug flow, since the flow field is constantly fluctuating (16).

In a stationary process the statistical characteristics of properties do not vary with time. As a descriptive example, the bubble length for slug flow with $D_H = 10\,mm$ follows a close to log-normal distribution (17). As the number of measured bubble lengths approach infinity, the standard deviation for the distribution approach will come to rest at a specific value. An example of this close to log-normal distribution is presented in Figure 4.4.

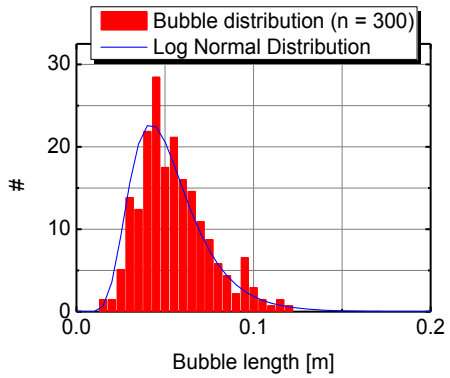

Figure 4.4: L_B distribution (17)

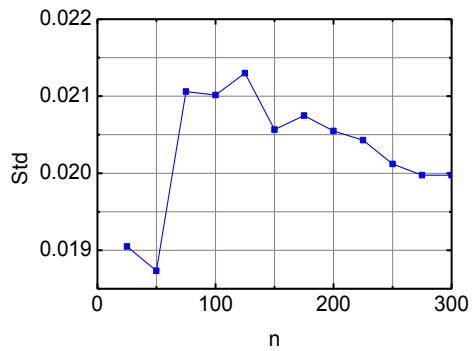

Figure 4.5: Standard deviation

This way of measuring bubble length distribution is referred to as *ensemble averaging*. In ensemble averaging a large number of identical experiments is considered in which measurements are repeated at specific locations and specific times after the initiation of each test. Figure 4.5 illustrates how the standard deviation closes in on a constant value for increasing the sample size.

The instantaneous volume-averaged value of the same property ξ is defined as

$$\left[\!\left[\xi(t_0,\vec{r}_0)\right]\!\right] = \frac{1}{\Delta V}\int_{\Delta V} \xi(t_0,\vec{r}_0)dV \qquad 4.6$$

- $\Delta V >$ characteristic scale of spatial fluctuations that are to be filtered out.
- $\Delta V \ll$ characteristic size of physical system

- $\Delta V <$ characteristic size over which significant macroscopic flow field property variations can occur.

Models and correlations are often however based on double averaging, so as to be able to remove all discontinuities in two-phase flow. Properties and flow parameters needs to be averaged to become continuous and have continuous derivatives. Composite time and volume averaging is the most widely applied concept. For one-dimensional flow volume averaging leads to area averaging. For any property ξ, the composite time- and flow-*area*-averaged value is defined as

$$\left\langle \overline{\xi}^{t}(t_0, z_0) \right\rangle = \frac{1}{A\Delta t} \int_{t_0-\frac{\Delta t}{2}}^{t_0+\frac{\Delta t}{2}} \int_A \xi(t_0, z_0, r, \theta) dA dt \qquad 4.7$$

4.3 Flow Area Averaged One-dimensional Flow

For the specified system at hand it is of interest to work with parameters that are both averaged in time and *area*, therefore the following definitions are based on composite averaging. For flow-area-averaged one-dimensional flow parameters the following expressions result from continuity of phase volumes (see Figure 4.6 for explanation of terms):

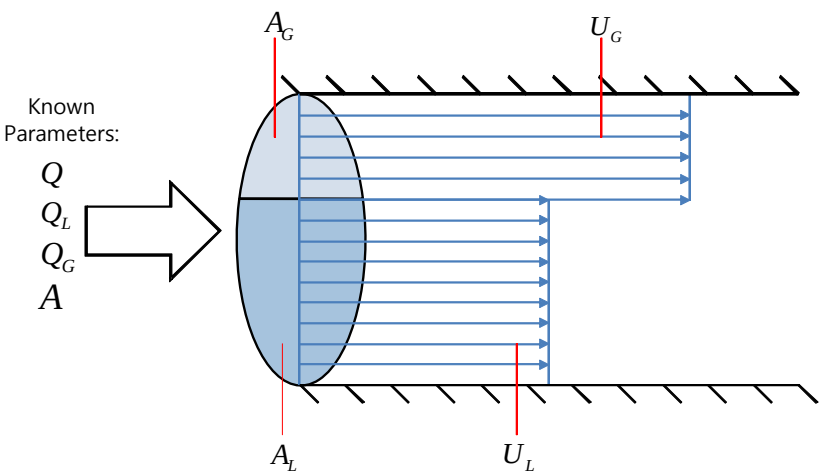

Figure 4.6: Schematic for two-phase pipe flow

The total volumetric flux (Mean velocity) is defined as

$$j = Q / A \qquad 4.8$$

and the volumetric flux for each phase

$$\begin{aligned} U_G &= Q_G / A_G \\ U_L &= Q_L / A_L \end{aligned} \qquad 4.9$$

A_G and A_L is usually difficult to obtain for slug/plug flow. It is related to the slip velocity between the two phases, as can be seen in Figure 4.6, and has to be determined through experimentation. The superficial velocities are defined as

$$\begin{aligned} j_G &= Q_G / A \\ j_L &= Q_L / A \end{aligned} \qquad 4.10$$

and from continuity

$$Q = Q_G + Q_L = U_G A_G + U_L A_L = (j_G + j_L)A \qquad 4.11$$

Void fraction, α, is a widely used term, and are defined by the gas fraction (area averaging) as

$$\alpha = \alpha_G = A_G / A \qquad 4.12$$

which yields the obvious relation

$$\alpha + \alpha_L = 1 \qquad 4.13$$

where α_L is the void fraction for the liquid phase.

By use of the previously introduced definitions the following relations can be constructed:

$$j_G = \alpha U_G$$
$$j_L = (1-\alpha) U_L \qquad 4.14$$

The mass flux, G, equals

$$G = \frac{\rho_G Q_G + \rho_L Q_L}{A} = \rho_G j_G + \rho_L j_L \qquad 4.15$$

The volumetric quality of the mixture, β, is, in a similar fashion to the void fraction, defined as

$$\beta = Q_G / Q = j_G / j \qquad 4.16$$

and the void quality, χ, as

$$\chi = G_G / G \qquad 4.17$$

The slip velocity between the two phases is defined as

$$U_r = U_G - U_L \qquad 4.18$$

and the slip ratio as

$$S_r = U_G / U_L \qquad 4.19$$

From these relations the *fundamental void-quality relation* is derived from

$$\begin{aligned}\chi &= G_G / G \\ &= G_G / \left(\rho_G j_G + \rho_L j_L\right) \\ &= G_G / \left(\rho_G \alpha U_G + \rho_L (1-\alpha) U_L\right)\end{aligned}$$

which yields

$$\rho_G \alpha U_G + \rho_L (1-\alpha) U_L = G_G / \chi$$

dividing by $\rho_L (1-\alpha) U_L$ to obtain

$$\frac{\rho_G}{\rho_L} S_r \frac{\alpha}{1-\alpha} + 1 = G_G / \left(\chi \cdot \rho_L (1-\alpha) U_L\right)$$

Now use the relation

$$G_L = \rho_L (1-\alpha) U_L = G - G_G$$

to obtain

$$\frac{\rho_G}{\rho_L} S_r \frac{\alpha}{1-\alpha} = \frac{G_G}{\chi\left(G - G_G\right)} - 1$$

and finally by use of the void quality relation the *fundamental void-quality relation* is obtained as

$$\frac{\chi}{1-\chi} = \frac{\rho_G}{\rho_L} S_r \frac{\alpha}{1-\alpha} \qquad 4.20$$

i.e. an increase in slip velocity will result in a decrease in void fraction.

4.4 Dimensionless Numbers

When plug flow at a meso-scale T-junction is to be regarded in later chapters the behaviour of the flow, as always in fluid dynamics, should be related to some important dimensionless numbers which compares different physical phenomena, trends and ingredients up against each other. Some of these will have their definitions introduced in this sub-chapter.

The Reynolds number is considered to be well known to all mechanical engineers with interest in fluid dynamics, and is assumed to need no further introduction. The experimental setup and regime for applicability of the model that shall both be introduced later only regards low Reynolds number

flow, i.e. the Reynolds number were kept below 2300 ($\mathrm{Re}_L < 2300$, and characteristic length as $D_H = 600\mu m$) calculated by use of the liquid phase's fluidic properties and the average velocity of the flow, which is not far from the average velocity of the liquid slug. This fact shall be readdressed in a later chapter. Even so it shall be shown in later chapters that the inertia effects of the plug flow field can still play an important role due to high-speed flow when addressing the physical trends for the split ratio.

The Reynolds number for the liquid and the gas phase, are defined as

$$\mathrm{Re}_L = \frac{G_L D}{\mu_L}$$
$$\mathrm{Re}_G = \frac{G_G D}{\mu_G} \qquad 4.21$$

respectively.

Further the weber number should receive some attention. It compares inertia to interfacial tension, and is defined as

$$We = \frac{\rho U^2}{\sigma} \qquad 4.22$$

where U is a characteristic velocity scale and σ the interfacial tension between the two phases.

The Bond number compares gravity to interfacial tension, and is defined as

$$Bo = \frac{\Delta\rho g l^2}{\sigma} \qquad 4.23$$

where $\Delta\rho$ is the difference in fluid densities between the two phases, g gravity, and l a characteristic length scale.

Finally, and for the subject at hand most importantly, the Capillary number compares interfacial tension to the viscous forces. It is defined as

$$Ca = \frac{\mu U}{\sigma} \qquad 4.24$$

Here the viscosity is generally the larger one out of the two phases. A low value of Ca indicates that the stresses due to interfacial tension are strong when compared to viscous stresses. Droplets or bubbles nearly minimize their surface area under such conditions by producing spherical ends. In the opposite situation with Ca being high large deformations away from spherical shapes of the interfaces occurs. This means that the curvature of the bubble nose for plug flow in meso-scale channels will increase, i.e. the nose region of the bubble will take a "sharper" form due to the viscous stresses.

5 Meso-scale Plug Flow

Plug flow is a flow pattern frequently encountered in micro and meso scaled channels when D_H is typically less than $1\,mm$. It can be described as consecutive liquid plugs and gas bubbles where the bubble cover almost the entire cross section and the gas holdup in the liquid plug is zero, i.e. no gas is entrained in the liquid plug as illustrated in Figure 5.1.

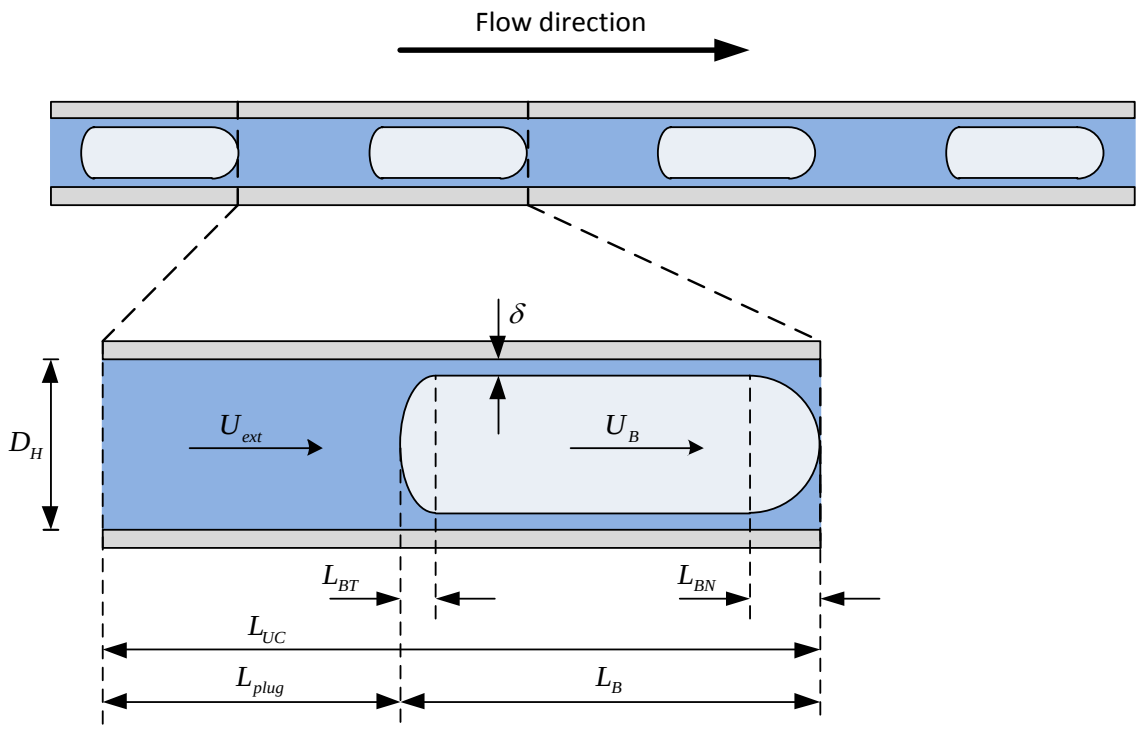

Figure 5.1: Plug flow in meso-scale channel

The bubble is separated from the wall by a thin liquid film of thickness δ. The bubble can be viewed as a gas cylinder propagating forward in time with a bubble velocity of U_B and total length L_B. The nose and rear end of the bubble has the lengths L_{BN} and L_{BT}, respectively, and takes up some part of the bubble's total length. The liquid plug has a mean velocity

represented by U_{ext} and its length is represented by L_{plug}. This gives a total unit length of a unit cell represented by L_{UC} equal to

$$L_{UC} = L_{plug} + L_B \qquad 5.1$$

When the phases in the channels are at rest the nose of the bubble will take a spherical shape, as shall be shown in subchapter 5.2 . The curvature of the bubble nose and tail will deviate and the nose will sharpen ones the velocity of the mixture is increased.

5.1 Flow Regime Map

A flow regime map created by Chung and Kawaji (2004) (1) and Owejan et al. (2005) (2) is presented in Figure 5.2 , and they used $D_H = 530\mu m$ and $D_H = 1mm$ respectively. Their results have been combined in the same graph for easier comparison of the flow pattern borders' location. The flow regime borders constructed by Owejan et al. are presented in red.

From a simple investigation of the borders that divides the different regions it can easily be seen how the border for churn flow moves into the region of plug/slug, slug-annular and annular flow as the diameter is increased. The diameter of interest in this thesis lies in between the diameters that this flow pattern map is constructed from, and hence it can be concluded for the time being that the borders for the different regimes will lie in the areas over where the curves have shifted while moving from smaller to larger hydraulic diameter in comparison to that of present interest. This flow pattern map will later be used to conclude upon the presence of plug flow for the superficial velocities used for experimentation, and this fact will receive support from images taken of the flow field.

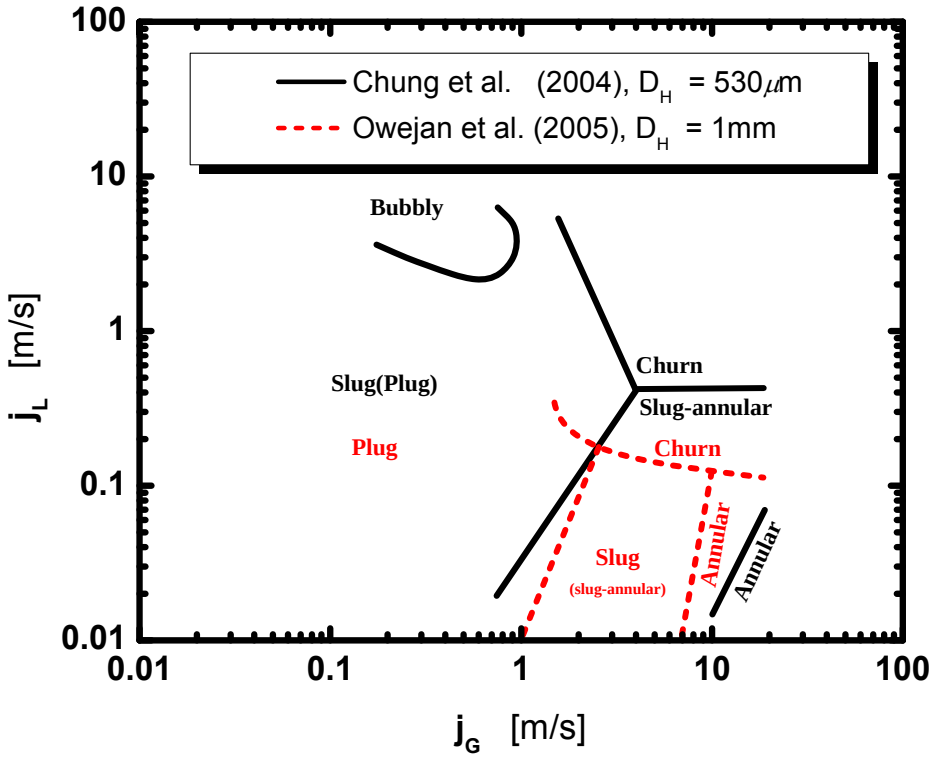

Figure 5.2: Flow regime map for meso-scale plug flow

As can be seen in the map stratified flow does not occur for $D_H \leq 1\,mm$ ((1) & (2)). All other major flow regimes can occur in meso-scale channels. On the other hand a brand new flow pattern has interestingly made its appearance, namely the slug-annular flow pattern. Studies on this flow pattern have been conducted by several authors, among them He et al.(2011) (18) and Wang et al.(2011) (19). They took illustrative images of the flow field that clearly view the characteristics of this new flow regime as well as plug flow and annular flow (He et al.). Figure 5.3 (a) illustrates evidence of plug/slug flow, slug-annular flow and annular flow. Figure 5.3 (b) further illustrates the characteristics of the slug-annular flow pattern, which clearly is slightly different from that in figure $(a)\,(ii)$.

Slug-annular flow is an intermediate flow pattern located between slug flow and annular flow with respect to superficial velocities. It has not been observed for two-phase gas liquid flow in macro-scale channels. Investigation on this flow regime is relatively recent. In general the velocity

of the gas in the centre is much lower for plug flow in comparison to annular flow due to the liquid bridges that slows down the gas phase. The characteristics of slug-annular flow locate themselves in between the two neighbouring flow patterns' characteristics.

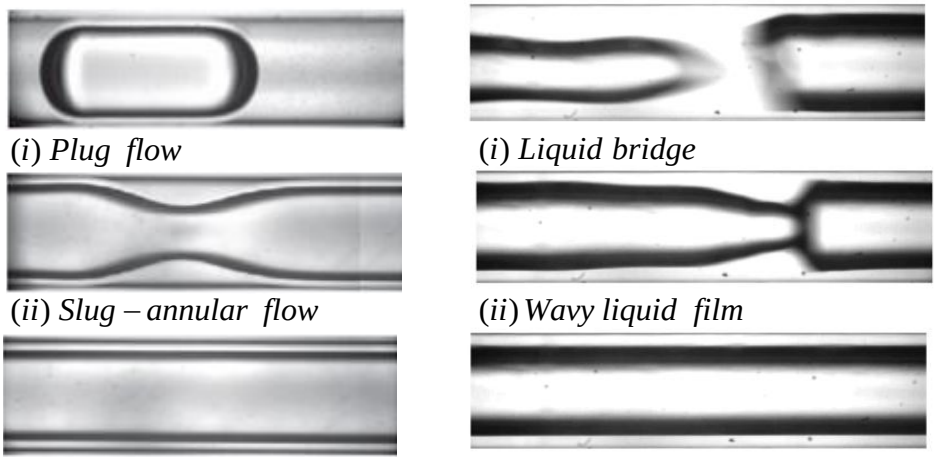

(i) *Plug flow* (i) *Liquid bridge*

(ii) *Slug – annular flow* (ii) *Wavy liquid film*

(iii) *Annular flow* (iii) *Smooth liquid film*

(a) *He et al.* (2011), *Flow patterns* (b) *Wang et al.* (2011), *Slug – annular flow*

Figure 5.3: Flow patterns by He et al.(2011) (18) & Wang et al.(2011) (19)

As already stated this thesis will primarily have its point of interest in the plug flow regime, but even so it is helpful for the insight of split ratio to compare it for also different flow pattern. This can help increase our knowledge of the physical trend of the two phases close to a T-junction. This is performed in chapter 6

5.2 Interfacial Tension

The reason why bubbles, sometime referred to as droplets, occur is mainly due to the immiscibility of, and the interfacial tension between, the two phases. Interfacial tension is a *force per unit length* which pulls the interface with a magnitude $\sigma \sim [N/m]$. Therefore if a spatial imbalance is present in σ over the interface flow along the interface from the low to the high interfacial tension regions will occur. This phenomenon is known as

Marangoni flow (13). Interfacial tension can be thought of as energy per unit area which acts to minimise the total surface area so as to reduce the free energy of the interface. Imagine stretching a piece of rubber material as presented in Figure 5.4. After stretching the piece of rubber to some extent in the same plane as it is located and keeping it there, a certain amount of energy is stored in the surface. Further on if it is given a pressure increase on one side so that it takes on the form that resembles a part of sphere more energy is needed. Between step two and three in the figure, step two is the form that has the lowest amount of available energy distributed in its surface. For a volume the shape that takes up the least amount of energy is hence a sphere, whereas the example regarded simply a surface.

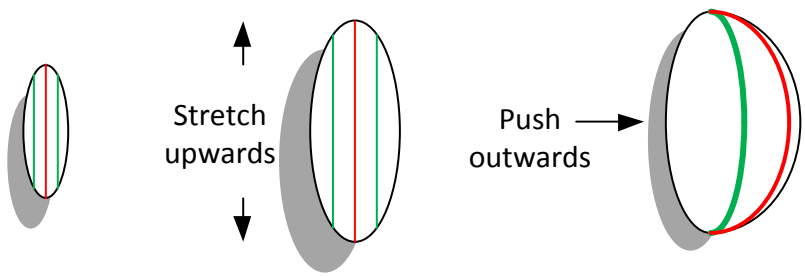

Figure 5.4: Tension example

That is why a droplet will take a spherical shape. This is presented in Figure 5.5, assuming zero velocity. Of course if the radius of the droplet exceeds that of the channel, or $D_H/2$ for a square shaped cross section, the droplet must adapt its shape due to the presence of walls while keeping its interfaces between the two phases curved, as is illustrated in bubble *d* in the figure.

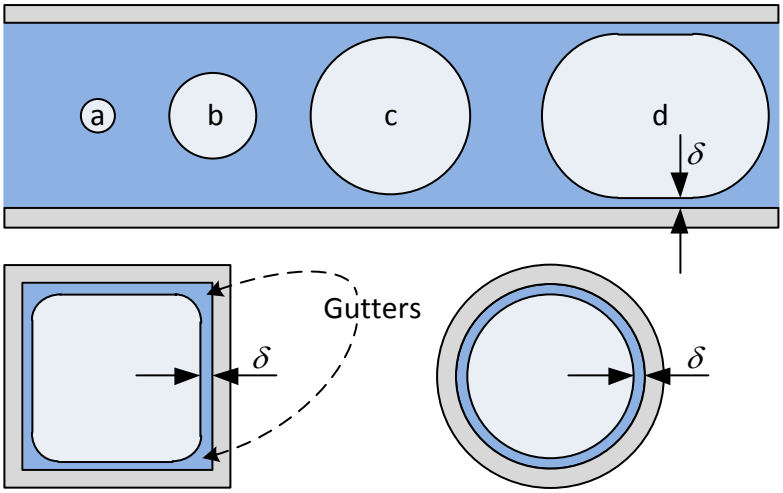

Figure 5.5: Droplets and bubbles in a channel

The curvature introduces a pressure jump, known as the Laplace pressure between the inside and the outside of the droplet. It is defined as

$$\Delta P = \frac{\sigma}{R_1 R_2 / (R_1 + R_2)} \qquad 5.2$$

where R_1 and R_2 are the principal radii of curvature. For a spherical case where $R_1 = R_2$ it can be seen from Figure 5.6 that the same expression is obtained by setting the sum of forces equal to zero

$$\begin{aligned} &\Sigma F = 0 \\ &\Rightarrow \Delta P \, \pi R^2 = 2\pi R \, \sigma \\ &\Rightarrow \Delta P = \frac{2\sigma}{R} \end{aligned} \qquad 5.3$$

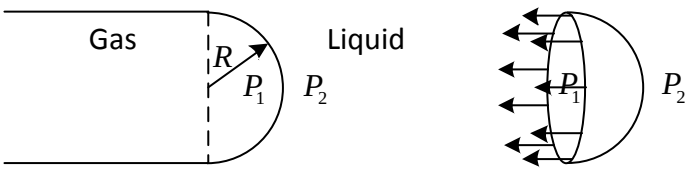

Figure 5.6: Laplace pressure

5.3 Macro-, Meso- and Micro-scale Channels

As introduced in subchapter 4.1 macro-, meso- and micro-scale channels are defined and distinguished through regions for the hydraulic diameter as

- $D_{H,macro} > 1mm$,
- $1\,mm > D_{H,meso} > 100\ \mu m$,
- and $100\ \mu m > D_{H,micro} > 10\ \mu m$,

and this with good reason. The physical ingredients that govern the flow field vary drastically when changing the hydraulic diameter so as to move from one of these three regions to another.

5.3.1 Negligible Impact from Gravitational Effects

It is common knowledge in fluid mechanics that if a two-phase mixture of gas and liquid is at rest in a channel the liquid will place itself at the bottom and the gas at the top due to the higher density of the liquid together with gravitational forces. If the flow is put into motion, and keeping the superficial velocities of both phases relatively low, stratified flow would occur. As the hydraulic diameter is decreased and moving into the meso-scale region this phenomenon is countered by interfacial tension, rendering effects of gravity negligible. This fact is quantified by use of the Bond number which compares gravity to interfacial tension. Gravity has a negligible impact once the hydraulic diameter is decreased below $D_H \leq 1\,mm$ (13), which the previous definition is based upon. Therefore, while working in the meso-scale region, the flow field is insensitive to channel orientation and gravitational forces.

For plug flow in a meso-scale channel the variations in bubble length are far less present in comparison to the example given in chapter Figure 4.2 , with its macro-scale hydraulic diameter. As shall be pointed out through evaluation of the bubble length measurement in the experiment this effect is

regarded as negligibly small, and assumed to be absent due to the lack of gravitational effects in the mixer.

5.3.2 Bubble velocity, Void Fraction and Volumetric Quality Relations

For plug flow in meso-scaled channels the bubbles generally moves with a higher velocity than the average velocity of the channel. This implies of course that the liquid phase, from continuity (see Figure 4.6), has an average velocity U_{ext} which are lower than the average velocity j. Hence $U_r > 0$ and $S_r > 1$. Several authors, e.g. the textbook Two-phase Flow Heat Transfer (1993) (20) and the scientific paper by Chung and Kawaji (2004) (1), states this fact. This fact implies a relation between void fraction and volumetric flux of the form

$$\alpha = \frac{j_G}{C_1 j} \qquad 5.4$$

where the use of $C_1 = 1.2$ is agreed upon by many authors to perform well (20), (21), (22). This relation further on implies the relation

$$U_B = C_1 j \qquad 5.5$$

were

$$U_B = U_G \qquad 5.6$$

with reference to the book by Lee et al. Two-Phase Flow Heat Transfer (1993) (20).

Ali et al. (1993) (23) recommended using the relation

$$\alpha = 0.8\,\beta \qquad 5.7$$

between the void fraction and volumetric quality. This relation is almost the same as setting $C_1 = 1.2$ and using equation 5.4. Since both relations are purely empirical, the rest of this thesis will take use of equation 5.4 with $C_1 = 1.2$.

When the hydraulic diameter closes in on the micro-scale regime drastic changes in the relation between void fraction and volumetric quality has been recorded by e.g. Chung and Kawaji (2004) (1) as well as other researchers. The relation between the two parameters changes from a close to linear relation (see experimental data marked with green circles) to a nonlinear relation as can be seen in Figure 5.7.

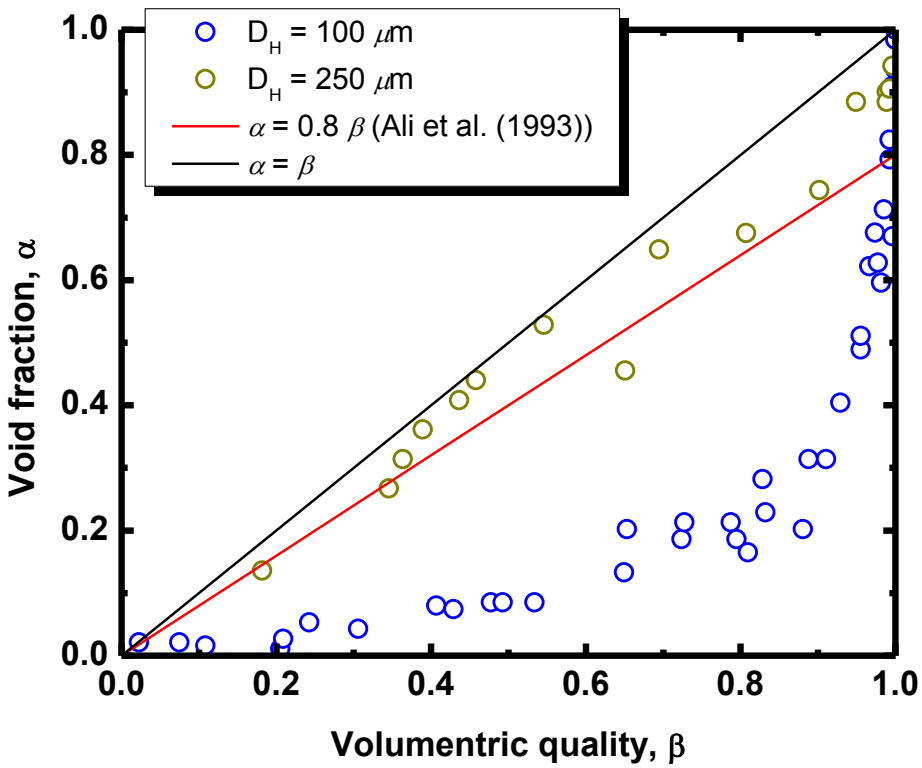

Figure 5.7: Void fraction and volumetric quality relationship

Since the bubble velocity is higher than the average velocity continuity states that the average velocity of the liquid is hence lower. In this text the average velocity of the liquid, as already introduced, is defined by the term U_{ext}.

Then, by investigating a unit cell, there will be a mean flux Q_{exit} flowing out of the control volume that equals

$$Q_{exit} = A(U_{ext} - U_B) \qquad 5.8$$

which will take a negative value as long as the bubble velocity is higher than the mean velocity.

The slip ratio is found, by use of the equations introduced in this subchapter, to be

$$S_r = \frac{U_G}{U_L} = \frac{Cj - j_G}{j - j_G} \qquad 5.9$$

And hence yields the fact that $U_G > U_L$ as it should.

5.4 Capillary Action

Capillary action is the ability of a liquid to flow in narrow spaces without the assistance of, and in opposition to, external forces like gravity. The effect can be seen in channels with small D_H. It occurs because of inter-molecular attractive forces between the liquid and solid surrounding surfaces. If D_H becomes sufficiently small, then the combination of surface tension and adhesive forces, the tendency of dissimilar particles or surfaces to cling to one another, between the liquid and the container will act to lift the liquid, in opposition to e.g. gravity for vertical flow. Hence, for sufficiently small D_H, vertical and horizontal flow in channels can be treated similarly.

5.5 Pressure Distribution and Gradient

For single phase flow in a straight pipe the pressure gradient due to wall friction is constant, given by

$$\left(-\frac{dP}{dx}\right)_{fr,liq} = f\frac{1}{D_H}\frac{1}{2}\rho V^2 \qquad 5.10$$

where the symbol j, total volumetric flux, corresponds to the mean velocity. The friction factor for single phase laminar flow, obtained analytically, is

$$f = \frac{64}{\mathrm{Re}_d} \qquad 5.11$$

These equations can be found in any fluid mechanic textbook. The pressure drop along a streamline, by use of Bernoulli's equation (excluding gravity effects and assuming constant channel size to keep velocity constant), is

$$P_1 - P_2 = \left(-\frac{dP}{dx}\right)_{fr,liq} \Delta L \qquad 5.12$$

When bubbles and plugs are introduced the complexness increases drastically. There is no exact solution for the spatial velocity and pressure profile in the flow field. Many semi-empirical correlations exist for determining the pressure gradient for plug flow. They largely depend on the shape of the cross section and its size, properties of both fluids, and of course the velocity. One of these methods for calculating the pressure drop will be introduced, but firstly a simplified reasoning for the axial absolute pressure and pressure gradient is performed to give a simplified picture of how the pressure varies along the liquid plug and the gas bubble. Also an example of how pressure, measured at a point, varies as a function of time is included. This is helpful to get insight into the trend of the pressure variations in time and space for plug flow, as well as describing the increase in complexity.

Firstly this simplified reasoning will be conducted on the bases of a laminar flow assumption. The experimental conditions suggest likewise, so this will be the basis throughout the entire reasoning to not cloud it more than necessary. The main assumption is to treat absolute pressure as linearly

decreasing over the liquid plug, similarly to that of single-phase flow. Further on the pressure drop along the body of the bubble is assumed to be negligible, i.e. constant pressure within the bubble, except for the nose and tail region. Due to viscous effects between the thin film region and the bubble, the gas within the bubble will move in vortexes, but even so the assumption will not be far from the truth for cases where the viscosity ratio λ ($\lambda = \mu_G / \mu_L$) and density ratio (ρ_G / ρ_L) are small (i.e. $\lambda \ll 1$ and $\rho_G / \rho_L \ll 1$). So from these two assumptions the *instantaneously* recorded pressure distribution in a channel with a plug flow pattern should resemble that which is presented in Figure 5.8(a). Figure 5.8(b) will receive more attention in subchapter 5.5.2 . The green line represents pressure drop for single phase flow with the same working fluid used as the continuous phase for the plug flow. The black curve represents the pressure variations for plug flow, as is well explained in the figure.

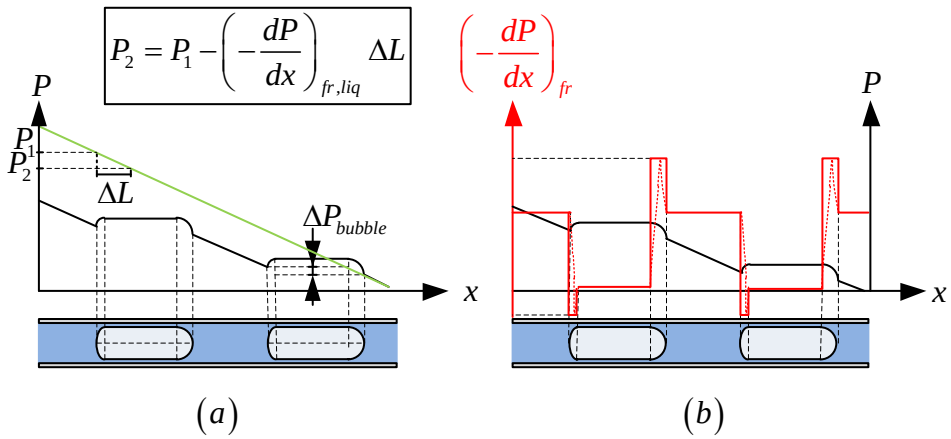

Figure 5.8: Simplified pressure distribution

Exactly how the pressure varies close to the nose and tail of the bubble is uncertain. This will also depend on where in the cross sectional area the pressure is measured, since also the plug includes vortexes and hence also variations in pressure and velocity.

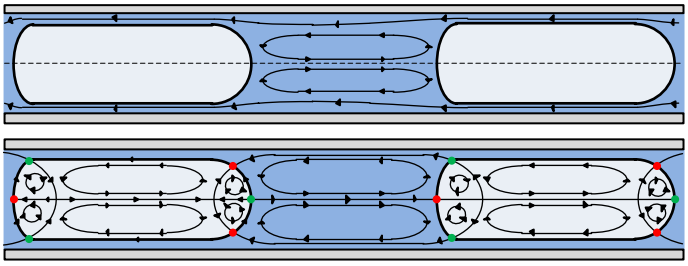

Figure 5.9: Vortexes and stagnation points (13)

A schematic presentation of vortexes and stagnation points is presented in Figure 5.9. The reasoning for finding locations of vortexes and stagnation points can easily be conducted with use of the slip velocity ratio. The stagnation points on the interface are classified between the converging points marked with red circles and the diverging points marked in green. At stagnation points the angle between the interface and the streamline takes on an angle of 90°. From variations in velocity along different stream lines pressure changes over the cross section arises. While experimenting the pressure is measured by attaching pressure taps at one side of the channel. This would therefore indicate that the pressure is measured along the wall, inside the liquid plug and the film region. Additionally the interface between the two phases does not only curve along the nose and tail, which indicates pressure difference due to interfacial tension, but also in the middle of the bubble due to the bubbles curvature that follows that of the channel itself. This fact yields pressure drop between the centre of the bubble and the film region. For circular channels the curvature of the pipe and bubble body have equal shape and their difference would only depend on the film height. There is more uncertainty implemented in the case of square shaped cross sections due to the gutter zones in the corner regions.

Secondly, for high velocities the viscous forces will change the shape of the bubble nose and tail from that seen in Figure 5.5 with spherical shapes to the form that is presented in Figure 5.10. This is due to an increase in viscous drag and inertia effect on the bubble shape that follows from an increase in velocity. The figure is taken from Choi et al. (2010) (24) who investigated the bubble behaviour and the pressure drop over a single bubble. As can be seen in the figure also the tail of the bubble deviates

from a spherical shape when velocity increases; the curvature increases. This would indicate that the pressure drop over the tail of the bubble is lower in comparison to that of over the nose interface, and decreasingly so as velocity increases. In Figure 5.8 this would indicate that the frictional pressure drop marked for the tail region, which are negative, will draw closer to the zero-pressure drop line. Also the distance of the tail in the axial direction which it covers will decrease making that region in the graph slimmer.

The flow is only axial, with the exception of the regions close to the bubble nose and bubble tail, which leads to the conclusion that the pressure stays fairly constant over a cross section of any shape, with additional change in pressure due to interfaces along the bubble body.

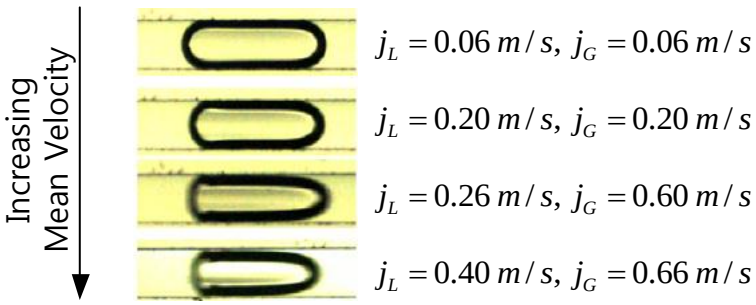

Figure 5.10: Change in shape of interface due to inertial and viscous effects (24)

All these introduced factors from simple reasoning are important for obtaining a picture of how the pressure will vary in space and time, and should be kept in mind also for the upcoming chapters. It also points out the complexities that are involved when it is of interest to mathematically describe the velocity and pressure fields, with several stagnation points and vortexes.

5.5.1 Pressure Drop over a Single Bubble

A correlation for the pressure drop over a single bubble, i.e. ΔP_{bubble} (see Figure 5.8 as x increases along the bubble), has been proposed by Wang et al. (2011) (19), and is defined as

$$\Delta P_{bubble} = 3.15 \frac{2\sigma}{h} Ca^{2/3} \qquad 5.13$$

By moving from the bubble nose and upstream along decreasing x value in Figure 5.8 the absolute pressure along the nose increases more rapidly in comparison to the single phase pressure gradient slope, and afterwards decreases over the tail over the bubble. This is due to the fact that the curvature of the bubble tail and nose has opposite directions. The absolute pressure difference from these two contributions is what is represented by ΔP_{bubble}.

5.5.2 Pressure Evaluation Based on Single Phase Flow Assumption

Some helpful pictures of how the pressure gradient varies in the axial direction of the flow, as well as in time when measuring the pressure at one point, has been made for explanatory reasons. It is based on Figure 5.8 together with the simplified statement that the pressure gradient over an interface, either nose or tail of the bubble, is higher than that due to wall friction. Figure 5.8(b) presents the pressure *gradient* at an *instant in time* along a part of the channel, marked in red. The figure also shows the absolute value for the derivative of absolute pressure with respect to x, marked in black. It should be pointed out that the pressure along the tail of the bubble actually increases with x, and hence the pressure gradient is negative.

The case is slightly different when regarding the trend of absolute pressure at a point in space as a function of time. This pressure will theoretically

depend on the number of bubbles in the channel between the measuring point and the outlet where it is assumed that the pressure is held constant (The case with upstream constant pressure would yield the same oscillating result). The number of bubbles in this region will depend on the bubble and plug length, and vary between a specific possible maximum and minimum value. An example of this theoretical absolute pressure and pressure gradient as it varies in time is presented in Figure 5.11 and Figure 5.12. The points in the part of the figure that illustrates the plug flow (marked with red filled and black outlined circles) represent the point where pressure is measured. As can be seen the downstream region from the measuring point includes between one and two bubbles, and this variation affects the upstream pressure. Exit pressure and bubble length are kept constant.

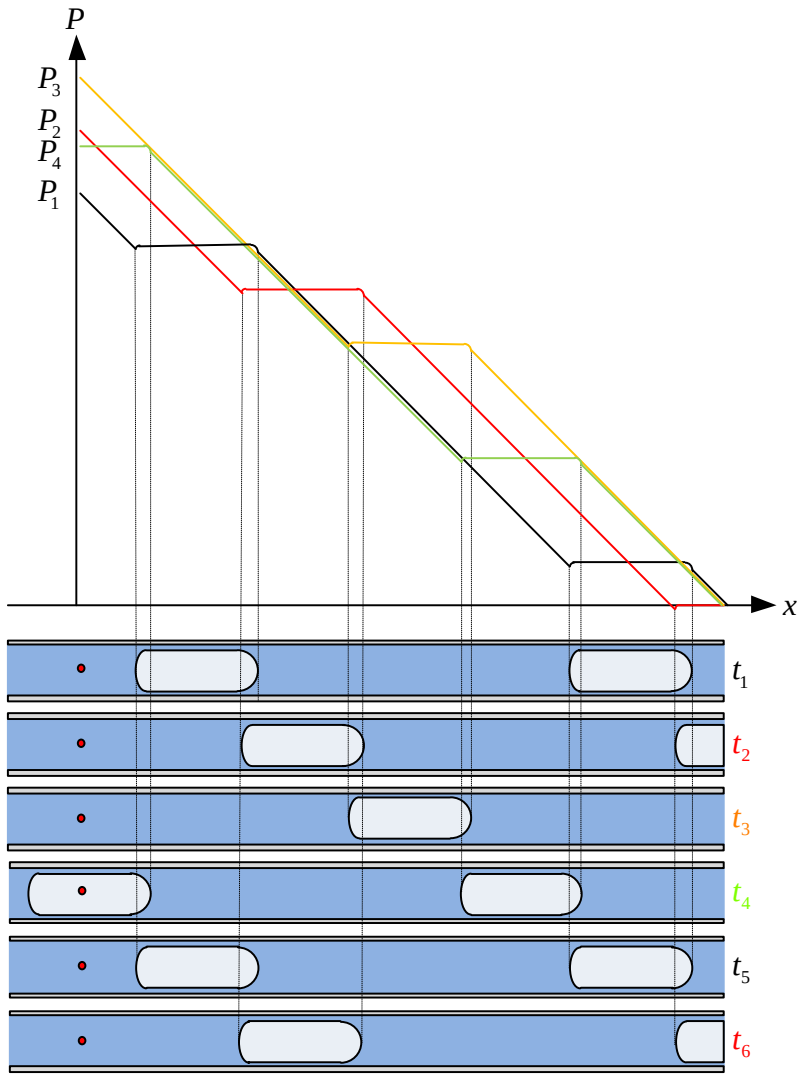

Figure 5.11: Spatial pressure distribution as a function of time

It is expected that the sudden increase and drop in pressure due to bubbles exiting the system, and their interfaces rapturing, will induce pressure waves that propagates upstream. This further increases the complexity of the flow. Theoretically this phenomenon will induce small variations in the mean velocity continuously.

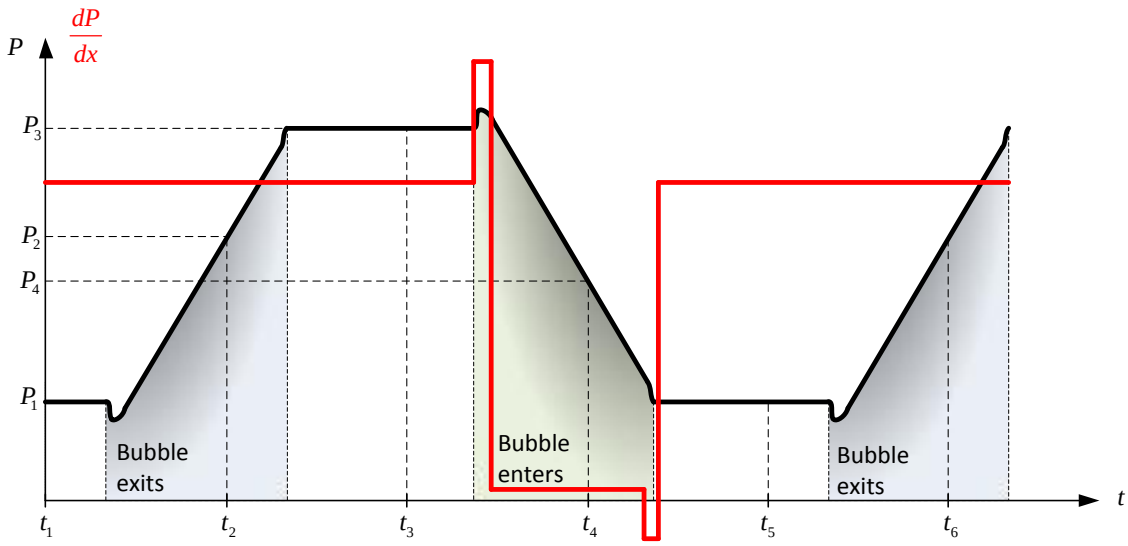

Figure 5.12: Absolute pressure and pressure gradient as a function of time measured in a point

Figure 5.13 (a) represents the pressure gradient as bubbles pass the point where the gradient is measured. (a) illustrates actually the same as was presented in the graph in Figure 5.12, but for a longer time interval to more clearly see the trend of the gradient. t_1 and t_2 indicates the location of the bubble at that instant with increasing time as the subscript value increases. Figure 5.13 (b) represents an assumed pressure difference between two points, where the bubble length is shorter than the distance between the two points, as a function of time, and only one bubble is present in the entire system so that the downstream conditions stay constant. The last introduced figure will be helpful for when pressure shall be measured in later chapters. If this curve can be recreated experimentally to reveal a similar trend it can be concluded that all the assumed pressure variations so far introduced is close to the physically correct pressure variation since they are

all based on the same assumptions, and hence these assumptions can be useful for modelling of the split ratio at a T-junction, which will be discussed in chapter 6 .

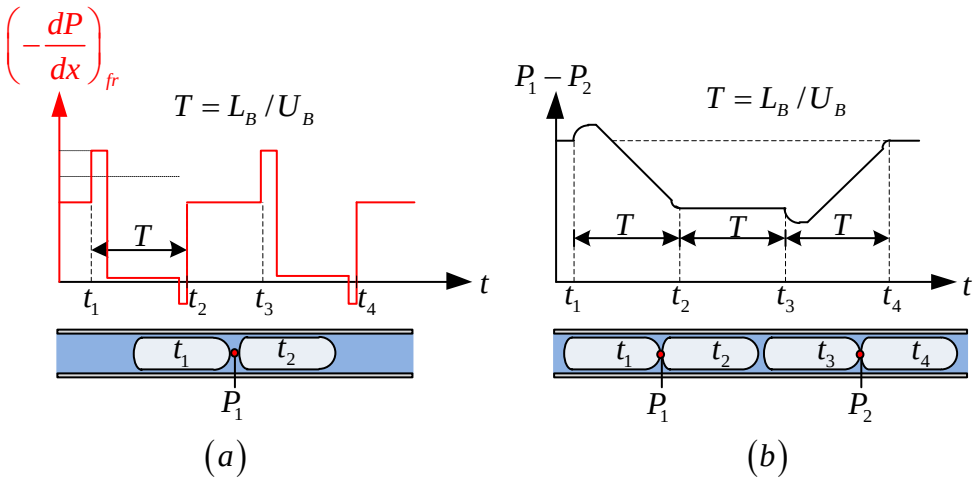

Figure 5.13: Pressure gradient & absolute pressure variations in time

5.5.3 Pressure Averaging in Time

When modelling a time averaged pressure curve will be usefull. This is illustrated in Figure 5.14.

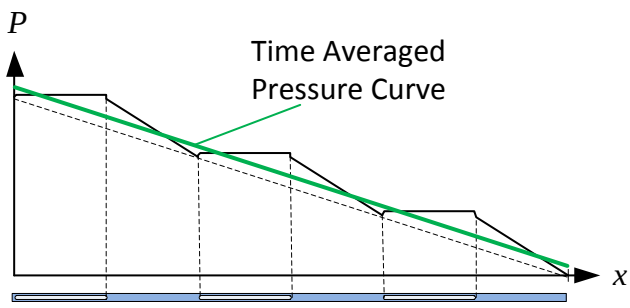

Figure 5.14: Time averaged pressure curve

By use of equation 4.5 the averaged local pressure is obtained from

$$\overline{P} = \frac{1}{\Delta T}\int_{T1}^{T2} P(t)dt \qquad 5.14$$

where $\Delta T = T_2 - T_1$. If ΔT is increased the average pressure will converge towards a specific average value for constant flow conditions (as was similarly explained in subchapter 4.2). Similarly an average value for the frictional pressure drop term $\overline{\left(-dP/dx\right)_{fr}}$ along the channel can be useful to obtain. The usefulness of these values will be further discussed in later chapters.

5.5.4 Single Phase Pressure Slope vs Pressure Drop over a Bubble

At this point some curiosity of which contribution, single phase pressure drop or pressure drop over a bubble with a certain length, will make the steepest frictional pressure drop along the channel. Based on previously introduced relations Figure 5.15 shows how the theoretical pressure drop along the channel varies with variations in bubble length as an example to answer for this curiosity. The outlet pressure and void fraction are kept constant. In the figure the volume flow rates for both the dispersed and continuous phase are kept constant. Hence a decrease in bubble length will yield an increase in bubble frequency. The different values and lengths in the figure are all proportional correct when compared to the calculations based on using water and air as working fluids, except the film region which have been magnified to more clearly illustrate the bubbles in the channel and the slope of the single phase frictional pressure drop. The figure shows the pressure as recorded for an instant in time. The channel hydraulic diameter is set to $D_H = 600 \mu m$, as is used in the experimental setup.

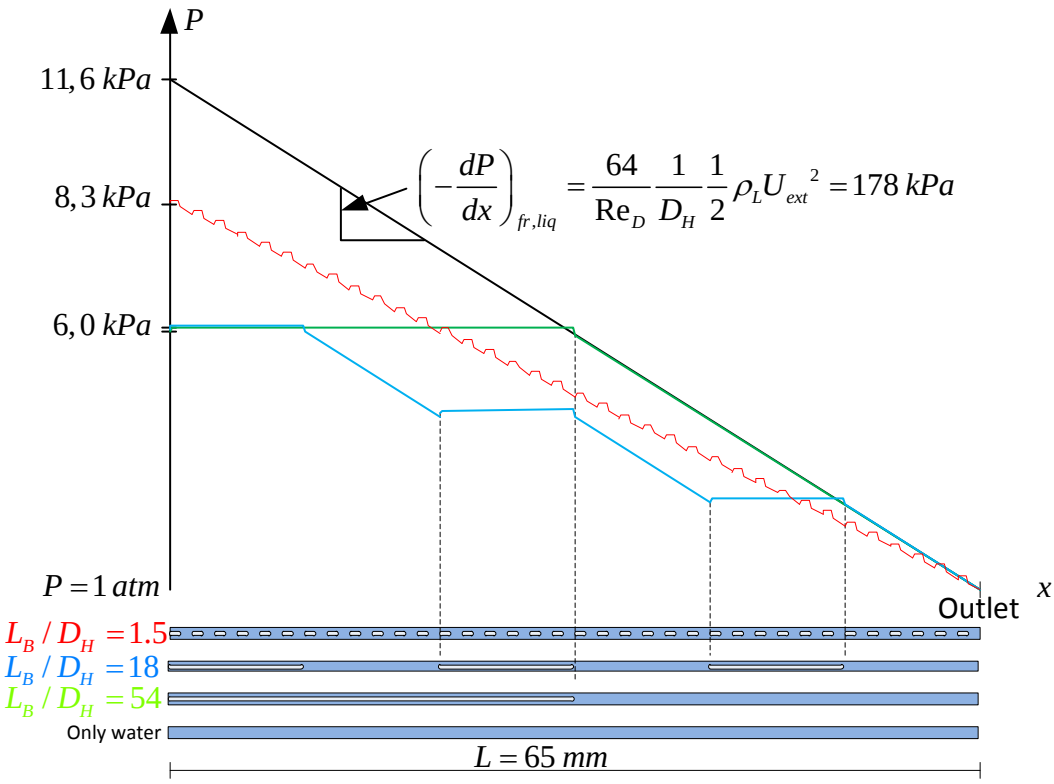

Figure 5.15: Single Phase Pressure Drop VS Pressure Drop over a Bubble

The pressure drop over a bubble of any length under the same conditions as has been used in the experimental setup and calculated with use of equation 5.13 is $(-\Delta P_{bubble}) \approx 70\ Pa$. Since the frictional pressure drop for single phase flow is $(-dP/dx)_{fr} \approx 178\ kPa$ the critical bubble length to yield a similar frictional pressure drop would be $L_B / D_H \approx 0.65$. From this it is easy to see that for bubble lengths of this order Taylor bubbles will no longer be present, referring to Figure 5.5; instead the flow pattern will adjust itself and take on a bubbly flow pattern (see Figure 4.1 & Figure 5.2). Hence the current setup to be investigated later on is in no risk of having a higher pressure drop due to short bubbles when compared to that of single phase flow.

To support this conclusion the next subchapter introduces a second method for estimation of the total pressure drop for two phase flow to better conclude upon this fact.

5.5.5 Empirical Two-phase Frictional Pressure Drop

Two empirical methods for calculating pressure drop are introduced to compare with the previous example. All equations are summarized in the textbook by M. Ghiaasiaan (2008) (16). The markings L and liq, and G and gas has the same meaning respectively.

The Reynolds number for the respective phases is calculated from equation 4.21. If the flow is laminar for both phases the friction factor is obtained as

$$\begin{aligned} f_L' &= 64/\mathrm{Re}_L \\ f_G' &= 64/\mathrm{Re}_G \end{aligned} \qquad 5.15$$

similarly to equation 5.11. Further on the single phase frictional pressure drops for each phase is respectively

$$\begin{aligned} \left(-\frac{dP}{dx}\right)_{fr,liq} &= f_L' \frac{G_L^{\,2}}{2D_H \rho_L} \\ \left(-\frac{dP}{dx}\right)_{fr,gas} &= f_G' \frac{G_G^{\,2}}{2D_H \rho_G} \end{aligned} \qquad 5.16$$

From this point the *Lockhart-Martinelli* method is introduced. The *Lockhart-Martinelli* method (1949) (16) uses the *Martinelli* factor defined as

$$X = \sqrt{\left(-\frac{dP}{dx}\right)_{fr,liq} / \left(-\frac{dP}{dx}\right)_{fr,gas}} \qquad 5.17$$

and the frictional pressure drop is defined as

$$\left(-\frac{dP}{dx}\right)_{fr} = \left(-\frac{dP}{dx}\right)_{fr,liq} \Phi_L^{\,2} \qquad 5.18$$

where

$$\Phi_L{}^2 = 1 + \frac{C}{X} + \frac{1}{X^2} \qquad 5.19$$

The model is based on a simple and inaccurate model, and it is therefore better to treat it as purely empirical. Mishima & Hibiki (1996) proposed the following relation for the constant C

$$C = 21(1 - e^{-0.319\,D_H}) \qquad 5.20$$

based on data obtained for $D_H = 40\,mm$ and air and water used as working fluids. Lee & Lee (2001) derived the following correlation for C using experimental data from many sources as well as their own ($D_H = 0.4 - 4\,mm$)

$$C = A\left[\frac{\mu_L{}^2}{\rho_L\,\sigma\,D_H}\right]^q \left[\frac{\mu_L\,j}{\sigma}\right]^r \mathrm{Re}_{L0}{}^s \qquad 5.21$$

where for laminar flow conditions for both phases $A = 6.833 \times 10^{-8}$, $q = -1.317$, $r = 0.719$, $s = 0.577$ and $\mathrm{Re}_{L0} = GD_H / \mu_L$. Other constants are used for turbulent flow conditions, but are excluded in this thesis since they will not be of use.

An example of using this method to calculate the frictional pressure drop by use of the previously presented parameters yields $(-dP/dx)_{fr,\,Mishima} \approx 91\,kPa$ and $(-dP/dx)_{fr,\,Lee} \approx 94\,kPa$ by use of the correlations by Mishima & Hibiki and Lee & Lee respectively.

This way of estimating the pressure drop does not account for changes in frequency, but only estimates the resulting total frictional pressure drop for plug flow. From calculation this would indicate a bubble length of $L_B / D_H \approx 1.3$ and $L_B / D_H \approx 1.2$ for Mishima & Hibiki and Lee & Lee respectively by use of the same procedure as in subchapter 5.5.4 (use of pressure drop correlation over a bubble given by Wang et al. (2011) (25)). When bubbles take on a length of this small magnitude another

phenomenon is expected to happen with a grave impact for the physical ingredients that are present in the junction region, and without further explanation for the time being, this type of plug flow with extremely short bubbles will not be investigated further. See next chapter for a more thorough explanation for this decision.

6 Meso-scale Plug Flow at a T-junction

Schematic of a T-junction is presented in Figure 6.1. W represents mass flow rate. The numberings 1,2 and 3, refers to the main, run and branch channel respectively. G and L represents gas and liquid respectively.

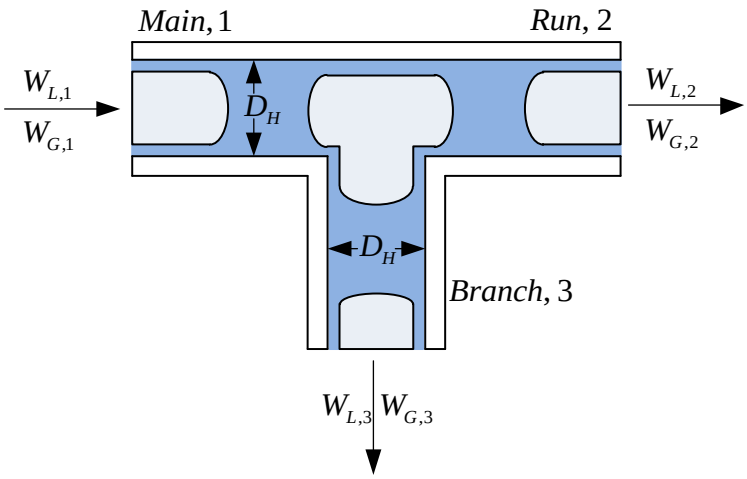

Figure 6.1: T-junction schematic with $D_H = 600\ \mu m$

The occurrence of mal-distribution at a meso-scale T-junction has already been established. Its appearance is unavoidable. This phenomenon, where $\alpha_1 \neq \alpha_3$ and $\beta_1 \neq \beta_3$, is the main topic of interest in this thesis. There is no exact method to describe why this happens, and exactly which physical ingredients that have an effect, and lastly how great the contributions for each of these ingredients actually are relatively to each other.

Prediction models for modelling of the split-ratio at a T-junction usually take into account the superficial velocities, but omit the effect from varying bubble length on the split ratio. In general these models poorly predict the split-ratio, and as shall be seen through comparison of experimental data obtained by different authors the appearances of sudden unexplainable phenomena is present; when comparing results between different authors

the split ratio differ from each other even though the inlet superficial velocities and geometry of the T-junction are almost the same. To try to find a reason behind these unexplainable trends it was suspected by Hong et al. that the effect of bubble length should be regarded and implemented for better prediction of the split ratio. Hong et al. (2010) have reported that the distribution of plug flow depends strongly on the bubble length. This interesting new discovery will be introduced and thoroughly explained in chapter 7 , but firstly a review of other state of the art knowledge in the literature is carried out.

6.1 Use of a Particular Plot

A particular method of plotting is frequently used to present the split ratio. An example plot is presented in Figure 6.2. Some experimental data from Hong et al. has been used to illustrate this method.

.

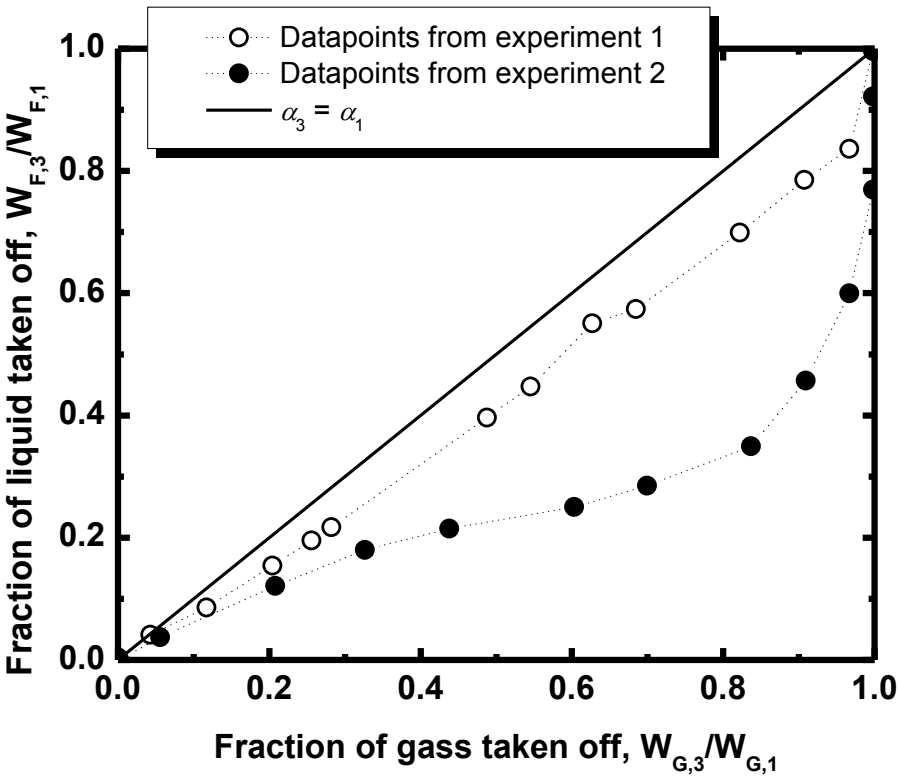

Figure 6.2: Split ratio example plot

This plot is not to be confused with Figure 5.7 even though they share some resemblance. In the graph *W* represents the mass flow rate. By use of relations introduced in chapter 4 the following relation holds:

$$\frac{W_{G,3}}{W_{G,1}} = \frac{Q_{G,3}\,\rho_G}{Q_{G,1}\,\rho_G} = \frac{j_{G,3}\,A}{j_{G,1}\,A} = \frac{j_{G,3}}{j_{G,1}} \qquad 6.1$$

and similarly for $W_{L,3}/W_{L,1}$. The upper right corner of the graph represents zero flow rate in the run, and vice versa for the lower left corner of the graph. The reason for why not only 1 point is plotted in the graph for each experiment is that the total flow j_2 and j_3 in the run and branch respectively can be varied by altering the downstream pressures. To do this valves can be connected to both the branch and the run. By increasing and decreasing the openings of the valves the total flow rates in the run and the branch will change. This will also lead to change in absolute pressure in the main channel unless the two valves are carefully adjusted. The conditions in the main should stay constant.

If a points is located above the diagonal line (perfect distribution line) it implies a decrease in void fraction in the branch when compared to that in the main, i.e. $\alpha_1 > \alpha_3$ (keep in mind that void fraction is measured for the gas phase). Likewise for a point located below the diagonal line $\alpha_1 < \alpha_3$. For the data included in the figure experiment two always involve a higher increase in void fraction in comparison to the void fraction in the main for any alteration of the flow rates j_2 and j_3. Also experiments with different flow rates in the main can be compared in the same graph to see how superficial velocities affect the split ratio. Usually one of the superficial velocities is kept constant while the other varied to see more clearly the effect variations in each of the superficial velocities have on the split ratio.

Continuity in all three channels as well as for the entire system yields

$$
\begin{aligned}
j_1 &= j_{L,1} + j_{G,1} \\
j_2 &= j_{L,2} + j_{G,2} \\
j_3 &= j_{L,3} + j_{G,3} \\
\\
j_{L,1} &= j_{L,2} + j_{L,3} \\
j_{G,1} &= j_{G,2} + j_{G,3}
\end{aligned}
\qquad 6.2
$$

The plot (Figure 6.2) also implicitly presents the volumetric quality in the branch channel. The volumetric quality is defined as (see eq. 4.16)

$$\beta_3 = \frac{Q_{G,3}}{Q_3} = \frac{j_{G,3}}{j_3}$$

This relation with continuity yields

$$
\begin{aligned}
j_3 &= j_{G,3} + j_{L,3} \\
&= \frac{1}{\beta_3} j_{G,3} \\
&= \frac{j_{G,1}}{\beta_3} \frac{j_{G,3}}{j_{G,1}}
\end{aligned}
$$

Rearranging to get

$$j_{G,1} \frac{j_{G,3}}{j_{G,1}} + j_{L,1} \frac{j_{L,3}}{j_{L,1}} = \frac{j_{G,1}}{\beta_3} \frac{j_{G,3}}{j_{G,1}}$$

$$j_{L,1} \frac{j_{L,3}}{j_{L,1}} = \left(\frac{j_{G,1}}{\beta_3} - j_{G,1} \right) \frac{j_{G,3}}{j_{G,1}}$$

and hence yields the relation

$$\frac{j_{L,3}}{j_{L,1}} = \frac{j_{G,1}}{j_{L,1}} \left(\frac{1-\beta_3}{\beta_3} \right) \frac{j_{G,3}}{j_{G,1}} \qquad 6.3$$

between superficial velocities and volumetric quality in the main and the branch.

This equation relates the x- and y- axis in the plot to the volumetric quality in the branch as well as the inlet conditions in the main. Similarly for the void fraction, by use of equation 5.4 the equation

$$\frac{j_{L,3}}{j_{L,1}} = \frac{j_{G,1}}{j_{L,1}}\left(\frac{1-C_1\alpha_3}{C_1\alpha_3}\right)\frac{j_{G,3}}{j_{G,1}} \qquad 6.4$$

relates the x- and y- axis of the plot to the void fraction in the branch and the information about the flow conditions in the main. The diagonal line in Figure 6.2 represents the points were the volumetric quality and the void fraction in the main and branch are equal (and thereby the run as well, from continuity). This would yield no mal-distribution.

This plot will be used frequently throughout the rest of this thesis. Also constant void fraction and volumetric quality lines will be plotted in the same graph to be able to see how their values change when altering j_3, and hence also j_2.

6.2 Split Ratio Evaluation

The interest in investigating split ratio for two-phase flow through a *meso*-scale T-junction is relatively recent. Much related work by other authors dates back only a couple of years (meso-scale channels). Some authors that have investigated systems in close relation to that of interest in this thesis are presented in Table 6.1.

Author	D_H $[m]$	Cross section	Fluid	ρ kg/m^3	μ $Pa \cdot s$	σ N/m		j_L m/s	j_G m/s	j m/s	Re_L	Re_G	Ca $\times 10^2$
He et al. (2011) (18)	0.0005	Square	water	997.1	0.000902	0.073	min	0.028	1.12	1.1	15	38	1.4
			nitrogen	1.16	0.000017		max	0.35	17.6	18.0	193	600	22
Azzi et al. (2010) (26)	0.001	Circular	water	998.2	0.001	0.073	min	0.09	2.5	2.6	90	167	3.5
			air	1.2	0.000018		max	0.42	4.9	5.3	419	327	7.3
Wang et al. (2011) (25)	0.0005	Square	water	998.2	0.001	0.073	min	0.042	2.55	2.6	21	87	3.6
			nitrogen	1.16	0.000017		max	0.5	25.48	26.0	250	869	36
Wang et al. (2011) (19)	0.0005	Square	water	998.2	0.001	0.073	min	0.05	4.2	4.3	25	140	5.8
			air	1.2	0.000018		max	0.28	12.7	13.0	140	423	18

Table 6.1: Related authors and their experimental conditions

The used superficial velocities for all mentioned authors are mapped in Figure 6.3. As can be seen in the flow pattern map they have also performed experiments for split ratio where the flow takes on different flow patterns other than plug flow. The flow pattern borders by Owejan et al. is marked in red, the same as the superficial velocities for Azzi et al. since their experimental setup resembles each other the most (see the table for detailed specifications).

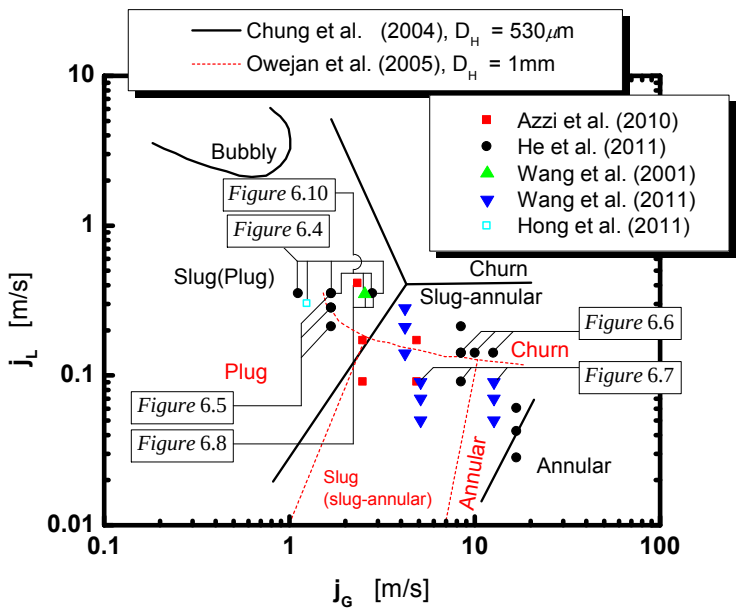

Figure 6.3: Mapping of superficial velocities for experiments by other authors

There are numerous comparisons between all these data that can be performed. Due to this large amount of possible comparisons, only the ones regarded important will be introduced in this chapter to simplify the comparison as much as possible without losing important factors to reveal physical trends for the split ratio. Seven comparisons are included in this chapter. They each evaluate variations in split ratio as a function of different parameters. The objective is to evaluate how much each of these parameters affects the split ratio, and how. Split ratio for annular flow has been excluded entirely. Every performed comparison is marked in Figure 6.3.

Before the comparisons are introduced it should also be mentioned that the split ratio data between different flow pattern flow was investigated, but no specific physically meaningful trend was found to characterize the change in split ratio when moving from one flow pattern to another. That is, one fact that stands out and deserves attention is that the split ratio curve resembles each other in shape and steepness regardless of the three flow patterns. Before the parametric study is performed it is referred to Figure 6.4 and Figure 6.5 for a preliminary discussion on this subject. All split ratio curves, regardless of what have changed between them, shows that the branch is usually rich on gas and increasingly so for increased j_3 when operating within the slug flow regime. This phenomenon has been observed by all mentioned authors. This is explained as follows (hypothesis by the author based on mentioned physical ingredients): the inertia of the liquid is much higher than the gas. The liquid also requires more energy to be brought into the branch channel due to the sudden change in angular velocity. This allows the light gas phase to more easily escape into the branch channel as a function of the oscillating pressure and velocity distribution in all three channels.

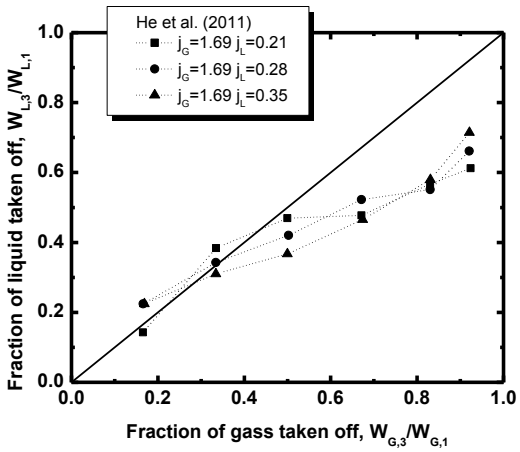

Figure 6.4: Plug flow. Variations in liquid superficial velocity (18)

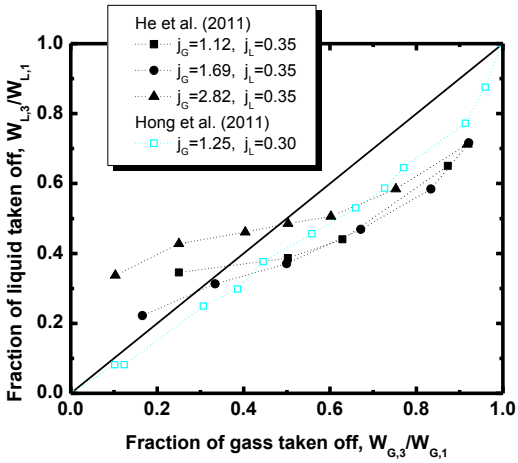

Figure 6.5: Plug flow. Variations in gas superficial velocity (18) (3)

The first comparison (He et al.) evaluates how the split ratio is affected by changes in liquid superficial velocity. See Figure 6.4. When closely studied it can be seen that this figure in fact contain inconsistencies, i.e. the change in fraction of gas taken off to the branch show no physically meaningful trend since all three curves cross each other at several locations in a chaotic fashion. When something exactly similar is seen for comparison of split ratio (still plug flow, He et al. & Hong et al.) as a function of gas superficial velocity (see Figure 6.5) evidently there has to be some other physical ingredient affecting the split ratio which He et al. were not able to point out. When the split ratio curves of He et al. is compared to one of the curves by Hong et al. (Cyan collared split ratio curve) the comparison grows even more chaotic.

The third and fourth comparison relates split ratio to changes in gas superficial velocities again, but this time for when operating within the slug-annular flow regime to see if the superficial velocities have any effect on the split ratio this time. Figure 6.6 shows surprisingly that by increasing the gas superficial velocity the run takes on an increasing amount of gas, i.e. places a large amount of the split ratio curve above the diagonal line representing perfect distribution. This can be explained by the nature of the slug-annular flow. Since it much resembles the annular flow pattern as well, and the liquid largely is located in the film region with high gas velocity in the centre of

the pipe, this seems physically reasonable as the gas' pathway is unblocked (as long as no liquid bridges is present in the flow field, see Figure 5.3).

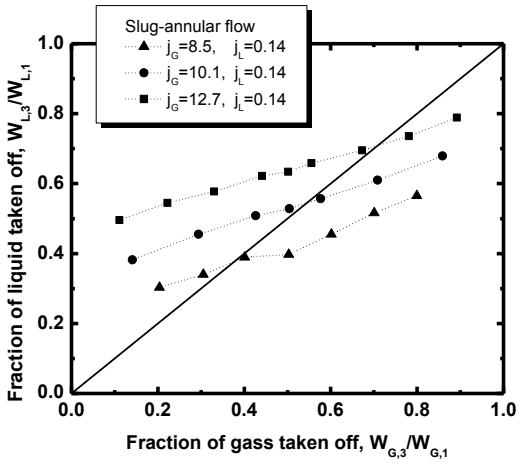

Figure 6.6: Slug-annular flow. Variations in gas superficial velocity (18)

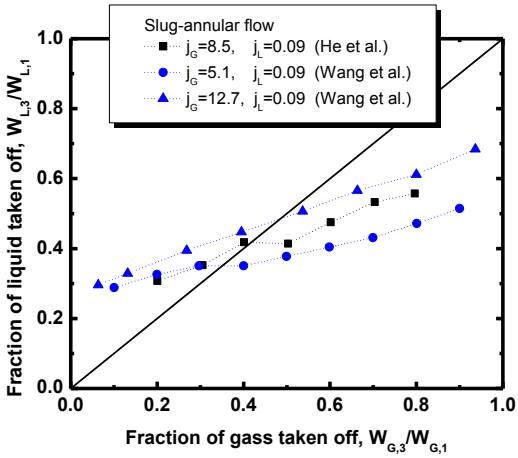

Figure 6.7: Slug-annular flow. Variations in liquid superficial velocity. Comparison between results from different authors (19) (18)

Figure 6.7 compares results from different authors (He et al. against Wang et al.) to try and verify the experimental data. It is suspected by the superficial velocities that the split ratio graph by He et al. should locate itself in the mid-region between the data by Wang et al. Besides for low total flux in the branch the verification is fairly satisfactory. Only small changes in split ratio have been observed for changes to liquid superficial velocities within the slug-annular flow regime, similarly to that of Figure 6.4, and is therefore excluded from this thesis. For validation of this statement it is referred to publications by the authors presented in Table 6.1.

Further on three other parameters have been varied to see how they affect the split ratio, namely the shape of the cross section, the hydraulic diameter and the viscosity of the liquid phase. In Figure 6.8 the superficial velocities for all three sets of data is almost similar. This variation in superficial velocities should have a negligible effect on variations between the split ratio curve, given the previous reasoning for plug flow. As can be seen the curve

by Azzi et al. differs greatly from the two curves obtained by Wang et al. and He et al. The experimental data by Azzi et al. uses circular shaped channels while Wang et al and He et al. uses square shaped channels (see Table 6.1), and the hydraulic diameter has been doubled. Still at this point it is proven difficult to reveal any strict physical trends. Regrettably no more data to support the comparison for changes in hydraulic diameter have been located in the literature that has matching superficial velocities.

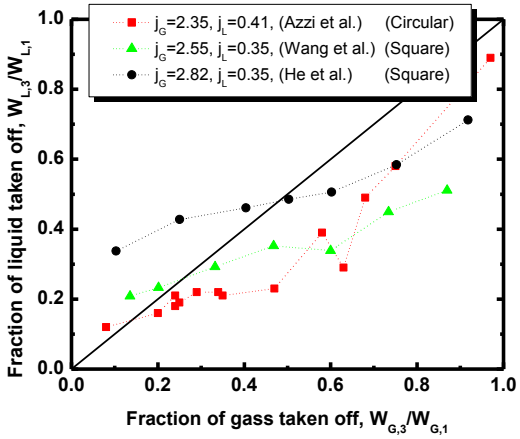

Figure 6.8: Variations in diameter and cross section shape. Plug flow. (26) (19) (18)

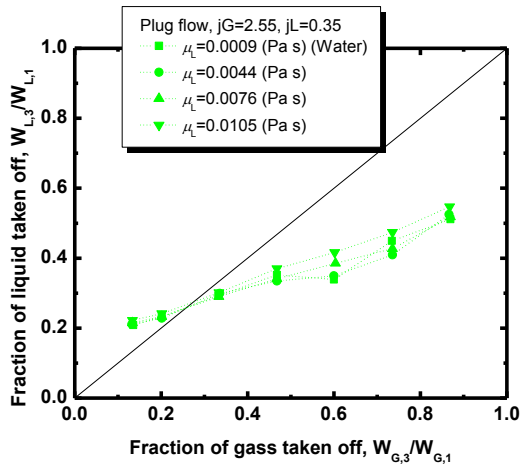

Figure 6.9: Variations in viscosity. Plug Flow. (25)

In Figure 6.9 a comparison of split ratio as a function of liquid viscosity is presented, taken from Wang et al. (2011). In the flow regime map the its set of superficial velocities is marked in green. It can easily be seen that even for change in viscosity of an order of ten the split ratio curve stays fairly constant. Hence viscosity changes for values within these limits, and relative to that of the gas, i.e. the gas phase has a much lower viscosity than the liquid phase, is negligible.

Even though few strict physical trends could be discovered for the split ratio when operating in the plug flow regime (as this thesis particularly focus on) , there is still one important that has surfaced: There has to be some other physical parameter that has not been kept constant throughout the experiments for all mentioned authors which is the reason for the

inconsistencies found through comparing their split ratio data. Figure 6.10 clearly illustrates this by comparing results from Wang et al. with those of He et al. To see this keep a close look at how the superficial velocity for gas varies while moving from between the curves in one direction.

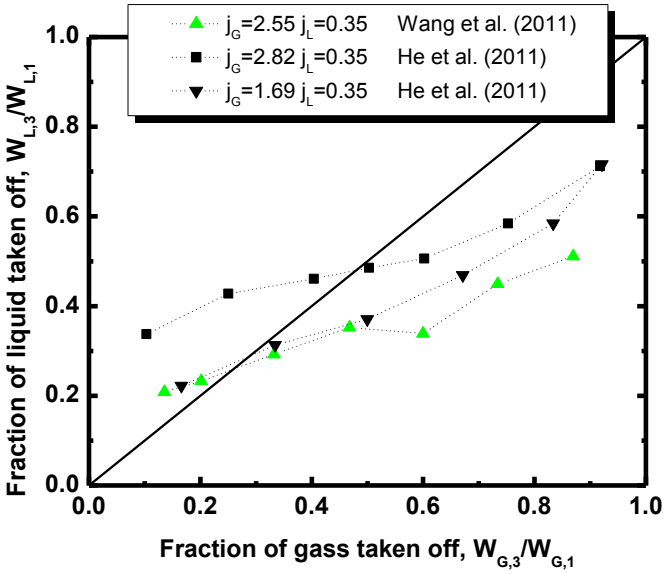

Figure 6.10: Split ratio inconsistency from superficial velocities

One possible parameter that has not been taken into account by any of the mentioned authors is the bubble length (or frequency, both strongly related through the unit cell length). Since none of the authors have thoroughly explained under what conditions the two phases have been mixed it is not possible to investigate it at this point. This possible reason for explaining the chaotic behaviour of the split ratio through implementing the bubble length into the equation was discovered by Hong et al., and shall receive much attention in the next chapters.

6.3 Pressure Distribution and Pressure Gradient

At the T-junction the flow field is exposed to a kind of sudden expansion. Therefore theory related to sudden contraction and expansion is reviewed to back up the proposed picture of how the pressure is assumed to vary close to the junction region. To take use of Bernoulli's equation every pressure

evaluation is therefore regarded as being on the same streamline(s) going from upstream to downstream.

6.3.1 Sudden Expansion and Contraction

When a sudden expansion or contraction is present in a pipe containing single phase flow the pressure along the pipe is affected. For laminar flow conditions (far upstream/downstream of the expansion/contraction point) the pressure is constant over the cross section since the radial velocity is zero, but the velocity changes in the axial direction from continuity. This review will be used when the time averaged pressure drop from the main to the run and main to the branch is evaluated later. The Bernoulli equation for energy conservation along a streamline with loss term is used (horizontal flow assumed), and it is defined as

$$P_1 - P_2 = \frac{1}{2}\rho(u_2{}^2 - u_1{}^2) + K_{12}\frac{1}{2}\rho u_1{}^2 \qquad 6.5$$

where *12* refers to the frictional pressure drop due to separation when the fluid moves from the inlet to the outlet pipe. In this equation pressure and velocity are averaged over the cross section. Otherwise the loss coefficient cannot be defined practically. The frictional pressure drop over a sudden expansion and sudden contraction are illustrated in Figure 6.11 (a) and (b) respectively. The subscripts SE and SC imply the sudden expansion and the sudden contraction, respectively.

For the case of sudden expansion, an analytical solution exists. This is not included since it will not be of direct use. Instead the physical phenomena is of interest. In the edge regions, clearly illustrated in the figure, separation occurs. Vortexes is present, and this separation results in a loss of energy of the size $K_{12,SE}\rho u_1{}^2/2$. At the same time the area increases and this in turn results in a decrease in velocity and increase in pressure. The dashed line in the graph (still referring to sudden expansion) would be the pressure change if no separation and frictional pressure drop were present.

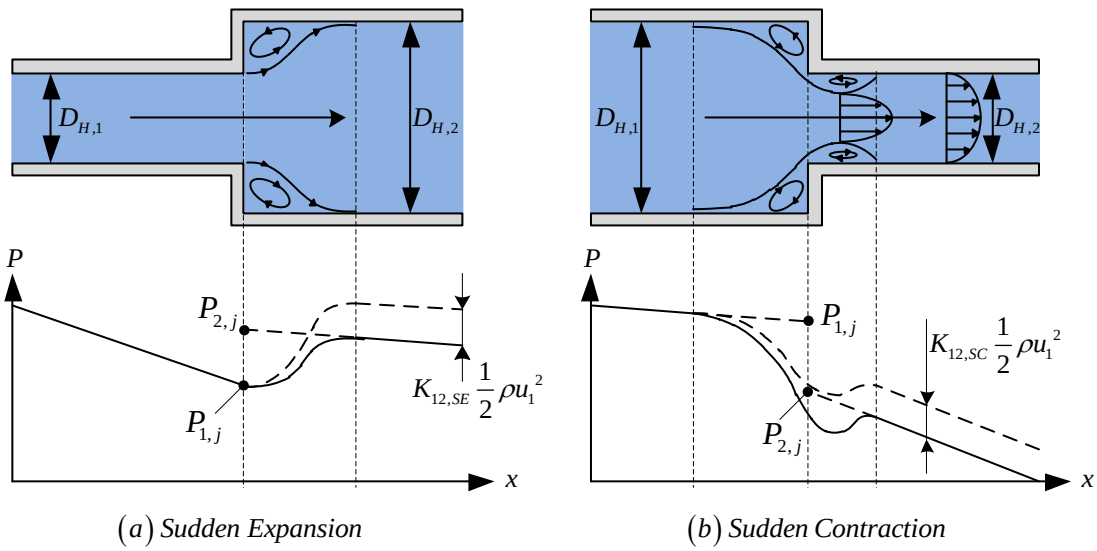

Figure 6.11: Pressure drop from SE / SC

For sudden contraction the case is slightly different. Separation will for this case occur in two new regions inside the small pipe as illustrated in Figure 6.11 (b). Due to this phenomenon the velocity in this region actually exceeds that for when the flow has again become stationary in the smaller outlet pipe. This is well illustrated with velocity distributions over both cross sections in figure (b). Hence the pressure decreases even more for this region as can be seen in the graph.

The term $P_{k,j}$ were $k=1,2$ refers to the extrapolated junction pressures. In next subchapter pressure distribution for plug flow at a T-junction will be evaluated. Since the pressure always oscillates, time averaging is necessary and the junction pressures will be extrapolated from these average values. This is convenient for modelling. Even though it is assumed that the split ratio oscillates as a function of time (due to the position of the bubbles) the interest is mainly for split ratio when average in time, and hence the use of time averaged junction pressures is accounted for.

6.3.2 Pressure at a T-junction

After the T-junction, the flow area doubles (assuming $D_H = const$ as illustrated in Figure 6.1). This leads a decrease in velocity for both outlet channels and hence an increase in pressure similarly to what was explained about single channel with sudden expansion. How much the velocity decreases depends on the downstream pressure in each outlet channel, and as previously stated can be altered by valves installed downstream of the junction point.

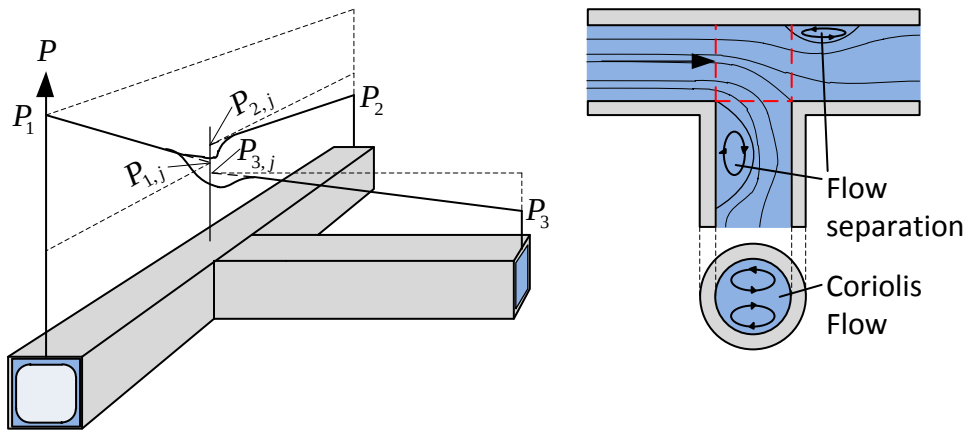

(a) *Junction pressure* (b) *Flow field*

Figure 6.12: Pressure and flow field at T-junction

Figure 6.12 (a) illustrates the pressure drop over the junction region along the flow directions from main to run and main to branch. The pressure variation along the junction region is of special interest. The junction region is marked in red in figure (b), and shall receive frequent attention in later sections. The frictional pressure drop in each of the channels far away from the junction region can be treated similarly to what was explained in the previous chapter. Of course the steepness of the curves depends on the average velocity in each channel, and hence the main channel has the steepest curve, since no other channel can have higher velocity.

Figure 6.12 (b) illustrates different streamlines going from main to run or main to branch. Due to the sudden angling of the pipe which the two phase flow has to follow separation will again occur as illustrated. It is also suspected that separation will occur in the run channel. Due to angular

inertia the flow field will be affected by Coriolis force which give rise to vortexes in the cross section. This further increases the complexity. Needless to say, as this reasoning is based on single phase flow at the moment, the pressure distribution and velocity field should be even more complex when bubbles are present. It should be possible to assume that the plug flow regime consists of consecutive annular and single-phase liquid flows, but then the bubble interfaces further clouds the description. In this thesis the pressure will be averaged over the T-junction to obtain the time-averaged junction pressures $\overline{P_{1,j}}$, $\overline{P_{2,j}}$ and $\overline{P_{3,j}}$ as illustrated in Figure 6.13. This is the fashion in which experimental data are treated, and also on the basis the model is constructed.

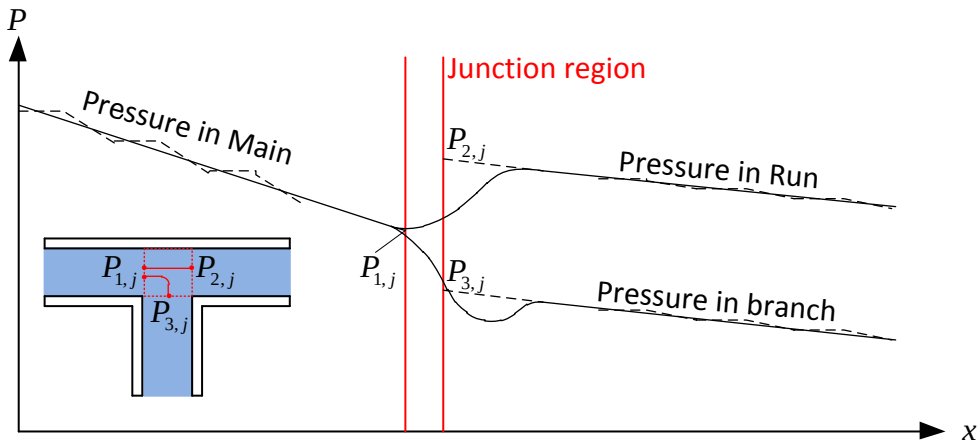

Figure 6.13: Time averaged pressure variations in close to T-junction

Actually the junction region has at this point been positioned closer to the centre of the junction than where separation occurs. Even so, empirically obtained coefficients for pressure losses shall include these losses. In the figure the dashed lines represents instantaneous axial absolute pressure for the plug flow. The solid lines represents the decreasing average pressures. From the review of flow true a sudden expansion it is natural to believe that the junction pressure for the branch should be located above that of the main due to decrease in velocity. Here it has been placed below to illustrate that pressure losses due to friction and separation might overcome the increase in pressure due to a decrease in the velocity.

6.4 Control of Bubble Frequency and Length

Some authors have focused on manipulating the inlet flow rates and geometries to try and achieve a specifically desired unit length, bubble length and thereby also a desired bubble frequency for the inlet conditions. Even though mal-distribution at a meso-scale T-junctions seems to be inevitable, by altering the inlet conditions with a given technique this can be used to tune the inlet conditions so as to obtain the "desired" mal distribution. As mentioned in chapter 2 electrical components usually involve variations in temperature distribution over the region that is to be cooled. By careful positioning of the heat exchanger and the possibility of altering the inlet conditions, it would be possible to construct the system so that the quality would be high in the channels that has a lower need of heat transportation, while a flow pattern with lower quality could be injected into those channels that require a higher amount of cooling rate in the electrical device. Yamada et al. (2008) (14) developed an active technique for precise control of bubble/droplet division for use in micro/meso-scale channels. This scheme involves hydrodynamic control of droplet division. Without necessitating any physical or chemical actuations this scheme tunes the volume ratio of the droplets. For further information of this scheme, see the paper by Yamada et al. (2008). If such a technique can be implemented in the application of interest, which includes a T-junction similarly to that which is presently investigated, knowledge of the split ratio in combination with this controlling scheme can help to obtaining a preferred mal-distribution.

7 Bubble Length Importance on Split Ratio

As previously stated this thesis is a continuation of the MSc thesis by Hong et al. (3). Hong et al. were able to rigorously conclude upon the fact that the bubble length is actually one of the main parameters for specifying the split ratio. Of course other factors will also have a role, for instance the superficial velocities was shown to have an influence by Wang et al. (2010 & 2011) (19) (25), He et al. (2011 & 2011) (18) (27) and Azzi et al. (2010) (26), but from Hong et al.'s work it can be seen clearly how important this parameter really is for the split ratio in comparison to the superficial velocities or other already mentioned parameters. It can easily be seen from a comparison between the mentioned authors' experimental data with experimental data by Hong et al. that variations in the bubble length has a much greater effect than the superficial velocities.

Hong et al. conducted several experiments where only the bubble length was varied. Other parameters such as viscosity ratio, density ratio, superficial velocities and geometry specifications were kept constant. This was made possible by use of different mixers for the experimental setup. Thereafter, by taking the reader through a slightly complex but at the same time elegant reasoning, the bubble length effect on the split ratio can clearly be seen. Keep in mind definitions and terminology introduced in previous chapters; they will not be reviewed in the present chapter. Their experimental data will be reviewed in this chapter. By being able to conclude upon the split ratio's dependency on bubble length this fact will in chapter 10 be the primary ingredient in the recipe for constructing a model.

Hong et al. also proposed a model for prediction of the split ratio, but a critical shortcoming in the model were discovered by the present author. Hence the model was found inapplicable for the use of prediction of the split ratio. Therefore their model will not be reviewed in this thesis, but

instead only the newly constructed model will be included (see chapter 10). It should, at the same time, be emphasized that both models base their derivation upon the extended Bernoulli equation and the use of a time averaged pressure drop over the junction region.

7.1 Proof of Bubble Length Importance on the Split Ratio

Proof of the importance of bubble length was performed through experimentation. A systematic evaluation of the obtained data leads the conclusion that the bubble length for the bubbles in the main channel is the main parameter for deciding the split ratio.

Hong et al. included 11 different sets of experimental data in their line of reasoning. Some experimental data from their previous work were not included. This was done so as to not cloud the line of reasoning more than necessary. Each of the chosen experiments has been chosen so that the objective could be reach by the right comparisons between these experiments. The data from each of the 11 experiments are mapped in Figure 7.1 by their superficial velocities.

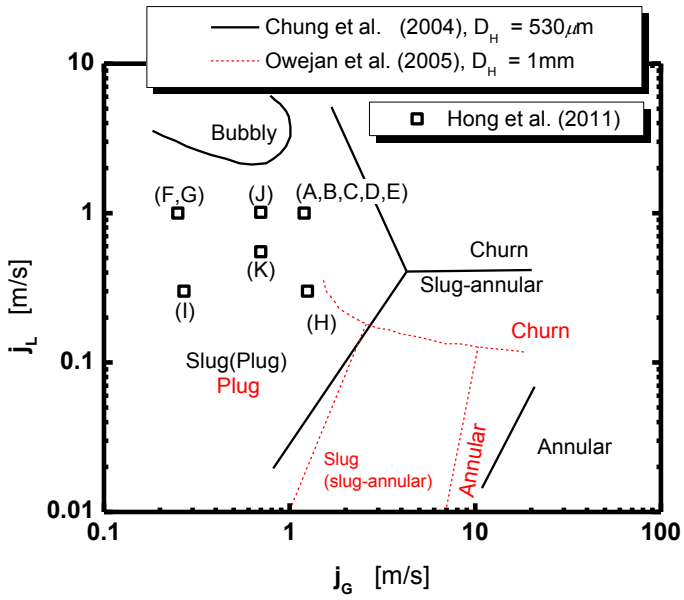

Figure 7.1: Superficial velocities for experimental data by Hong et al.

The experimental setup took use of five different mixers. By different combinations of mixers with variations in superficial velocities, different bubble lengths were obtained even though the superficial velocities were held constant, and this is the reason for 5 different experiments with the same superficial velocities. Table 7.1 summarizes the experimental conditions used by Hong et al. including the bubble lengths. The bubble lengths have been non-dimensionalized by use of the hydraulic diameter.

Case	$j_{G,1}$ (m/s)	$j_{L,1}$ (m/s)	Mixer	L_B / D_h	Comments
A	1.2 ±0.03	1.0 ±0.04	1	93	Bubble length effect
B			2	31	
C			3	12	
D			4	5	
E			5	2.5	
F	0.25 ±0.01	1.0 ±0.01	1	74	
G			5	1.6	
H	1.25	0.3 ±0.01	1	162	Flow rate effect
I	0.27			89	
J	0.7 ±0.02	1.01	4	2.5	
K		0.55	5		

Table 7.1: Specifications for experimental data by Ju Hyuk Hong (2011)

The reasoning will, for clarity, be divided into 2 main sections and one side-note section. Each of the sections has its own objective, and when added together will prove that the bubble length is the main parameter for determining the split ratio at the T-junction.

The two sections and the side note are described as follows:

1) Section 1

Examine effect L_B for a fixed set of superficial velocities.

2) Side note

When $L_B \geq 30D_h$ a special phenomenon occurs. This shall prove itself helpful for section 3. Also the presence of separation shall be discussed, among some other important aspects.

3) Section 2

Examine effect of superficial velocities on the split ratio for *a:* L_B *large* (further explained in side note) while letting j_G and j_L vary, and *b:* L_B small and fixed ($L_B = 2.5D_h$) with variations in j_G and j_L.

7.1.1 Section 1

Proceeding with section 1 Figure 7.2 presents split ratio curves for five cases containing different bubble lengths (see Figure 7.1 case A to E). From this plot the effect of bubble length is examined by keeping the flow rates constant.

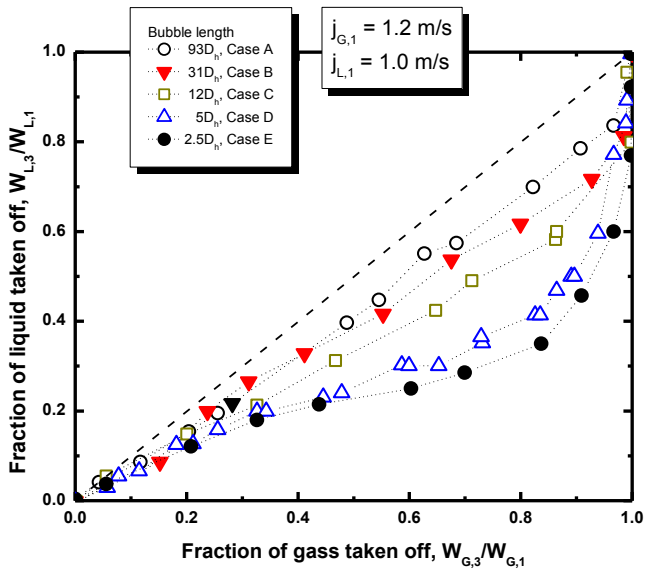

Figure 7.2: Fixed flow rates and variations in bubble length

The plot clearly illustrates how the fraction of gas in the branch increases as the bubble length is decreased, and without any exceptions as was observed in the data for several other authors in the previous chapter. For short bubbles the void fraction in the branch deviates largely from the diagonal line, i.e. short bubbles give high mal-distribution rate. Also it is worth to

notice that through comparison between A and B there is almost no difference between the branch qualities between these two even though the bubble length is three times higher for case A than B. Both case A and B appears to be close to the diagonal line, i.e. close to the type of distribution that is preferable in most cases (perfect distribution). This line of reasoning clearly confirms the mal-distribution for flow fields that include short bubbles, and in general the grave impact bubble length has on the split ratio.

7.1.2 Side note

From comparison between experiments A, B, F, I, H in Figure 7.3 only negligible deviations in split ratio is observed. All these experiments have $L_B > 30D_H$. It can thereby be concluded that when $L_B > 30D_H$ (3) changes in L_B loses its effect on the split ratio. For this comparison no attention was given to the superficial velocities. Hence, even at this point before the investigation of changes in superficial velocities have been conducted, it can already be seen that the superficial velocities play no role for the split ratio for cases with $L_B > 30D_H$.

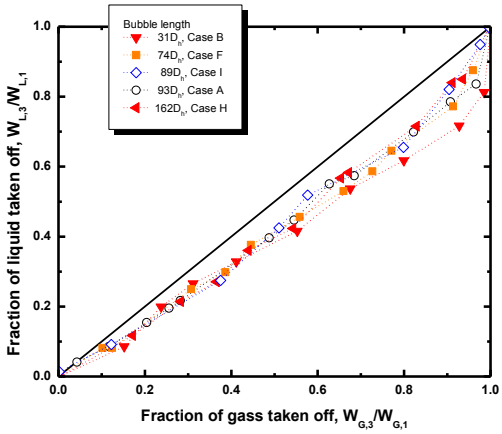

Figure 7.3: Long bubbles. Variations in superficial velocities

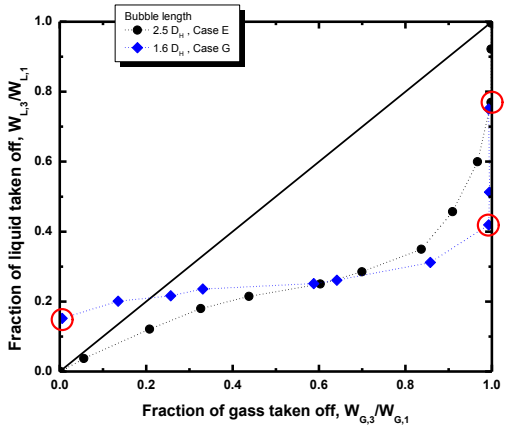

Figure 7.4: Separation for short bubble lengths

Figure 7.4 contains split ratio for cases with extremely short bubbles, on the verge of transforming into bubbly flow (see subchapter 5.2). Even the

separation is observed in three cases. At some point, when the mass flow rate in the branch is lowered (left hand side of the plot), all bubbles follow straight to the run, and opposite when the total flow rate in the run is decreased down to a certain point. Hong has explained the reason for the separation as follows: When bubbles become very short, they tend to follow the stream of the liquid that has much higher density and viscosity. During the work on this thesis another theory of describing the physical ingredients for the differences between the split ratio for long and short bubbles were proposed, and the proposal agrees well with that of Hong et al. It divides the split phenomena for the plug flow into two regimes as a function of the bubble length. Referring to Figure 7.5, for bubbles above a certain critical length $L_{B,crit}$ the split at the junction is affected primarily by what shall be referred to as the *squeezing* effect. Hence it is named the *squeezing regime*. Because the size of the bubble is large enough to cover the entire junction region and parts of the channels both upstream and downstream the following liquid plug can only affect the bubble by *pushing* it from behind. Finally when the tail of the bubble is located in the junction region the plug located behind will squeeze it so as to divide it into two parts, as is illustrated in Figure 7.5 (b).

For $L_B < L_{B,crit}$ the size of the bubble is not large enough to block the possible pathways for the liquid located in the following plug. The size of the thin film region increases and the velocity of the liquid as well. An increase in velocity yields higher viscous drag on the bubble surface and renders possible the event of having the entire bubble following the high-velocity liquid flow, as is well illustrated in Figure 7.6. Figure 7.6 (a) represents high flux in the branch which leads to all bubbles following the liquid into this channel, resulting in separation as seen in the right hand side in Figure 7.4. Figure 7.6 (b) represents the opposite case with high flux in the run, and thereby also separation by bubbles following the high velocity liquid phase.

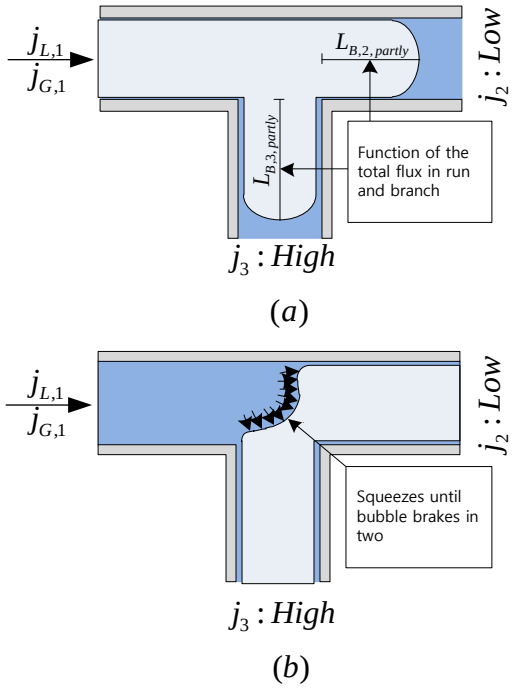

Figure 7.5: Split at T-junction with long bubble length

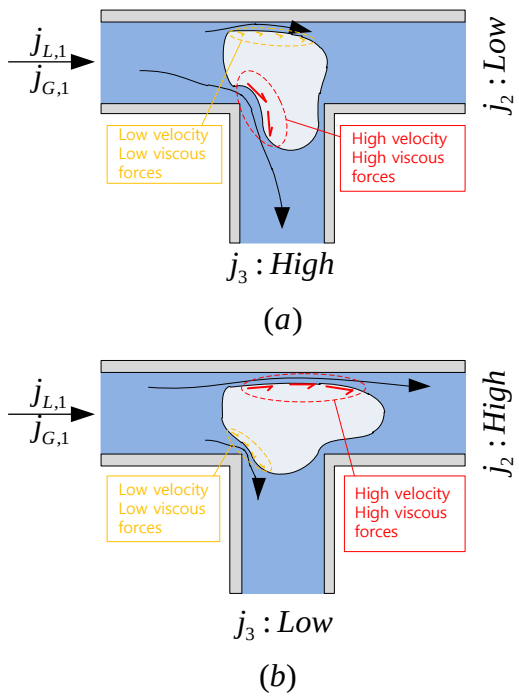

Figure 7.6: Split at T-junction with short bubble length (L_B=1.5 D_H)

$L_{B,crit}$ is assumed to cover a region instead of taking on a constant value, and this region is named transition region, for transition between squeezing and viscous effects. This parameter will be a function of the bubble length, hydraulic diameter and, most certainly, the capillary number. It is expected that for a decrease in Ca the critical bubble length will take on a higher value, e.g. if the surface tension between the two phases is increased, but this has not been proven.

7.1.3 Section 2

The second section investigates the influence from superficial velocities while keeping the bubble length constant. Since plug flow with $L_B \geq 30D_h$ has been proven to have a small amount of mal-distribution, and as long as the bubble lengths are kept above this value, changes in either superficial velocity or bubble length has little to no effect on the split ratio. By comparing the different superficial velocities for the cases A, F, H and I in Figure 7.3 (excluding B since its bubble length is close to $30D_h$) it can be concluded that neither of the superficial velocities have an impact on the

split ratio for long bubbles. For short bubbles Hong et al. compared cases E, J and K. They all include plug flow with equal bubble length, and are illustrated in Figure 7.7.

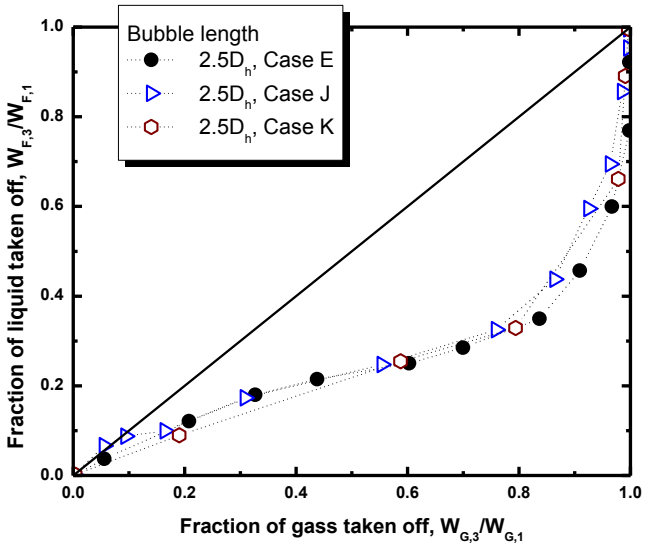

Figure 7.7: Split ratio for short bubbles with varying superficial velocities

For short bubbles as well as for long bubbles it is clear that variations in superficial velocities have a minor effect in comparison to that of the bubble length. Thus it can be concluded that once the bubble length is given, changes in the superficial velocity of each phase in the main channel have insignificant effect on the flow split ratio in the plug flow regime.

Finally in this side note section it will be important to point out that even though the superficial velocities might not have a big effect on the split ratio as the bubble length they are still important. One reason to back up this reason is located at the mixer for the two phases. L_B is largely determined by choice of mixture, but varies at the same time for variations in superficial velocities for the same mixer. This fact was strictly concluded upon by Sung Geun Jo (2011) (28),and the reader is referred to this thesis for further description details for different mixers. Therefore it can be concluded with data from Hong et al. that variations in superficial velocities together with

mixer geometry make changes to the bubble lengths, while the bubble length is the main parameter affecting the split ratio.

7.2 Bubble Length Importance Unknown

From a thorough literature review no evidence has been discovered about other researchers' knowledge of the bubble length importance. This fact is hence assumed to be the main reason why several authors have struggled with describing the physical trend of the split ratio rigorously without discontinuities and exceptions when comparing experimental data. It has been seen in several cases that researchers have obtained extensive experimental data but leaving the bubble length, or the unit cell frequency, out of the investigation. At the same time as they have managed to point out some effects of the split ratio related to physical trend which is in agreement with others, they fail to be able to describe the physical trend fully due to exactly this fact of omitting the bubble length importance.

8 Experimental Setup

The experimental setup is presented schematically in Figure 8.1. The T-junction plate is made of transparent acrylic plates for visualizing purposes. Two plates were mounted together to form a square shaped channel with $D_H = 600\ \mu m$ as illustrated in Figure 8.2.

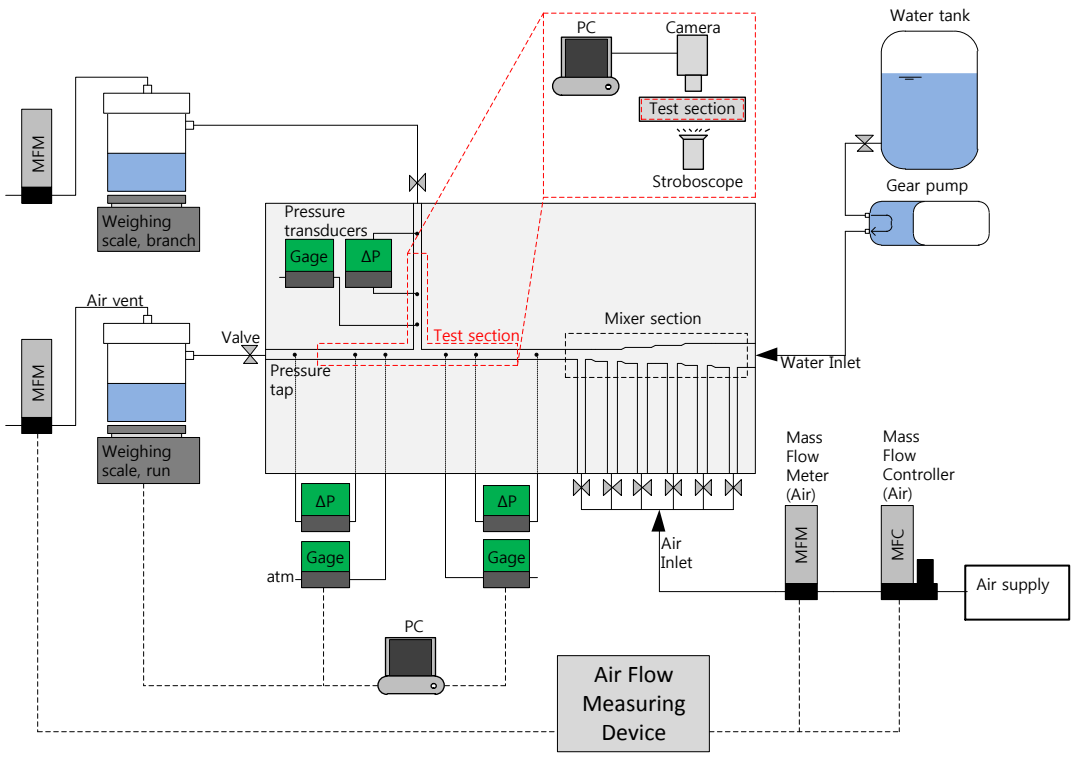

Figure 8.1: Schematic of experimental setup

Water and air was used as working fluids at room temperature. Ranges for superficial velocities used were

$$j_G = 0.3 \pm 0.01\, m/s$$
$$j_L = 0.3 \pm 0.01\, m/s$$

With a corresponding surface tension between the two phases of $\sigma = 0.073\, N/m$. Water was supplied from a tank while the air taken from the building supply line at thr pressure of 7 bar. Use of superficial velocities in combination with channel dimension yields the Reynolds numbers of $\mathrm{Re}_d \approx 360$, $\mathrm{Re}_L \approx 180$ and $\mathrm{Re}_G \approx 10$, which evidently corresponds to laminar flow. The conditions yield the capillary number of $Ca \approx 0.008$ and the Bond number of $Bo \approx 0.05$. Through comparison with flow regime map constructed by Chung and Kawaji (2004) (1) and Owejan et al. (2005) (2), the flow was assumed to be in the plug flow regime for all conducted experiments (see Figure 9.1 in the following chapter).

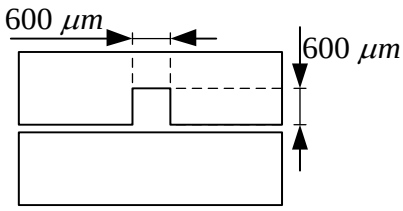

Figure 8.2: Channel construction

The acrylic plates include the T-junction, one liquid inlet, six gas inlets and a total of twelve pressure taps. It is schematically presented in Figure 8.3 with dimensions.

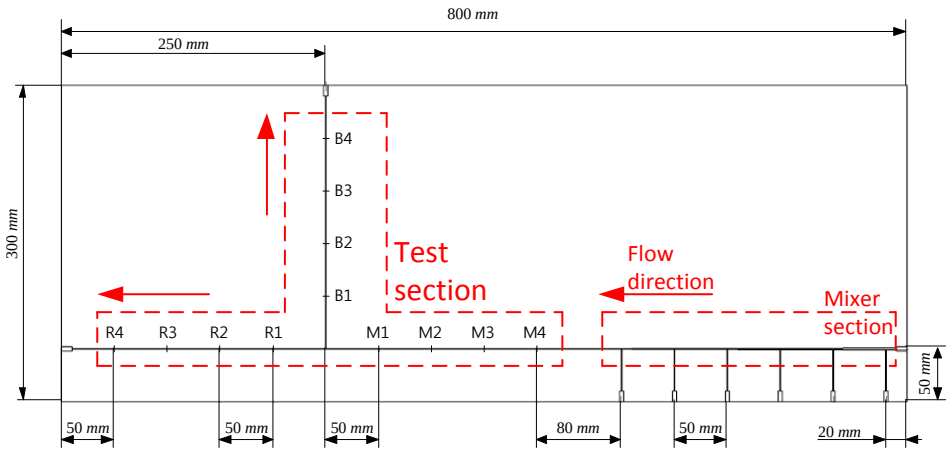

Figure 8.3: Test section with mixer integrated

The mixer section was fabricated together with the T-junction. Only one inlet for air is used at a time. Use of different inlets make different bubble lengths due to the variations in outlet diameter after the mixing region. The water enters the mixer region in the axial direction. This minimizes the risk of

bubbles breaking up before entering the T-junction region due to any sudden expansions and/or contractions. Needless to say if bubbles were to break up prior to the junction region and receive variations in the length due to instabilities it would be inapplicable to evaluate both the split ratio and pressure data as functions of bubble length. Many other types of external mixers were tested but failed at this specific point of grave importance.

Pressure taps were drilled in the test section with locations described in Figure 8.3 (M1-M4, R1-R4 and B1-B4). The distance between pressure taps, and the pressure taps to the junction point are all $50\,mm$. To obtain the extrapolated junction pressures the average pressures at a specific point and the channels' average pressure gradients were measured with use of pressure transducers (see Figure 8.1). The average gage pressure in each channel was measured at the points M1, R1 and B1 for the main, run and branch respectively. The average pressure gradient in the main was found from

$$\overline{\frac{dP}{dx_1}} = \frac{1}{2\Delta L\,\Delta T}\int_{t_0}^{t_1}\left(P_{M4} - P_{M2}\right)dt \qquad 8.1$$

where $\Delta L = 50\,mm$, and similarly for the run and the branch. The pressure taps numbered M3, R3 and B3 was not used. The average pressure at the reference point M1 was kept constant at $\overline{P_{M1}} = 10 \pm 2\,kPa$ for any adjustment made to the two downstream valves. The reference pressure was kept as low as possible to avoid leakage, which was frequently encountered for higher pressures. It was seen during experimenting that even seemingly negligible amounts of leakage had great impact on the pressure distribution. Since the frictional pressure drop is proportional to the square of the average velocity it is extremely important to keep the superficial velocities as constant as possible for good readings of pressure data.

Valves were connected downstream (see position in Figure 8.1) to both the run and branch channels for enabling adjustment in the total fluxes through

the two outlet channels. The air and water is separated in tanks afterwards. The water flow rate is then measured by use of electronic weight scales connected to a computer. The flow rate of water in the main is found from continuity by adding the flow rate in the run and the branch. Water is injected through a constant volume flow rate gear pump. Similarly the mass flow rate of air is controlled by a Mass Flow Controller (MFC) and measured by use of three Mass Flow Meters (MFM); one for each of the three channels.

Matlab was used to analyse the bubble length for each case. For any adjustments made to the flow conditions (valves, flow rates and use of mixer) the bubble length was thoroughly checked to ensure that it included negligible variations before recording the split ratio and the pressure data.

8.1 Mixers

To obtain different bubble lengths for a given superficial velocity of each phase different mixers were used. Parameters that have an impact on the final bubble length are

- the hydraulic diameter of each of the three connected channels
- the angle between each of them
- gravity effect if any of the diameters are larger than $D_H \approx 1\,mm$

To construct a device that is able to vary all these parameters in a continuous fashion is quite the difficult task. Therefore it was decided during construction of the experimental rig to take use of several mixers. For every time a change is made to the mixer it will result in a step increase or decrease in the bubble length.

Jo et al. (2011) (28) studied the impact of different parameters on the bubble length. Variation in angle between the two inlet tubes and the outlet tube were seen to have an effect, but at the same time relatively minor in comparison to simply changing the sizes of the channels and thereafter reducing/expanding the outlet channel to fit the main channel in the T-

junction plate. What is meant by this can be simply explained with help of Figure 8.4. In general the bubble length in the outlet of the mixer is largely related to the diameter of the outlet channel. As long as plug flow is maintained, the gas can only enter the outlet for a short period of time before the flow is cut by the liquid phase. Then the pressure at the gas inlet has to build itself up again to make the next bubble. Hence inclination angle can only change the bubble length to a certain extent. Therefore the approach illustrated in the figure were used in the experimental setup, and proved to be utmost useful. Simply by constructing several mixers with variations in outlet diameter bubbles with different lengths could easily be obtained. Of course it was important to avoid brake-up of the bubbles so as to conserve its volume. Carefully designed connectors had to be used to ensure this.

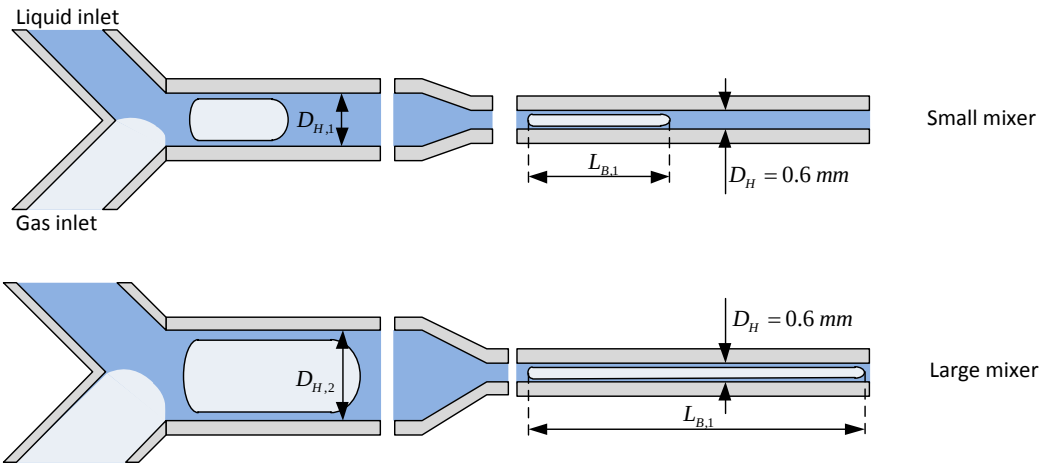

Figure 8.4: Mixer design

In chapter 6.4 a passive technique for altering the inlet flow to obtain desired bubble length and unit length of the entire plug were reviewed, constructed by Yamada et al. (2008) (14). It is assumed that, by implementation of this technique into the experimental setup, a higher degree of independency could have been achieved in varying the bubble length while running the experiment, but due to lack of equipment and available time to order new necessary devices it was not possible to try out.

Even so it is assumed that a more continuous amount of experimental data would have been obtainable from implementation.

8.2 Uncertainty

After calibration the uncertainty for each of the pressure transducers were found to be less than $0.01\,kPa$. This uncertainty factor is regarded sufficient to obtain relatively accurate pressure readings when compared to variations in pressure introduced in the next chapter. On the other hand a miss-calibration with regards to reference value between the four pressure transducers took place where no exact uncertainty rate can be placed. This fact results in, as shall be seen, possibly high uncertainty in absolute values. The variations in pressure reading, i.e. obtained trends for variations in flow rate, are still valid with the given uncertainty $0.01\,kPa$ as an upper limit. Superficial velocity measurement has an upper limit of uncertainty set to $0.001\,m/s$ for both air and water.

9 Experimental Data

It is of interest to see how increasing the bubble length affects not only $j_{G,3}$ and $j_{L,3}$, but also the time averaged extrapolated junction pressures. Hong et al. (3) proved that, by decreasing the bubble length while keeping the inlet flow rates constant, the fraction of gas in the branch increased. On the other hand, extrapolated pressure data was not provided. In the present work, data for split ratio and extrapolated junction pressures has been obtained for four cases with variations in bubble length while keeping the superficial conditions constant. It is suspected that an increase of gas fraction in the branch will yield a lower time-averaged pressure drop between the main and the branch to overcome frictional forces, i.e. the head-loss due to flow from the main to the branch is lowered as a result of increasing void fraction. Superficial velocities are mapped in Figure 9.1. Conditions for all performed experimental cases are listed in Table 9.1.

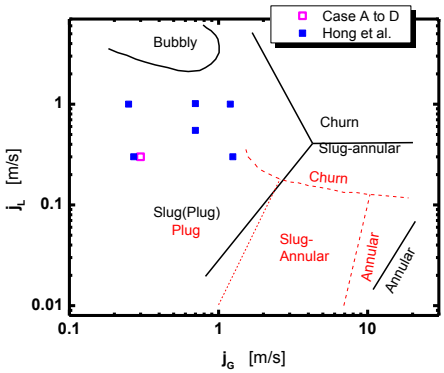

Figure 9.1: Superficial velocities

Case	$j_{G,1}$ (m/s)	$j_{L,1}$ (m/s)	L_B/D_h	P_{M1} (kPa)
A			37	
B	0.3	0.3	10	10
C	±0.01	±0.01	6.6	±2
D			5	

Table 9.1: Experimental conditions

9.1 Split Ratio

Split ratio data for case A to D is presented in Figure 9.2. All four cases show well behaved split ratio trends as a function of total flow rates and bubble length. When plotted together with constant j_3/j_1 lines the split ratio curves clearly show variations in trend for $0.2 < j_3/j_1 < 0.3$ and $0.7 < j_3/j_1 < 0.8$. Case

D with its shortest bubbles is affected by this variation in trend prior to the other cases. This variation in trend has already in earlier chapters been addressed and its occurrence anticipated. The regime located in the middle of the transition borders marked in Figure 9.3 will from this point be referred to as the *centre regime*, and shall receive more attention through evaluation of capillary forces in sub-chapter 9.3 .

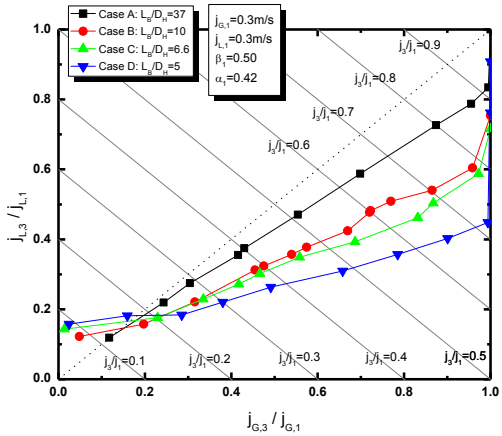

Figure 9.2: Split ratio

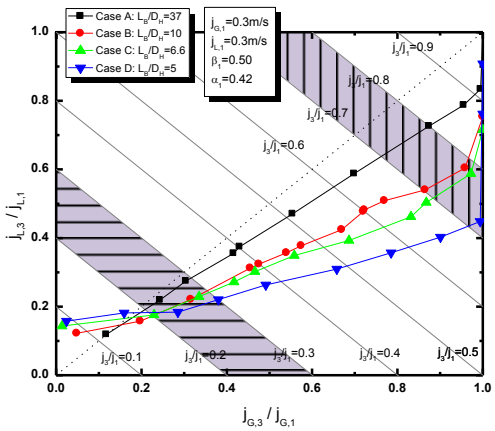

Figure 9.3: Transition borders

Separation was observed to occur for both low and high branch flow rates for cases B to D. Cases B to D show good trend for when separation occurs in both ends of the plot in Figure 9.2; short bubbles are separated first (case D) with case C and B following in a fashion related to increasing bubble length. Separation did not occur for case A.

Figure 9.4 compares the obtained data with case A to E of Hong et al. (see Table 7.1). This comparison is performed for validation of the obtained data. The currently obtained data is marked in the same fashion with symbol and lines as in Figure 9.2, and data by Hong et al. is simply presented by lines. As is seen in the figure, all split ratio curves follows a strict relation to variations in bubble length. The same applies for when compared to Hong et al.'s case F to K, but has been excluded from to figure so as to not make it too chaotic to evaluate. This further strengthens the conclusion about the minor influence on split ratio due to variations in superficial velocities alone.

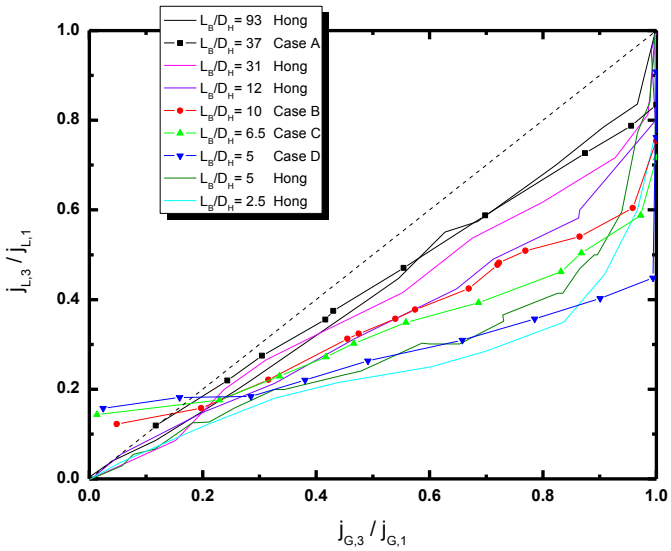

Figure 9.4: Validation of split ratio data through comparison with Hong et al.'s case A to E

Data by Hong et al. also illustrates the apparent change in trend, and hence physical ingredients for when moving to the far edges for total flow in the branch channel. The centre regime is even narrower for data by Hong et al. due to a higher capillary number.

9.2 Void Fraction as Function of Bubble Length

Prior to evaluating the pressure data, an interesting point shall receive some attention, namely the strict relation between void fraction/volumetric quality and corresponding bubble length. This is evaluated inside the centre regime. Hong et al. did not provide pressure data, and no other sources in the literature that has evaluated both pressure and bubble length has been discovered, so this fact render impossible the validation of pressure data as function of bubble length together with other sources. Therefore only this evaluation of void fraction as function of bubble length is applicable for comparison between data by Hong et al. and the currently obtained data.

Recall equations 4.16 and 5.4 which relates void fraction with volumetric quality. In Figure 9.5, volumetric quality has been obtain through linear interpolation between data points along constant j_3 / j_1 lines for

$j_3 / j_1 = 0.3, 0.4, ..., 0.8$. Volumetric quality data for case D at $j_3 / j_1 = 0.8$ has been excluded since the comparison shall be performed only for the centre regime.

Figure 9.6 presents void fraction as a function of bubble length along constant j_3 / j_1-lines. The data shows a good trend for the centre regime with little change for different total fluxes, with exception of high j_3 / j_1=0.8 for very short bubbles (Figure 9.6, pink line). As the bubble length decreases the centre regime for which this evaluation is performed grows narrower more rapidly, as was previously stated.

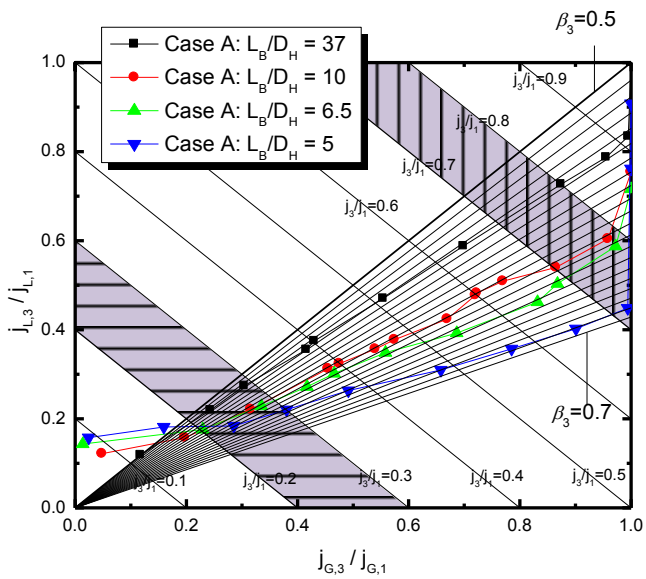

Figure 9.5: Split ratio plotted together with constant j3/j1 and b3 lines

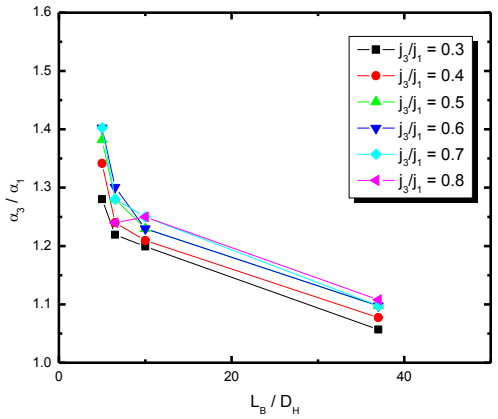

Figure 9.6: $\alpha_3/\alpha_1 = f(L_B/D_H)$, Case A to D

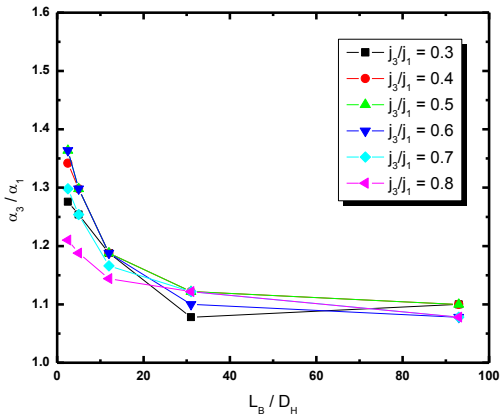

Figure 9.7: $\alpha_3/\alpha_1 = f(L_B/D_H)$, Hong et al. Case A to E

The same interpolation has been performed for data by Hong et al. Figure 9.7 illustrates void fraction as function of bubble length for case A to E by Hong et al. The same trend is seen, and at this point with even smaller variation for different constant j_3/j_1 -lines. A comparison between all currently obtained data together with that of Hong et al. is presented in Figure 9.8. It is hard to distinguish between the lines, but this fact only further strengthens the possibility of concluding upon a strict relation between void fraction and bubble length when operating inside the centre regime. For all cases it can be seen how the void fraction stays fairly constant for long bubbles in comparison to short bubbles. For short bubbles the increase in void fraction takes on a trend which resembles a proportionality with $\sim 1/L_B$.

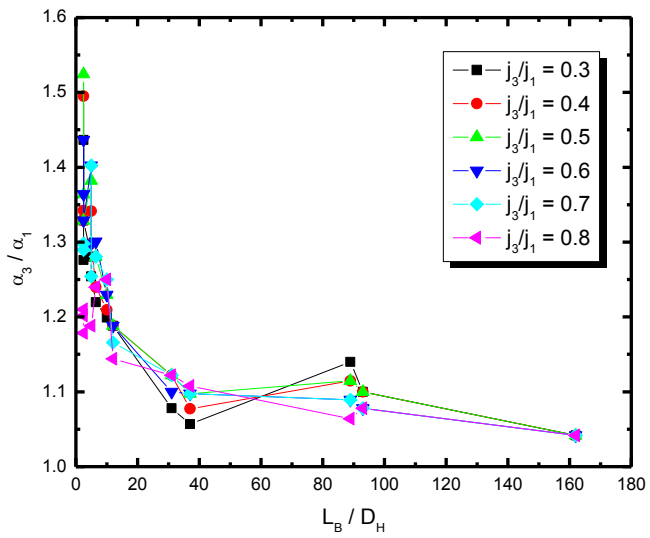

Figure 9.8: $\alpha_3 / \alpha_1 = f(L_B / D_H)$ (case A to D, and all data by Hong et al.)

Before moving on with evaluation of the border regions and the outer ends with regards to j_3 / j_1 it can be said that all data reveals a good trend between void fraction and bubble length. It is interesting to see how little alpha change with variations in j_3 / j_1 while operating inside the centre regime. On the other hand without use of the extended Bernoulli equations it is impossible to predict the *total fluxes* in each of the two outlets, which of course also is of interest to many different applications. This is why it is still of interest, if possible, to construct a well performing model by use of the extended Bernoulli equations.

9.3 Observed Flow Pattern, Bubbly Flow and Separation

The centre regime is defined as having a plug flow pattern in all three channels. This is illustrated in Figure 9.9 to Figure 9.12 for cases A to D, respectively. Plug flow in all three channels was observed for all four cases, but when attempting to take use of mixer 5 the bubble lengths was very short, and hence bubbly flow in the outlet channel with low flow rate was frequently encountered. All four introduced images are taken for the centre regime.

Figure 9.9: $L_B / D_H = 37$, Case A

Figure 9.10: $L_B / D_H = 10$, Case B

Figure 9.11: $L_B / D_H = 6.5$, Case C

Figure 9.12: $L_B / D_H = 5$, Case D

Through the image analysis, bubbly flow was seen to occur frequently for case C and D. Also in some cases the flow pattern seemed to be on the transition region between plug and bubbly flow for case B. Figure 9.13 and Figure 9.14 illustrates close to transition between plug and bubbly flow, and strictly bubbly flow in the branch for shorter bubbles respectively.

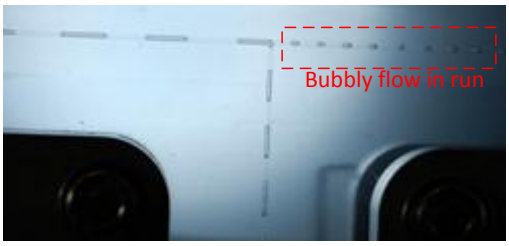

Figure 9.13: $L_B / D_H = 10$, case B

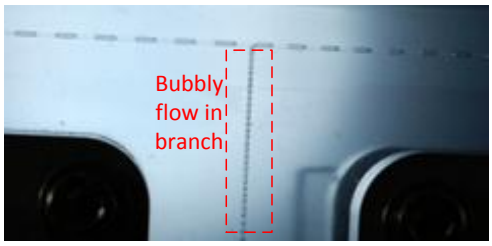

Figure 9.14: $L_B / D_H = 5$, Case D

For bubble lengths shorter than $L_B / D_H = 5$ the centre regime grew quickly smaller (the centre regime must have plug flow in all three channels). This is easy explained by the fact that at some point plug flow in both outlet channels is simply impossible, i.e. for plug flow in main with $L_B / D_H \leq 2$ bubble flow will always occur in at least one of the two outlet channels.

When j_3 / j_1 moves towards transition lines for separation, instabilities has been observed, i.e. time dependant variations with either separation or

sporadic bubbly flow in the outlet channel of low total flux. An example of this occurrence is demonstrated in Figure 9.15 and Figure 9.16 for case D. Both pictures were taken during constant operating conditions with no adjustments made to either upstream pumps or downstream valves. This is regarded as a transition region between the plug/bubbly flow and the phase separation.

Figure 9.15: Sudden bubbly flow occurrence

Figure 9.16: Close to separation

For the currently used setup with used flow conditions the transition areas has been defined to start at $0.2 < j_3 / j_1 < 0.3$ and $0.7 < j_3 / j_1 < 0.8$ through evaluation of split ratio curves as well as two-phase K coefficients, which will be introduced in the following chapter. The location of these transition borders, as well as for when separation occurs, is expected to be a function of the Capillary number and the bubble length. Even so it should be kept in mind that variations in either viscosity and/or interfacial tension has not been tested in relation to variations in total fluxes. Hence it cannot not be strictly concluded that the capillary number is the correct parameter. This assumption is in need of further validation, but has not been carried out in this thesis. Separation was not encountered for case A, but seen for all the three other cases, B to D. Hong et al observed separation for high run flow rate in case G, and in both case E and G for high branch flow rates. Case E had $L_B / D_H = 2.5$ and G had $L_B / D_H = 1.6$. The low capillary number for the current experimental data in comparison to that of Hong et al. explains the differences in j_3 / j_1 for when separation occurs. Separation occurs easier for the currently used flow rates due to their low values which decreases the capillary number, i.e. the viscous forces are not great enough to break the surface of the bubbles, and hence the bubbles can withstand viscous drag

forces and move their entire bodies into the channel with higher flow rates. This happens before the pressure in the channel with the low flow rate manages to drop a sufficient amount so as to break the bubble surface.

There is not enough data to carry out a mapping of the critical value for separation or location of transition borders between the centre regime and the outer regions. The critical value to determine when separation occurs should also be a function of the bubble length as well as the capillary number. Through examination of separation points in Figure 9.2 and Figure 7.4, it is clear how separation occurs more easily for less extreme values of j_3 / j_1 when the capillary number is lowered. Also low capillary numbers have shown separation to occur for L_B / D_H up to 10, while for Hong et al. separation has only been observed for when L_B / D_H is less than 2.5, and hence this comparison defends the previous assumption of having separation/transition borders related to bubble length and capillary number.

9.4 Single-phase K Coefficients

Experiments were also conducted for single-phase flow with an average velocity in the main channel similar to that of the two-phase flow experiment ($j_1 = 0.55 \pm 0.02\,[m/s]$). The obtained data for extrapolated junction pressure drops, $\overline{P_{1,j} - P_{2,j}}$ and $\overline{P_{1,j} - P_{3,j}}$, is presented in Figure 9.17. The same experiment was performed twice with use of two different test sections and small changes in average velocity in the main. The second experiment took use of the same setup as were used for the two-phase experiment. All data obtained for the single phase flow experiment is included in attachment A.

The data shows good trends for variations in j_3 / j_1. As expected, and in accordance with previous reasoning with regards to pressure drop due to frictional forces, $\overline{P_{1,j} - P_{3,j}}$ increases more rapidly than $\overline{P_{1,j} - P_{2,j}}$ for high branch fluxes. This is physically reasonable. On the other hand, a point worth noticing is the fact that $\overline{P_{1,j} - P_{2,j}}$ appears negative for all values of j_3 / j_1. $\overline{P_{1,j} - P_{2,j}}$ should be zero for $j_3 / j_1 = 0$. This is assumed to have occurred due

to error in calibration of the pressure transducers in the experimental setup. This shall receive more attention in the upcoming sections, since it also occurred during experimenting on two-phase flow.

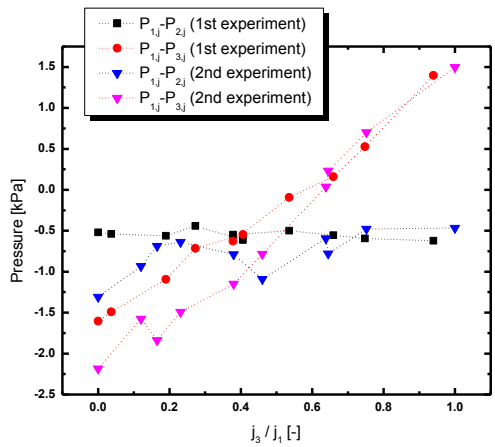

Figure 9.17: Sing phase pressure drop

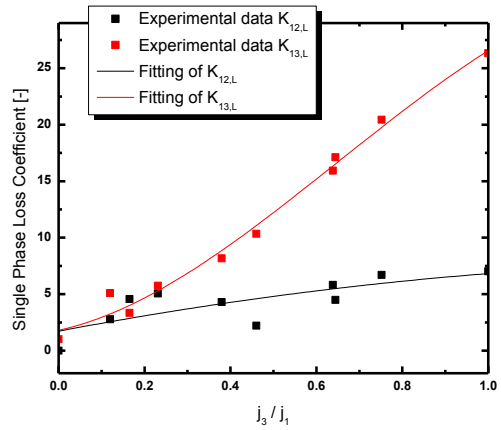

Figure 9.18: $K_{12,L}$ and $K_{13,L}$

The objective of experimenting on single phase flow was to obtain loss coefficients for the liquid phase, which shall be used during model construction to predict split ratio for two-phase flow. These K values are obtain from the single phase Bernoulli Equation given as

$$P_1 - P_2 = \frac{1}{2}\rho(u_2^{\,2} - u_1^{\,2}) + K_{12,L}\frac{1}{2}\rho u_1^{\,2} \qquad 9.1$$

$$P_1 - P_3 = \frac{1}{2}\rho(u_3^{\,2} - u_1^{\,2}) + K_{13,L}\frac{1}{2}\rho u_1^{\,2} \qquad 9.2$$

$K_{12,L}$ and $K_{13,L}$ represents the K-loss coefficients along a streamline from main to run and main to branch respectively. Due to the apparent error in pressure data the obtained data has been *shifted* in the y-direction so as to appear physically reasonable while the trends are assumed to be less erroneous, judging from previous discussion with regards to pressure behaviours in comparison to observed trends. Even for wrongly calibrated equipment the trends can still be obtained, and hence evaluating the pressure data still has meaning. Data for the K coefficients, calculated by use of equation 9.1 and 9.2, is presented in Figure 9.18.

The following correlations have been constructed for the K coefficients through fitting:

$$K_{12,L} = 1.72 + 7.22\frac{j_3}{j_1} - 2.12\left(\frac{j_3}{j_1}\right)^2$$
$$K_{13,L} = 1.805 + 8.213\frac{j_3}{j_1} + 33.924\left(\frac{j_3}{j_1}\right)^2 - 17.390\left(\frac{j_3}{j_1}\right)^3 \qquad 9.3$$

with and error of ±1.2 and ±1.5 for $K_{12,L}$ and $K_{13,L}$, respectively.

9.5 Pressure Measurement

Extrapolated junction pressure drops as function of j_3 / j_1 has been measured experimentally. They are presented in Figure 9.19 and Figure 9.20 for $\overline{P_{1,j} - P_{2,j}}$ and $\overline{P_{1,j} - P_{3,j}}$ respectively with four graphs in each plot, one for each of the four cases A to D with their respective bubble lengths. At first sight the presented data gives simply a chaotic impression. Pressure data was found to be extremely sensitive to upstream conditions in comparison to the split ratio data. This occurrence is easily explained by referring to the Bernoulli equation; change in pressure is a function of the square of change in velocity along a streamline. Another proof of this sensitivity is the appearing perfect split ratio trends when compared to split ratio data by Hong et al., with all four curves being relatively smooth, while the pressure data takes on such a chaotic appearance. During modelling each of these junction pressure drops shall be evaluated with each point of measuring's corresponding set of superficial velocities in all channels taken into account. This will reveal the fact that there is actual physical meaning in the presented data even though at this point this fact cannot be seen.

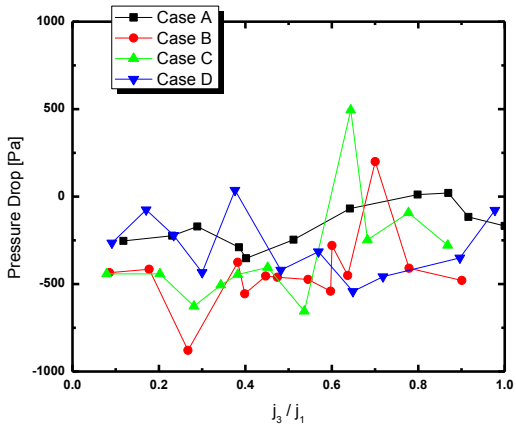

Figure 9.19: $\overline{P_{1,j} - P_{2,j}}$ as function of j_3 / j_1

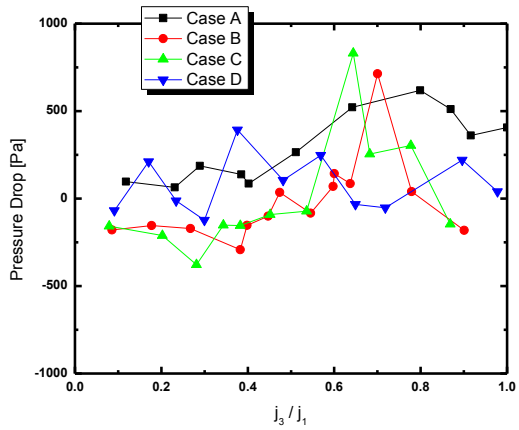

Figure 9.20: $\overline{P_{1,j} - P_{3,j}}$ as function of j_3 / j_1

All pressure data obtained from the experiment is included in attachment C together with their respective set of measured superficial velocities in all of the three channels. From previously performed reasoning of pressure behaviour it would be natural to assume that $\overline{P_{1,j} - P_{3,j}}$ for long bubbles should be much higher than $\overline{P_{1,j} - P_{3,j}}$ for short bubbles due to their apparent difference in void fraction (see Figure 9.2), but due to the junction pressure drop's sensitivity to variations in average velocities this expected trend is currently not easily recognizable in Figure 9.20. Measuring pressure with high accuracy proved to be very difficult in comparison to measuring flow rates. This fact renders some of the objective of this thesis inapplicable. A physical trend for the junction pressure drops has been found, and shall be introduced during the introduction of the model. This trend supports the hypothesis for variations in time averaged junction pressure drops (introduced in the following chapter), but due to the assumingly high uncertainty rate in the recorded experimental data it is inapplicable to perform the desired fitting for correlating the variation in bubble length to the split ratio phenomenon. This fact shall receive more attention in the following chapters. More data points and a lowering in uncertainty for the measured pressure values are assumingly needed to complete the desired fitting process between the pressure data and the bubble length.

No concrete conclusions have been given for the pressure measurement. Due to the apparent chaotic behaviour of the data, further discussion of the

pressure distribution, discovered trends and possible conclusions will be further addressed in the next chapter.

10 Model

Hong et al. proposed a model for prediction of the split ratio at the T-junction based on the extended Bernoulli equation. The model was not thoroughly validated, and hence present work focused on obtaining sufficient experimental data so that the validation of the model could be completed. While reviewing the model a problem with the derivation was discovered. This problem is without a doubt grave, and renders the model inapplicable for prediction of the split ratio. Therefore the derivation will not be reviewed here, but only the newly proposed model by the present author. At the same time it should be pointed out that a large fraction of the derivation of the new model is based on the same approach as was done by Hong et al, namely to take use of the extended Bernoulli Equation. One equation is used for a stream line from the main to the run and likewise one to the branch.

Since the plug flow regime is still far from thoroughly understood the most important aspect of investigation at this point will still be to obtain knowledge regarding the physical trend of the plug flow pattern in meso-scale channels. This has already been performed to some extent in the previous chapters. The most important new discovery is the trend of the average pressure drop variations as a function of bubble length, and hence split ratio as the total fluxes in the branch is held constant, which were presented in the previous chapter.

10.1 Model Derivation

The model is based on the time averaged pressure drop from main to run and main to branch. Since the bubble length is the main variable for the split ratio, the effect of the superficial velocity is neglected in determining the split ratio. The reason for addressing the variations in average pressure is

to be able to determine the total fluxes in each of the channels. Such time averaged junction pressures is a function of several contributions with respect to the flow conditions in the junction region for given time steps. The definition of the junction region has already been established; see Figure 6.12 (b) as well as Figure 10.1.

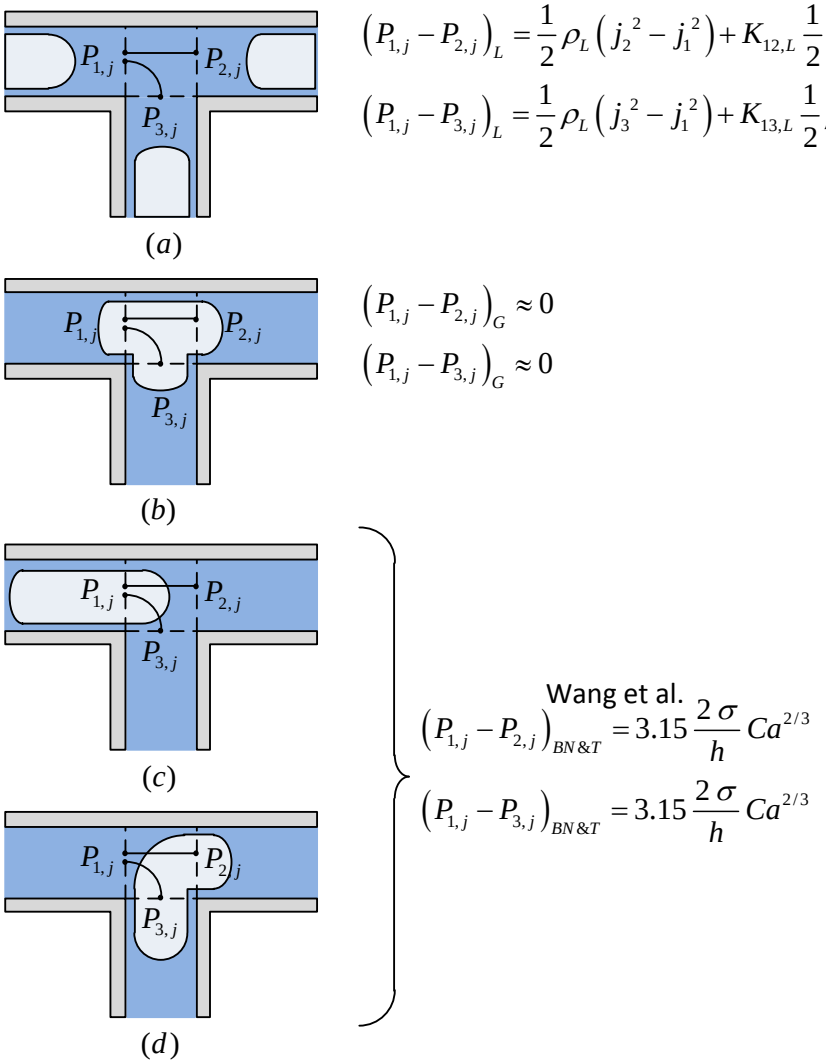

Figure 10.1: Average pressure drop contributions

The different contributions to the total average pressure drop is illustrated in Figure 10.1 and presented in equation 10.1.

$$\begin{aligned}\overline{P_{1,j}-P_{2,j}}&=\left(P_{1,j}-P_{2,j}\right)_L\frac{\sum\Delta t_L}{T}+\left(P_{1,j}-P_{2,j}\right)_G\frac{\sum\Delta t_G}{T}+\left(P_{1,j}-P_{2,j}\right)_{BN\&T}\frac{N\Delta t_i}{T}\\ \overline{P_{1,j}-P_{3,j}}&=\left(P_{1,j}-P_{3,j}\right)_L\frac{\sum\Delta t_f}{T}+\left(P_{1,j}-P_{3,j}\right)_G\frac{\sum\Delta t_G}{T}+\left(P_{1,j}-P_{3,j}\right)_{BN\&T}\frac{N\Delta t_i}{T}\end{aligned}\qquad 10.1$$

Equation 10.1 states that the average pressure drop for the junction pressures equals the sum of the liquid, gas and interfacial (bubble nose and tail) contributions, and each term multiplied by the respective time fraction occupying the junction region. This is in accordance with the evaluation of pressure distribution in time and space given in subchapters 5.5 and 6.3 . Figure 10.1 (a) illustrates pressure drop contribution due to the liquid plug covering the junction region. From the extended Bernoulli equation

$$P_1 - P_2 = \frac{1}{2}\rho\left(j_2^{\,2} - j_1^{\,2}\right) + K_{12}\frac{1}{2}\rho j_1^{\,2} \qquad 10.2$$

the pressure drop contribution is as presented in the right hand side of Figure 10.1 (a), namely

$$\begin{aligned}\left(P_{1,j} - P_{2,j}\right)_L &= \frac{1}{2}\rho_L\left(j_2^{\,2} - j_1^{\,2}\right) + K_{12,L}\frac{1}{2}\rho_L j_1^{\,2} \\ \left(P_{1,j} - P_{3,j}\right)_L &= \frac{1}{2}\rho_L\left(j_3^{\,2} - j_1^{\,2}\right) + K_{13,L}\frac{1}{2}\rho_L j_1^{\,2}\end{aligned} \qquad 10.3$$

Similarly the same approach applies when the bubble body covers the junction region as well, as is illustrated in Figure 10.1 (b), but since this pressure drop is small in comparison to that of the liquid it is neglected. The pressure drop contribution by the bubble nose and tail take use of the correlations proposed by Wang et al., see equation 5.13. They are presented in Figure 10.1 (c) and (d). Each of these three mentioned contributions for the average junction pressure drop has to be multiplied by the respective fraction of time occupying the junction region during a time interval T, where $T = \sum \Delta t_L + \sum \Delta t_G + N\Delta t_i$ (T larger than the time it takes for one unit cell to pass through the junction region, see chapter 4.2). Before substituting each of the pressure drop contributions into equation 10.1, a couple of terms shall first receive some special attention.

The single-phase K coefficients describing frictional loss over the junction region was proposed in chapter 9 . These coefficients shall cover all pressure

losses over the junction region from the main to the branch, and main to the run, due to separation, secondary flow occurrence and due to wall friction, as was thoroughly explained in subchapter 6.3.2 . The coefficients are given as

$$K_{12,L} = 1.72 + 7.22\frac{j_3}{j_1} - 2.12\left(\frac{j_3}{j_1}\right)^2$$
$$K_{13,L} = 1.805 + 8.213\frac{j_3}{j_1} + 33.924\left(\frac{j_3}{j_1}\right)^2 - 17.390\left(\frac{j_3}{j_1}\right)^3 \qquad 10.4$$

They are obtained for water, and shall be used to predict the pressure loss for when a plug cover the junction region. Both coefficients are functions of the total flux in the branch divided by the total flux in the main.

The total time a bubble occupies the junction region is obtained as

$$\begin{aligned}\frac{\sum \Delta t_G}{T} &= \frac{N \cdot \Delta t_G}{T} \\ &= f \cdot \Delta t_G \\ &= f\,\frac{L_B}{U_B} \cdot \frac{A_B}{A_B} \\ &= \frac{Q_G}{U_B \cdot A_B} \\ &= \alpha\,\frac{A}{A_B}\frac{U_G}{U_B}\end{aligned}$$

This includes the nose and tail of the bubble. Now, with use of equation 5.5 and assuming $\delta \to 0$, this relation yields

$$\frac{\sum \Delta t_G}{T} \approx \alpha \qquad 10.5$$

Hence it can easily be seen from continuity that the time fraction for the liquid phase to occupy the junction region is

$$\frac{\sum \Delta t_L}{T} = (1-\alpha) \qquad 10.6$$

The fraction of time a bubble nose covers the junction region can be derived by setting (keep in mind Figure 5.1)

$$\frac{N\Delta t_i}{T} = \frac{U_B}{L_B + L_L}\Delta t_i$$

where

$$\Delta t_i = \frac{D_H}{U_B}$$

Hence the total time fraction for the bubble nose to cover the junction region within the total time T equals

$$\frac{N\Delta t_i}{T} = C_{BT}\frac{D_H}{L_B + L_L} \qquad 10.7$$

Substituting equation 10.3, 5.13, 10.6 and 10.7 into equation 10.1, and neglecting the pressure drop contribution due to the body of the bubbles, results in time averaged junction pressure drops given as

$$\overline{P_{1,j} - P_{2,j}} = (1-\alpha)\frac{1}{2}\rho_L\left(j_2^{\,2} - j_1^{\,2}\right) + (1-\alpha)K_{12,L}\frac{1}{2}\rho_L j_1^{\,2} + 3.15\cdot C_{BT}\frac{2\sigma}{L_B + L_L}Ca^{2/3} \qquad 10.8$$

$$\overline{P_{1,j} - P_{3,j}} = (1-\alpha)\frac{1}{2}\rho_L\left(j_3^{\,2} - j_1^{\,2}\right) + (1-\alpha)K_{13,L}\frac{1}{2}\rho_L j_1^{\,2} + 3.15\cdot C_{BT}\frac{2\sigma}{L_B + L_L}Ca^{2/3} \qquad 10.9$$

The junction pressures $\overline{P_{1,j}}$, $\overline{P_{2,j}}$ and $\overline{P_{3,j}}$ has to be determined by use of e.g. the pressure drop correlation which were introduced in subchapter 5.5.5 , i.e. three more equations for this system. Equation 10.8 and 10.9 in addition to equation 6.2 (5 equations), 10.4 (2 equations) and 5.4 plus the three additional pressure relations to estimate the junction pressures results in a

system consisting of 13 equations and 13 unknowns. The unknowns are $\overline{P_{1,j}}$, $\overline{P_{2,j}}$, $\overline{P_{3,j}}$, j_2, j_3, $j_{L,1}$, $j_{L,2}$, $j_{L,3}$, $j_{G,1}$, $j_{G,2}$, $j_{G,3}$, $K_{12,L}$ and $K_{13,L}$.

The pressure equations are not completed at this point. They still lack physical impact from the split ratio phenomenon itself. At this point they are only applicable for prediction of the total fluxes in the run and the branch, but, as can be seen by carefully studying equation 10.8 and 10.9, no information affects the pressure drops due to the apparent mal-distribution. Actually by carefully investigating the two junction pressure equations it can be seen that they (if the bubble nose and tail term is excluded) are the same as for single-phase flow at a T-junction with a decrease in the diameter so as to raise the average velocity along a streamline. The mal-distribution phenomenon gives reason to believe that the time averaged pressure drops should be affected in some sense, which at this point they are not. Conclusively in this short but important reasoning the main question to be answered to finalize the derivation of the model is: how is the *junction pressure drops* affected by the presence of mal-distribution?

In general the split ratio phenomenon includes a high level of complexity. Several important physical ingredients have already been introduced in previous chapters to establish a physical understanding of it. Still this physical understanding is far from finalized. Because of this it is suggested that an empirical fitting has to be conducted to be able to propose a well-performing model. It shall be based on physical ingredients as far as possible. Pressure variations on a small time scale with fast oscillations (proportional to the frequency of the unit cell) are assumed to greatly impact the split ratio. For an increase in pressure drop over a short period of time the velocity will experience an increase in that respective channel, thereby allowing more of the phase currently situated in the junction region to enter the respective channel. Such effects are hard to measure, but a time averaged term that regards this effect has to be implemented into the average junction pressure equations (equation 10.8 and 10.9).

The objective of the model will be to strictly yield the trend in mal-distribution seen in the experimental data (as well as experimental data by Hong et al. which shows a similar trend), see Figure 10.2. The answer for model construction is embedded in this plot. In Figure 10.2 lines of constant volumetric quality as well as total flux in the branch has been added. One interesting way of addressing this plot arises if the mal-distribution is plotted with total flux as x-axis, see Figure 10.3. This figure is simply Figure 10.2 flipped horizontally and rotated 135°. A specific increase in mal-distribution strictly related to the bubble length is without a doubt present, but since knowledge of the pressure is necessary to predict the total fluxes, the question of *what happens to the pressure drop over the junction region once the mal-distribution is increased* has to be addressed.

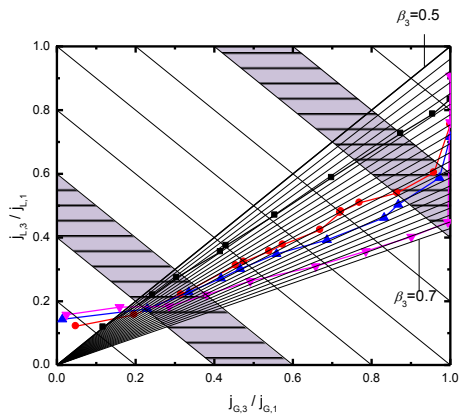

Figure 10.2: Split ratio curve with constant j_3 lines

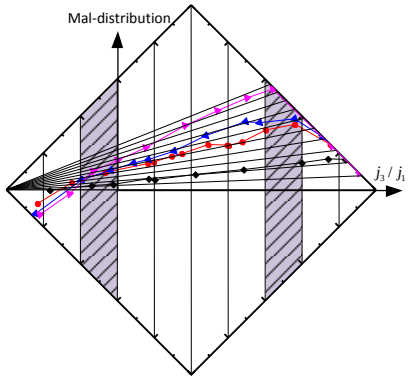

Figure 10.3: Split ratio as a function of j_3

Prior to possession of data for variations in the time averaged pressure drops over the junction region as a function of void fraction in the branch a hypothesis was formulated for the expected behaviour. When the velocity suddenly decreases due to sudden expansion the pressure in both the run and branch increase. As an example, let j_2 is set equal to j_3. So, as is illustrated in Figure 10.4, the pressure increases equally for both channels. The sudden expansion results in the already introduced frictional pressure losses, where the one for the branch is generally much larger. In this picture the flow is still in possession of a perfect distribution having $\alpha_3 = \alpha_1$ since the K-losses is applicable for single phase flow along a streamline. This is what

equation 10.8 and 10.9 presently models; prediction of j_2 and j_3 with no mal-distribution. If a sudden mal-distribution occurs it results in an increase in $j_{L,2}$ as well as a decrease in $j_{L,3}$. Since it is already assumed that the gas phase has negligible impact on the pressure drop over the junction region this fact has to result in an increase in frictional pressure loss between the main and the run. This assumption is based on common sense that if the amount of heavy liquid transported along a streamline is increased more energy will be lost due to friction. Hence, as is illustrated in Figure 10.5, an additional K-loss should affect the total time averaged pressure losses over the junction region. Since the branch is rich in gas ($\alpha_3 > \alpha_1$) $\overline{P_{2,j}}$ decreases while $\overline{P_{3,j}}$ increases.

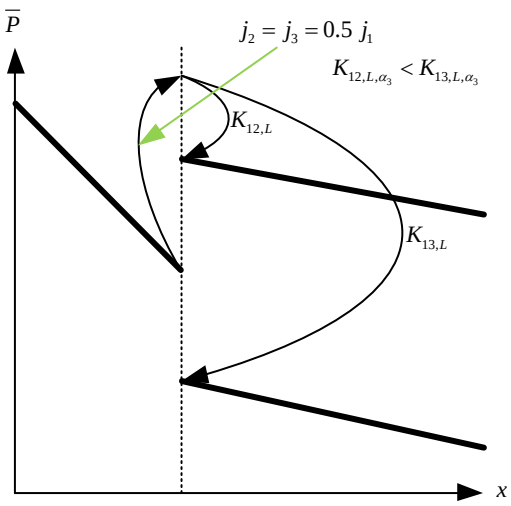

Figure 10.4: Pressure hypothesis

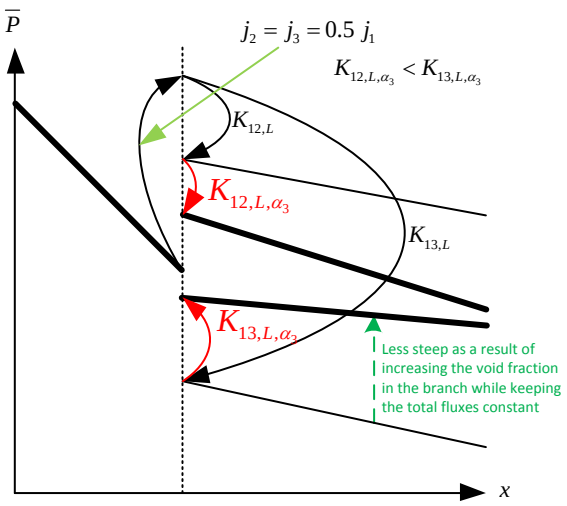

Figure 10.5: Additional pressure terms due to the occurrence of mal-distribution

Since Hong et al. has already pointed out the strict relation between bubble length and void fraction, this fact can also be implemented in the formulated hypothesis. An example of the formulated hypothesis is presented in Figure 10.6 and Figure 10.7, to clarify it further.

Example

$$L_{B,1} > L_{B,2}$$

Inlet cond.		Inlet cond.
Q_L	=	Q_L
$Q_{G,1}$	=	$Q_{G,1}$
$Q_{L,1}$	=	$Q_{L,1}$
j_3	=	j_3
⇩		⇩
α_3	<	α_3
$\overline{P_{2,j}}$	>	$\overline{P_{2,j}}$
$\overline{P_{3,j}}$	<	$\overline{P_{3,j}}$
$\overline{P_{1,j}} - \overline{P_{2,j}}$	<	$\overline{P_{1,j}} - \overline{P_{2,j}}$
$\overline{P_{1,j}} - \overline{P_{3,j}}$	>	$\overline{P_{1,j}} - \overline{P_{3,j}}$

Figure 10.6: Parametric study

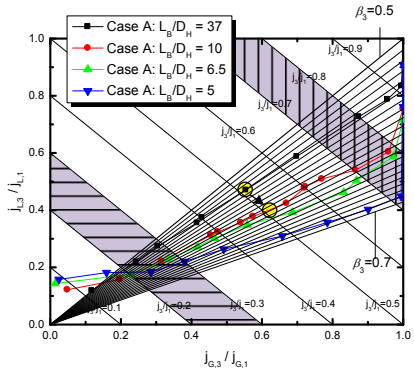

Figure 10.7: Increase in bubble length and hence also void fraction in the branch

When moving from the black line (long bubbles) to the red line (short bubbles) along a line of constant total flow rate in the branch the void fraction in the corresponding channel experiences an increase. By following the logic in Figure 10.6, the result is expected to be an increase in $\overline{P_{1,j} - P_{2,j}}$ and a decrease in $\overline{P_{1,j} - P_{3,j}}$ (Even though this was not very apparent in Figure 9.20 it will be made more clear when the additional K coefficients are regarded and small variations in fluxes taken into account). This change in time averaged pressure drop over the junction region has to be implemented into the model for the model to be fully applicable for prediction of the split ratio as well as total fluxes. At this point nothing particular has been stated about exactly *when* this mal-distribution effect takes place. Therefore recall the reasoning of time dependant variations in pressure distribution given in chapter 7 ; when this effect is averaged in time it should result in a contribution to the time averaged junction pressure drops on the form

$$\overline{\Delta P}_{Mal-dist} = (\alpha_3 - \alpha_1) K_{1k,L\alpha} \frac{1}{2} \rho_L j_1^2 \qquad 10.10$$

where $k = 2,3$. Here $(\alpha_3 - \alpha_1)$ equals the increase in gas transported from the main to the branch, and hence also represents the increase of liquid transported from the main to the run. The K coefficients have been marked with an additional alpha to distinguish them from the single phase K loss coefficients. They do not necessarily have to be the same as for single phase

flow due to the complexness of the time dependant pressure fluctuations, and at the same time there is no guarantee for how well the single phase K coefficients describes the flow behaviour for when a plug occupies the junction region. This change in pressure drop over the junction region should, since experimental data strictly shows a trend of the branch being rich on gas, be introduced into equation 10.8 and 10.9 as following:

$$\begin{aligned}\overline{P_{1,j}-P_{2,j}} &= (1-\alpha_1)\frac{1}{2}\rho_L\left(j_2^{\,2}-j_1^{\,2}\right)+(1-\alpha_1)K_{12,L}\frac{1}{2}\rho_L j_1^{\,2} \\ &\quad +3.15\cdot C_{BT}\frac{2\sigma}{L_B+L_L}Ca^{2/3}+(\alpha_3-\alpha_1)K_{12,L\alpha}\frac{1}{2}\rho_L j_1^{\,2}\end{aligned} \qquad 10.11$$

$$\begin{aligned}\overline{P_{1,j}-P_{3,j}} &= (1-\alpha_1)\frac{1}{2}\rho_L\left(j_3^{\,2}-j_1^{\,2}\right)+(1-\alpha_1)K_{13,L}\frac{1}{2}\rho_L j_1^{\,2} \\ &\quad +3.15\cdot C_{BT}\frac{2\sigma}{L_B+L_L}Ca^{2/3}-(\alpha_3-\alpha_1)K_{13,L\alpha}\frac{1}{2}\rho_L j_1^{\,2}\end{aligned} \qquad 10.12$$

By carefully studying equation 10.11 and 10.12, it can be seen that without the newly added terms to make up for the mal-distribution effect on the pressure drops over the junction region, the equations only predict the total flow rates in the run and branch assuming perfect distribution of the two phases. The newly added terms regard the heavy liquid phase to be the only factor that has an impact on the junction pressure drops due to the apparent mal-distribution. They are proposed on the observation of having a branch rich on gas. From a pure mathematical point of view these newly added terms will result in offsetting/altering the constant pressure curves from the location of constant j_3/j_1 lines in the split ratio plot. This occurrence has without a doubt physical meaning as long as the assumption that transportation of more liquid per time does in fact result in a higher loss of frictional energy.

Equation 10.11 and 10.12 together with the previously introduced set of equations to formulate the system of equations are the finalized set of equations to complete the proposed model. To evaluate if the model holds the K coefficients have to be evaluated. They should both be a function of

the bubble length as well as j_3 / j_1. The fractional flux in the run could be used as well, but are connected true continuity with the branch flux, and hence this is merely a choice of formulation. Theoretically they should apply outside the centre regime as well, but show variations in trend.

Data for $\overline{P_{1,j} - P_{2,j}}$ and $\overline{P_{1,j} - P_{3,j}}$ was presented in chapter 9 . The data showed little sign of trend when plotted against j_3 / j_1 with its chaotic behaviour. At the same time such an occurrence was anticipated due to $\overline{P_{1,j} - P_{2,j}}$ and $\overline{P_{1,j} - P_{3,j}}$'s sensitivity to variations in average velocities. By calculating $K_{12,L\alpha}$ and $K_{13,L\alpha}$ from equation 10.11 and 10.12 with use of measured junction pressure losses with their respective measured superficial velocities (j_1, j_2, j_3, α_1 *and* α_3), the trend presented in Figure 10.8 and Figure 10.9 for $K_{12,L\alpha}$ and $K_{13,L\alpha}$ respectively, was discovered.

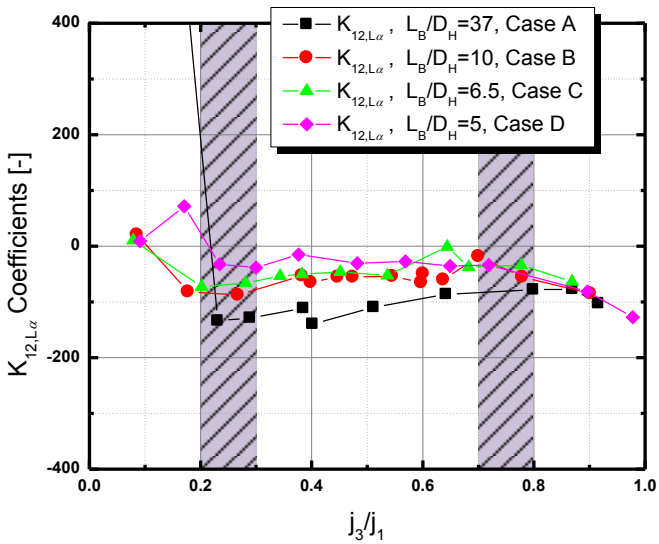

Figure 10.8: $K_{12,L\alpha}$

As discussed in chapter 9 these K-values ($K_{12,L\alpha}$ and $K_{13,L\alpha}$) reveals tremendous change in value for when moving outside the specified centre regime (see Figure 10.8 where one of the points for case A lies outside the plot). For case A with long bubbles and negligible mal-distribution for low branch flow rates ($\alpha_3 - \alpha_1$) moves towards zero, which explains the extreme behaviour seen in Figure 10.8.

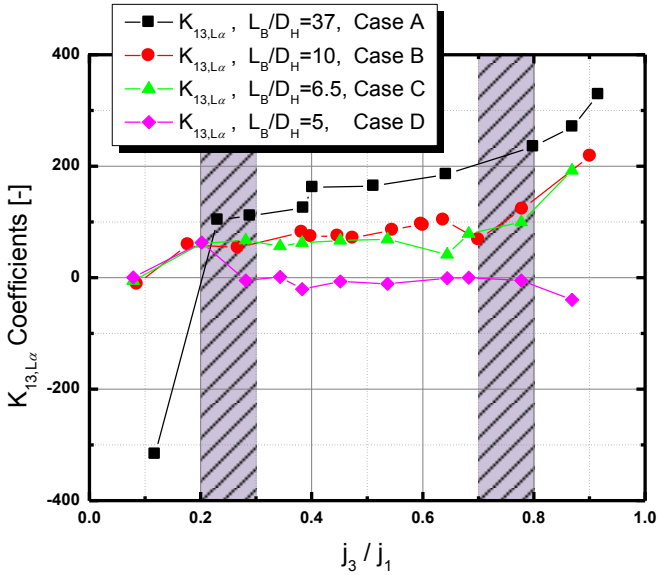

Figure 10.9: $K_{13,L\alpha}$

All cases have K coefficients located in a well behaved manner in reference to each other (and $K_{13,L\alpha}$ reveals a higher degree of change in comparison to $K_{12,L\alpha}$, which was anticipated), with exception of particularly one point. But recall that the mal-distribution rate between cases B and C is relatively minor. Also, as expected, $K_{13,L\alpha}$ shows a higher degree of change in comparison to $K_{12,L\alpha}$ due to much higher frictional losses for liquid moving from the main to the branch. It is of interest to correlate these obvious trends in $K_{12,L\alpha}$ and $K_{13,L\alpha}$ to j_3 / j_1 and the respective bubble lengths, but this will not be performed due to the limited amount of data that has been obtained. Instead it will be concluded that the observed trend for the new K coefficients agrees well with the previously introduced hypothesis, and this even after having little confidence in the apparent chaotic behaviour of obtained data for $\overline{P_{1,j} - P_{2,j}}$ and $\overline{P_{1,j} - P_{3,j}}$ in the previous chapter. To be fully able to make a well adjust fitting of this trend so as to complete the correlation between junction pressure drops and bubble length more data is needed for change in total fluxes as well as variation in bubble length. Curves for four different bubble lengths are regarded insufficient for conducting a fitting process when analysing Figure 10.8 and Figure 10.9.

Further validation of how well the model predicts the total flow rates as well as the split ratio is not applicable at this point. Instead, Figure 10.9 and Figure 10.8 work as validation of the fact that the model has physical meaning and shows promising behaviour for a possible well-performing method of modelling the split ratio at a meso-scale T-junction having one heavy and one light phase.

10.2 Negative K Coefficients

Calculation of the newly constructed K coefficients, $K_{12,L\alpha}$ and $K_{13,L\alpha}$, show good trends as function of the bubble length, but they appear to be negative (besides for $K_{13,L\alpha}$ in most of the cases). This conflicts with common sense. It implies that energy is actually *added* to the system, which is most definitely not be the case. This problem is assumed to have its roots from the calibration of equipment used in the experimental setup. Recall the fact that junction pressure drop was of the order of less than $1\,kPa$. A slight miss-calibration of the equipment is assumed to be the cause of this. Physically the K coefficients should always appear positive so as to extract frictional energy from the flow field due to wall friction, separation and secondary flow occurrence. On the other hand the obtained trends for variation in total fluxes are regarded to have high accuracy due to the high accuracy of each of the pressure transducers, i.e. it is only the calibration between different transducers that is the cause of the negative values for pressure drops as well as K-coefficients but the trends are conserved.

10.3 Criteria of Applicability

In subchapter 7.1.2 , an important aspect related to the possibility of sudden change in the physical ingredients once the bubble length reaches below a certain critical limit were discussed. A similar occurrence of change in physical ingredients for split ratio at an asymmetric T-junction has already been revealed to occur through image analysis. Hence below a certain limit for bubble length, $L_{B,crit}$, the physics will change and thereby render the

empirically fitted model inapplicable for use. A model for prediction of split ratio for this regime is not included in this thesis.

The criteria for applicability of the proposed model for prediction of split ratio is that all three channels, main, run and branch, must all have a plug flow pattern. Bubbly flow in either one of the two branches is not valid even though phase-separation is not encountered. The flow field must be laminar, and the channels meso-scaled. When the channel sizes closes in on the micro-scale regime ($D_H < 100\mu m$) new phenomena occur for the plug flow. As an example, see how slip velocity/void fraction as a function of volumetric flux presented in chapter 5 Figure 5.7 changes for when $D_H = 100\mu m$ in comparison to that in meso-scale channels. Even though it seems possible to construct loss coefficients that works across the regime-lines, due to the apparent change in physical ingredients these regimes should be referred to separately. Their borders should be thoroughly mapped through further experimentation evaluation of capillary number together with the corresponding bubble length.

10.4 Generalization of the Model

Due to limitations of the experimental setup it is at the moment not applicable to validate the model for variations in fluid properties and/or cross sectional size and shape. This is regrettable, and has to be worked out in future studies to ensure that the model is still applicable. It is assumed that changes in these parameters will have an effect on the split ratio and hence also the loss coefficients. A generalization of the model has to be performed. Such an addition to the model should be based on assumptions of the physical trend already discussed in previous chapters, and later on the model has to be fitted by use of empirical constants to perform well for any changes in fluid properties and/or geometry of the channels.

11 Conclusion

The mal-distribution phenomenon occurring at a asymmetric meso-scale T-junction for two-phase liquid and gas plug-flow has been investigated through a thorough literature review and experimentation. A model has been proposed for prediction of the split ratio and total flux in the run and branch based on the extended Bernoulli equations.

11.1 Physical Trend

The split ratio has shown to be heavily affected by the bubble length, as was proposed by Hong et al. (2011) (3). Changes in superficial velocities reveal close to negligible impact on the split ratio. A centre regime has been proposed for use where a set of physical ingredients are conserved, namely having plug flow pattern in all three channels. While operating within the centre-regime the branch stays rich on gas for all values of bubble lengths. Long bubbles yields a split ratio located closest to perfect distribution. For decreasing bubble lengths the void fraction in the branch experiences an increase. Location for border lines of the centre regime is a function of bubble length and capillary number (recall the discussion about capillary number in chapter 9.3). As the bubble length decrease the centre regime grows narrower. Increasing the total flux in the main also reveals a centre regime growing narrower. If the size of the centre regime is actually a function of the Capillary number needs further evaluation by experimenting with variable viscosities for the two phases and variable surface tension.

At a certain point of increasing total flux in the run, the bubbles tend to follow the high flow rate for the dispersed phase which leads to a deviation in split ratio trend (when operating outside the centre regime). Bubbly flow is encountered frequently outside the centre regime for sufficiently short bubbles, and also instabilities might occur.

Phase-separation has been observed for high flow rates in both run and branch with bubble lengths below a certain critical value. Occurrence of the separation of the gas phase to either the run or the branch shows a strict relation with the bubble length and capillary number (see chapter 9.3). Decreasing both bubble length and the total flux in the main results in faster occurrence of separation with regards to total fluxes in the respective outlet channel.

11.2 Time Averaged Junction Pressure Drops

In the experimental setup taps for measurement of pressure was drilled. A time averaged pressure distribution was obtained for all experiments through linear extrapolation. The objective of the pressure measurements was to investigate the time averaged junction pressure losses due to friction and separation within the junction region. The measured time averaged junction pressures revealed a chaotic behaviour. This behaviour was justified by addressing the exponential relation between variations in pressure and velocity given by the Bernoulli equation. A physically meaningful trend was by use of the obtained pressure data in the constructed model.

11.3 Model

A model based on the extended Bernoulli equation has been proposed. Since the time dependant flow field within the junction region is indisputably very complex it is inevitable to perform a fitting process since the time averaged Bernoulli equation was used. The proposed model introduces a new term that relates variations in pressure loss to the void fraction in each of the two outlet channels. It is based on the assumption that more energy is needed to transport the heavy liquid phase through the junction region. This assumption is physically sound. Once the apparent chaotic pressure data was used to calculate the additional loss-coefficients ($K_{12,L\alpha}$ and $K_{13,L\alpha}$) located within these term, a strict trend was located. They relate to variations

in bubble length and total fluxes in the outlet channels, as was anticipated. A fitting process was rendered inapplicable due to lack of a sufficient amount of data. Therefore this task of completing the correlation is mentioned in chapter 12 : Future Work. From the obtained amount of data it can be concluded that the model shows relatively good signs of being capable of predicting the split ratio once the loss-coefficients are correlated.

11.4 Void Fraction and Bubble Length Relation

Another interesting trend was revealed relating the void fraction in the branch directly to the bubble length parameter. For all cases it can be seen how the void fraction stays fairly linear for long bubbles in comparison to short bubbles. For short bubbles the increase in void fraction takes on a trend which resembles a proportionality with $\sim 1/L_B$.

12 Future Work

- Obtain a sufficient amount of experimental data for split ratio and junction pressure losses

- Perform fitting of $K_{12,L\alpha}$ and $K_{13,L\alpha}$ as a function of j_3 / j_1 and L_B from the sufficient amount of experimental data

- Generalize model to make it applicable for changes in D_H, shape of cross section, and fluid properties.

- Test if variations in total flux in the main, viscosity and surface tension relates similarly to the location of separation and centre regime borders. This should be performed to investigate how the Capillary number affects the flow pattern and split ratio.

- Further address the difficulties related to the outer regimes of the split ratio plot, i.e. for extreme values of j_3 / j_1.

- Further investigate separation as a possible function of j_3 / j_1, L_B, j_1, cross sectional shape and size, and fluid properties.

- Further investigate instability in transition regions to phase-separation

13 Acknowledgements

The author acknowledge help received from Professor Sang Yong Lee (이상용), PhD students Seok Kim (김석), Wooshik Kim (김우식), Joohan Bae (배주한), Junewoo Kee (기준우) and from Dr. Sangmo An (안상모), and wish to thank them for their contributions and numerous fruitful discussions. It was utmost helpful during both lab-work and in constructing the model. Much gratitude is given to my colleagues.

Their ability to welcome me as a foreigner in their lab and integrate me so that I was able to quickly function in this new and unfamiliar working environment at KAIST was exceptional. Their patience under the occurrence of language difficulties and cultural differences is highly appreciated.

I also thank my supervisor at NTNU Professor Maria Fernandino for supporting me in my decision of writing my thesis abroad.

14 Bibliography

1. *The Effect of Channel Diameter on Adiabatic Two-phase Flow Characteristics in Microchannels.* **Chung, P. M. and Kawaji, M.** 2004.

2. *Hydrogen-water Flow Regime Transitions Applied to Anode Flow Phenomena in a PEMFC.* **Owejan, J. P., Trabold, T. A. and Tighe, T. W.** 2005.

3. **Hong, Ju Hyuk and Lee, Sang Yong.** *On the Split of Two-Phase Plug Flow at Meso-Scale T-Junction: Influence of the Bubble Length.* 2011.

4. *Study of Flow Distribution and its Improvement on the Header of Plate-fin Heat Exchangers.* **Wen, Jian and Li, Yanzhong.** 2004.

5. *Two Phase Flow in Capillary Tubes.* **Suo, Mikio and Griffith, Peter.** 1964.

6. *The Effect of Flow Patterns On Two-Phase Flow in a T-Junction.* **Azzopardi, B. J. and Whalley, P. B.** 1982.

7. *Flow Distribution and Pressure Drop in Plate Heat Exchangers - II.* **Bassiouny, M. K. and Martin, H.** 1983.

8. *A Uniform Temperature Heat Sink for Cooling of Electronic Devices.* **Hetsroni, Gad, et al., et al.** 2002.

9. *Nonuniform Temperature Distribution in Electronic Devices Cooled by Flow in Parallel Microchannels.* **Hetsroni, G., Mosyak, A. and Segal, Z.** 2001.

10. *Micro and Meso Scale Compact Heat Exchangers in Electronics Thermal Management - A Review.* **Joshi, Y. and Wei, X.** 2005.

11. *Developing Adiabatic Two Phase Flow in Headers - Distribution Issure in Parallel Flow Microchannel Heat Exchangers.* **Hrnjak and Pega.** 2004.

12. *Microfluidic Devices for Cellomics: a Review.* **Andersson, Helene and Berg, Albert van den.** 2003.

13. *Dynamics of Microfluidic Droplets.* **Baroud, Charles N., Gallaire, Francois and Dangla, Rèmi.** 2010.

14. *Hydrodynamic Control of Droplet Division in Bifurcating Microchannel and its Application to Particle Synthesis.* **Yamada, Masumi, et al., et al.** 2008.

15. **Oertel, Herbert, et al., et al.** *Prandtl's Essentials of Fluid Mechanics.* 2001.
16. **Ghiaasiaan and Mostafa, S.** *Two-Phase Flow, Boiling & Condensation.* 2008.
17. **Wolden, Andre.** *Experimental Characterization of Slug Flow.* 2011.
18. *The Effect of Flow Pattern on Split of Two-Phase Flow Through a Micro-T-Junction.* **He, Kui, Wang, Shuangfeng and Huang, Jianzhen.** 2011.
19. *Phase Splitting of a Slug-annular Flow at a Horizontal Micro-T-junction.* **Wang, Shuangfeng, He, Kui and Huang, Jianzhen.** 2011.
20. **Lee, Sang Yong.** *Two-phase Flow Heat Transfer.* 1993 : s.n.
21. —. *Two-Phase Flow Heat Transfer.* 1993.
22. *Two-phase Plug Flow Distribution at a Meso-scale T-junction - Effect of Plug Bubble Length.* **Lee, Sang Yong, Hong, Ju Hyuk and Lim, Jin Seok.** 2010.
23. *Two-phase Flow in Narrow Channels Between Two Flat Plates.* **Ali, M. I., Sadatomi, M. and Kawaji, M.** 1993.
24. *Adiabatic Two-phase Flow in Rectangular Microchannels with Different Aspect Ratios: Part II - Bubble Behaviors and Pressure Drop in Single Bubble.* **Choi, C. W., Yu, D. I. and Kim, M. H.** 2010.
25. *Phase split of nitrogen/non-Newtonian fluid two-phase flow at a micro-T-junction.* **Wang, Shuangfeng, et al., et al.** 2011.
26. *Gas-liquid Two-phase Flow Division at a Micro-T-junction.* **Azzi, A., et al., et al.** 2010.
27. *The Effect of Surface Tension on Phase Distribution of Two-Phase Flow in a Micro-T-junction.* **He, Kui, Wang, Shuangfeng and Huang, Jianzhen.** 2011.
28. **Jo, Sung Geun.** *Effect of Gravity on Gas Plug Formation at Mini-scale Y-junctions.* 2011.

Attachment A: Single Phase Velocity and Pressure Data

Set	j_2	j_3	j_1	j_3 / j_1	Unit
1st Experiment					
1	0.564	0.000	0.564	0.000	[m/s]
2	0.544	0.021	0.565	0.037	[m/s]
3	0.456	0.107	0.563	0.190	[m/s]
4	0.411	0.154	0.565	0.273	[m/s]
5	0.333	0.227	0.560	0.406	[m/s]
6	0.348	0.212	0.560	0.378	[m/s]
7	0.260	0.300	0.560	0.536	[m/s]
8	0.191	0.369	0.560	0.659	[m/s]
9	0.140	0.416	0.556	0.748	[m/s]
10	0.034	0.523	0.557	0.940	[m/s]
2nd Experiment					
1	0.541	0.000	0.541	0.000	[m/s]
2	0.480	0.065	0.545	0.120	[m/s]
3	0.452	0.090	0.542	0.165	[m/s]
4	0.414	0.124	0.538	0.231	[m/s]
5	0.330	0.202	0.533	0.380	[m/s]
6	0.292	0.249	0.542	0.460	[m/s]
7	0.195	0.344	0.539	0.639	[m/s]
8	0.192	0.349	0.541	0.644	[m/s]
9	0.133	0.404	0.538	0.752	[m/s]
10	0.000	0.529	0.529	1.000	[m/s]

Set	$\overline{P_{1,j}}$	$\overline{P_{2,j}}$	$\overline{P_{3,j}}$	$\overline{P_{1,j}-P_{2,j}}$	$\overline{P_{1,j}-P_{3,j}}$	Unit	$K_{12,L}$	$K_{13,L}$
1st Experiment								
1	11.20	11.71	12.80	-0.52	-1.60	$[kPa]$	0.00	0.99
2	11.20	11.74	12.69	-0.54	-1.49	$[kPa]$	0.07	0.99
3	11.37	11.93	12.47	-0.56	-1.09	$[kPa]$	0.34	0.96
4	11.10	11.54	11.81	-0.44	-0.72	$[kPa]$	0.47	0.92
5	11.30	11.91	11.85	-0.61	-0.55	$[kPa]$	0.64	0.83
6	11.35	11.90	11.98	-0.55	-0.63	$[kPa]$	0.61	0.85
7	11.14	11.64	11.23	-0.50	-0.09	$[kPa]$	0.78	0.71
8	11.39	11.95	11.23	-0.55	0.16	$[kPa]$	0.88	0.57
9	11.34	11.94	10.82	-0.59	0.53	$[kPa]$	0.93	0.44
10	11.39	12.01	9.99	-0.62	1.40	$[kPa]$	0.99	0.13
2nd Experiment								
1	15.76	17.07	17.94	-1.31	-2.18	$[kPa]$	-0.01	0.99
2	15.21	16.15	16.79	-0.93	-1.58	$[kPa]$	0.22	0.97
3	15.32	16.01	17.16	-0.69	-1.84	$[kPa]$	0.30	0.96
4	15.63	16.26	17.12	-0.64	-1.49	$[kPa]$	0.40	0.94
5	15.34	16.13	16.49	-0.79	-1.15	$[kPa]$	0.61	0.85
6	15.53	16.62	16.31	-1.09	-0.78	$[kPa]$	0.70	0.78
7	15.44	16.04	15.41	-0.59	0.04	$[kPa]$	0.87	0.59
8	15.27	16.05	15.04	-0.78	0.23	$[kPa]$	0.87	0.59
9	15.32	15.80	14.62	-0.48	0.70	$[kPa]$	0.94	0.44
10	15.33	15.80	13.83	-0.47	1.50	$[kPa]$	1.00	0.01

Attachment B: Two-phase Flow Split Ratio Data

Case A				$L_B / D_H = 37$			
Set	$j_{L,1}$	$j_{L,2}$	$j_{L,3}$	$j_{G,1}$	$j_{G,2}$	$j_{G,3}$	unit
1	0.314	0.277	0.037	0.301	0.266	0.035	[m/s]
2	0.313	0.245	0.069	0.301	0.228	0.073	[m/s]
3	0.314	0.228	0.086	0.301	0.209	0.092	[m/s]
4	0.314	0.203	0.112	0.301	0.176	0.125	[m/s]
5	0.315	0.197	0.118	0.301	0.171	0.129	[m/s]
6	0.315	0.167	0.148	0.301	0.134	0.167	[m/s]
7	0.314	0.130	0.185	0.301	0.091	0.210	[m/s]
8	0.315	0.086	0.229	0.301	0.038	0.263	[m/s]
9	0.315	0.067	0.248	0.301	0.013	0.288	[m/s]
10	0.316	0.052	0.264	0.301	0.000	0.302	[m/s]
11	0.315	0.000	0.315	0.301	0.000	0.301	[m/s]

Case B				$L_B / D_H = 10$			
Set	$j_{L,1}$	$j_{L,2}$	$j_{L,3}$	$j_{G,1}$	$j_{G,2}$	$j_{G,3}$	unit
1	0.307	0.269	0.037	0.301	0.286	0.015	[m/s]
2	0.306	0.258	0.048	0.301	0.242	0.059	[m/s]
3	0.313	0.244	0.069	0.301	0.206	0.095	[m/s]
4	0.310	0.213	0.097	0.301	0.164	0.137	[m/s]
5	0.309	0.209	0.100	0.301	0.158	0.143	[m/s]
6	0.309	0.199	0.110	0.301	0.138	0.162	[m/s]
7	0.313	0.195	0.118	0.301	0.128	0.173	[m/s]
8	0.307	0.177	0.130	0.301	0.100	0.201	[m/s]
9	0.308	0.161	0.147	0.301	0.084	0.217	[m/s]
10	0.311	0.161	0.150	0.301	0.083	0.217	[m/s]
11	0.311	0.153	0.158	0.301	0.069	0.232	[m/s]
12	0.309	0.142	0.167	0.301	0.041	0.260	[m/s]
13	0.309	0.122	0.186	0.301	0.012	0.288	[m/s]
14	0.308	0.076	0.232	0.301	0.000	0.316	[m/s]

Case C				$L_B / D_H = 6.5$			
Set	$j_{L,1}$	$j_{L,2}$	$j_{L,3}$	$j_{G,1}$	$j_{G,2}$	$j_{G,3}$	unit
1	0.306	0.262	0.044	0.301	0.297	0.004	[m/s]
2	0.310	0.255	0.054	0.301	0.232	0.069	[m/s]
3	0.311	0.239	0.071	0.301	0.200	0.101	[m/s]
4	0.310	0.226	0.084	0.301	0.175	0.126	[m/s]
5	0.312	0.218	0.094	0.301	0.161	0.140	[m/s]
6	0.311	0.203	0.109	0.301	0.133	0.168	[m/s]
7	0.314	0.191	0.123	0.301	0.094	0.207	[m/s]
8	0.311	0.167	0.144	0.301	0.051	0.250	[m/s]
9	0.312	0.155	0.157	0.301	0.040	0.261	[m/s]
10	0.310	0.128	0.182	0.301	0.008	0.293	[m/s]
11	0.309	0.088	0.221	0.301	0.000	0.308	[m/s]

Case D				$L_B / D_H = 5$			
Set	$j_{L,1}$	$j_{L,2}$	$j_{L,3}$	$j_{G,1}$	$j_{G,2}$	$j_{G,3}$	unit
1	0.303	0.255	0.048	0.301	0.294	0.007	[m/s]
2	0.305	0.250	0.055	0.301	0.253	0.048	[m/s]
3	0.305	0.249	0.056	0.301	0.215	0.086	[m/s]
4	0.306	0.239	0.068	0.301	0.186	0.114	[m/s]
5	0.307	0.226	0.081	0.301	0.153	0.148	[m/s]
6	0.307	0.212	0.095	0.301	0.103	0.198	[m/s]
7	0.308	0.198	0.110	0.301	0.065	0.236	[m/s]
8	0.308	0.184	0.124	0.301	0.030	0.271	[m/s]
9	0.307	0.169	0.138	0.301	0.002	0.299	[m/s]
10	0.309	0.074	0.235	0.301	0.000	0.311	[m/s]
11	0.308	0.028	0.279	0.301	0.000	0.316	[m/s]

Attachment C: Two-phase Flow Pressure Data

Case A				$L_B / D_H = 37$				
Set	$\overline{P_{1,j}}$	$\overline{P_{2,j}}$	$\overline{P_{3,j}}$	$\overline{P_{1,j} - P_{2,j}}$	$\overline{P_{1,j} - P_{3,j}}$	Unit	$K_{12,L\alpha}$	$K_{13,L\alpha}$
1	8.36	8.62	8.27	-0.25	0.10	$[kPa]$	1055.5	-316.4
2	8.44	8.66	8.37	-0.22	0.06	$[kPa]$	-133.6	103.6
3	8.44	8.61	8.25	-0.17	0.19	$[kPa]$	-128.9	110.9
4	8.42	8.71	8.28	-0.29	0.14	$[kPa]$	-111.3	125.3
5	8.30	8.65	8.21	-0.35	0.09	$[kPa]$	-139.9	162.2
6	8.31	8.55	8.04	-0.25	0.27	$[kPa]$	-109.4	164.3
7	8.58	8.65	8.06	-0.07	0.52	$[kPa]$	-86.5	185.6
8	8.56	8.55	7.94	0.01	0.62	$[kPa]$	-78.2	235.1
9	8.70	8.68	8.19	0.02	0.51	$[kPa]$	-77.1	270.8
10	8.38	8.50	8.02	-0.12	0.36	$[kPa]$	-102.9	328.8
11	8.84	9.01	8.43	-0.17	0.41	$[kPa]$	-	-

Case B				$L_B / D_H = 10$				
Set	$\overline{P_{1,j}}$	$\overline{P_{2,j}}$	$\overline{P_{3,j}}$	$\overline{P_{1,j} - P_{2,j}}$	$\overline{P_{1,j} - P_{3,j}}$	Unit	$K_{12,L\alpha}$	$K_{13,L\alpha}$
1	9.74	10.18	9.92	-0.44	-0.18	$[kPa]$	20.3	-11.3
2	9.27	9.68	9.42	-0.42	-0.15	$[kPa]$	-81.7	59.4
3	8.80	9.68	8.97	-0.88	-0.17	$[kPa]$	-87.6	53.8
4	8.79	9.17	9.08	-0.38	-0.29	$[kPa]$	-53.0	81.7
5	8.73	9.28	8.88	-0.56	-0.15	$[kPa]$	-64.8	74.0
6	8.21	8.66	8.31	-0.45	-0.10	$[kPa]$	-55.3	74.8
7	8.17	8.64	8.14	-0.46	0.04	$[kPa]$	-55.3	71.0
8	8.28	8.76	8.36	-0.47	-0.08	$[kPa]$	-54.0	85.6
9	8.38	8.92	8.31	-0.54	0.07	$[kPa]$	-65.4	96.3
10	8.36	8.64	8.22	-0.28	0.14	$[kPa]$	-49.5	94.0
11	8.52	8.97	8.43	-0.45	0.09	$[kPa]$	-60.2	103.6
12	8.17	7.97	7.46	0.20	0.71	$[kPa]$	-18.4	68.4
13	8.46	8.87	8.42	-0.41	0.04	$[kPa]$	-55.1	123.1
14	8.26	8.74	8.44	-0.48	-0.18	$[kPa]$	-84.9	218.3

Case C				$L_B / D_H = 6.5$				
Set	$\overline{P_{1,j}}$	$\overline{P_{2,j}}$	$\overline{P_{3,j}}$	$\overline{P_{1,j} - P_{2,j}}$	$\overline{P_{1,j} - P_{3,j}}$	Unit	$K_{12,L\alpha}$	$K_{13,L\alpha}$
1	10.31	10.76	10.47	-0.44	-0.16	$[kPa]$	10.7	-5.4
2	9.57	10.01	9.78	-0.44	-0.21	$[kPa]$	-72.5	61.0
3	9.32	9.94	9.70	-0.63	-0.38	$[kPa]$	-66.0	67.0
4	8.91	9.42	9.07	-0.51	-0.15	$[kPa]$	-53.5	56.5
5	8.31	8.75	8.46	-0.45	-0.15	$[kPa]$	-50.1	62.7
6	8.27	8.68	8.36	-0.41	-0.09	$[kPa]$	-46.0	66.5
7	8.20	8.86	8.28	-0.66	-0.07	$[kPa]$	-52.3	68.8
8	8.31	7.81	7.47	0.49	0.83	$[kPa]$	-0.9	41.7
9	8.58	8.83	8.33	-0.25	0.25	$[kPa]$	-37.3	79.1
10	8.51	8.60	8.21	-0.09	0.30	$[kPa]$	-34.1	99.4
11	9.76	10.04	9.90	-0.28	-0.15	$[kPa]$	-63.3	192.3

Case D				$L_B / D_H = 5$				
Set	$\overline{P_{1,j}}$	$\overline{P_{2,j}}$	$\overline{P_{3,j}}$	$\overline{P_{1,j} - P_{2,j}}$	$\overline{P_{1,j} - P_{3,j}}$	Unit	$K_{12,L\alpha}$	$K_{13,L\alpha}$
1	11.15	11.41	11.22	-0.26	-0.07	$[kPa]$	9.0	-4.8
2	11.30	11.38	11.09	-0.07	0.21	$[kPa]$	71.7	-26.0
3	10.66	10.88	10.67	-0.22	-0.01	$[kPa]$	-32.4	29.8
4	10.01	10.44	10.13	-0.43	-0.12	$[kPa]$	-38.2	37.6
5	10.05	10.01	9.66	0.04	0.39	$[kPa]$	-15.0	20.1
6	9.07	9.49	8.97	-0.42	0.11	$[kPa]$	-30.8	39.0
7	8.05	8.36	7.80	-0.31	0.25	$[kPa]$	-27.2	42.5
8	8.08	8.62	8.11	-0.54	-0.03	$[kPa]$	-35.5	60.4
9	8.13	8.59	8.18	-0.46	-0.05	$[kPa]$	-34.0	69.9
10	10.88	11.23	10.84	-0.35	0.04	$[kPa]$	-81.1	217.0
11	11.06	11.14	10.84	-0.08	0.22	$[kPa]$	-127.5	470.7